

# Extracting quadratic propagators by refined graphic rule

---

Chongsi Xie<sup>a</sup> Yi-Jian Du<sup>1a,b</sup>

<sup>a</sup>*Department of Physics, School of Physics and Technology, Wuhan University,  
No.299 Bayi Road, Wuhan 430072, China*

<sup>b</sup>*Hubei Key Laboratory of Nuclear Solid Physics, School of Physics and Technology, Wuhan University,  
No.299 Bayi Road, Wuhan 430072, China*

*E-mail:* [chongsi.xie@whu.edu.cn](mailto:chongsi.xie@whu.edu.cn), [yijian.du@whu.edu.cn](mailto:yijian.du@whu.edu.cn)

ABSTRACT: One-loop integrands in Cachazo-He-Yuan (CHY) formula, which is based on the forward limit of tree-level amplitudes, involves linear propagators that are different from quadratic ones in traditional Feynman diagrams. In this paper, we provide a general approach to converting linear propagators in one-loop CHY formula into quadratic propagators, by refined graphic rule stemming from the recursive expansion of tree-level Einstein-Yang-Mills amplitudes. Particularly, we establish the correspondence between refined graphs and bi-adjoint scalar (BS) Feynman diagrams with linear propagators. Using this correspondence and graph-based relations of Berends-Giele currents in BS theory, the nonlocal terms accompanied by refined graphs can either be canceled out or be collected into local ones. Once the locality has been achieved, the integrand with linear propagators can be directly arranged into that with quadratic propagators. Following this approach, we first convert the linear propagators in single-trace Yang-Mills-scalar (YMS) integrands (with a pure-scalar loop) into quadratic ones. This result is then demonstrated to match the traditional one-loop Feynman diagrams. The discussions on single-trace YMS integrands are generalized to multi-trace YMS and Yang-Mills integrands.

KEYWORDS: Scattering Amplitudes, Gauge Symmetry

---

<sup>1</sup>Corresponding author

---

## Contents

<b>1</b>	<b>Introduction</b>	<b>1</b>
<b>2</b>	<b>CHY formula, refined graphic rule, tensorial PT factors and properties of BS currents</b>	<b>3</b>
2.1	Tree-level CHY	3
2.2	One-loop CHY formula from forward limit	5
2.3	Expanding the half integrands by refined graphic rule	6
2.3.1	Expansion of $\text{PT}(+, \boldsymbol{\sigma}, -) \text{Pf}[\Psi_{\mathbf{G}}]$	6
2.3.2	Expansion of $\text{Pf}'[\Psi_{n+2}]$	9
2.4	Tensorial PT factors and the problem of quadratic propagators	10
2.5	Properties of the BG currents in BS theory	13
<b>3</b>	<b>Four-point integrand with two gluons</b>	<b>15</b>
3.1	Four-point integrand with two gluons	15
3.2	The first class of graphs	18
3.3	The second class of graphs and approach-1 to canceling nonlocal terms	19
3.4	The third class of graphs and approach-2 to canceling the nonlocal terms	23
3.5	Compact expression of the four-point integrand with two gluons	26
<b>4</b>	<b>X-pattern and BCJ-pattern</b>	<b>31</b>
4.1	Example-1	31
4.2	Example-2	33
4.3	General X- and BCJ-pattern	34
<b>5</b>	<b>Spurious graphs and five-point integrand with three gluons</b>	<b>36</b>
5.1	Five-point example and spurious graphs	37
5.2	Compact expression of the five-point integrand with three gluons	41
<b>6</b>	<b>General discussions and the final result for single-trace YMS</b>	<b>44</b>
6.1	Topologies for a given partition	46
6.2	General cancellation between X- and BCJ-patterns	46
6.3	From linear to quadratic propagators	50
<b>7</b>	<b>Traditional Feynman diagrams and the extension to multi-trace YMS and YM</b>	<b>52</b>
7.1	The relationship with traditional Feynman diagrams	52
7.2	The extensions to multi-trace YMS and YM	54
<b>8</b>	<b>Conclusions and further discussions</b>	<b>55</b>

<b>A</b>	<b>Expansion formula of <math>\text{PT}(+, x_1, \dots, x_r, -) \text{Pf}[\Psi_G]</math></b>	<b>57</b>
<b>B</b>	<b>Expansion of <math>\text{PT}(+, \sigma_1, -) \text{PT}(\sigma_2) \cdots \text{PT}(\sigma_m) \mathcal{P}</math></b>	<b>57</b>
<b>C</b>	<b>All graphs with three gluons and all graphs for the effective current <math>\tilde{J}^\mu(p, q, r)</math></b>	<b>59</b>
<b>D</b>	<b>The cancellation map for the example in section 3.4</b>	<b>60</b>
<b>E</b>	<b>Two versions of graphic rules for a subgraph</b>	<b>60</b>
<b>F</b>	<b>Constructing a subgraph in a given partition and topology</b>	<b>63</b>
	F.1 Approach-1	64
	F.2 Approach-2	66
<b>G</b>	<b>Explicit examples for the construction of subgraphs</b>	<b>68</b>
<b>H</b>	<b>Quadratic propagators from refined graphic rule: an example with four gluons</b>	<b>69</b>
<b>I</b>	<b>Expressions of terms in (6.16): demonstrated by explicit examples</b>	<b>71</b>
<b>J</b>	<b>Feynman rule in YMS</b>	<b>73</b>
<b>K</b>	<b>KK relation for one-loop half integrands</b>	<b>73</b>

---

## 1 Introduction

In recent decades, there have been many significant progresses on perturbative scattering amplitudes, among which, Cachazo-He-Yuan (CHY) formula [1–5] provides a compact form of tree-level scattering amplitudes. In particular, according to CHY formula, a tree-level amplitude is expressed as an integral over scattering variables that are constrained by scattering equations. The CHY integrand, which contains the kinematic information of external particles, relies on theories and can be written as a product of two half integrands. CHY formula for various theories, such as bi-adjoint scalar (BS) theory, Yang-Mills-scalar (YMS) theory, Yang-Mills (YM) theory, Einstein-Yang-Mills (EYM) theory and gravity (GR) have already been established [1–5]. Moreover, it has also been shown to exist in effective theories [5].

A crucial feature of CHY formula is that the color-ordered BS amplitudes, whose CHY integrands are presented as a product of two Parke-Taylor (PT) [6] factors, play as the backbone of the CHY formula. CHY half integrands for other theories can be decomposed in terms of a proper combination of the PT factors. The expansion coefficients are constructed systematically by refined graphic rule [7, 8] which benefits from the recursive expansion formula of EYM amplitudes [9–15]. As a consequence of the expansion of

half integrands, the full amplitudes in other theories are finally written in terms of BS amplitudes. This has been effectively applied to the construction of local Bern-Carrasco-Johansson (BCJ) numerators that satisfy color-kinematics duality [16].

The CHY formula was generalized to one-loop amplitudes [17–19], based on an analysis of worldsheet structure. As pointed out in [18, 19], the CHY half integrands for an  $n$ -point one-loop amplitude could be obtained via taking the forward limit of  $(n + 2)$ -point half integrands at tree-level. This observation allows one to convert properties at tree-level to one-loop level. Following the forward limit approach, the one-loop BCJ numerators have been expressed by tree-level ones [20]. Although the forward limit provides a rather straightforward one-loop generalization of the tree-level CHY formula, the two  $(n + 2)$ -point PT factors with forward limits in fact can only produce propagators whose denominators are linear functions of the loop momentum [18, 19, 21–23]. This conflicts with traditional Feynman diagrams, in which the loop propagators involve quadratic function of loop momentum in the denominator. Many efforts have been made on converting the linear propagators into quadratic ones [18, 19, 21–33]. In [24] among these efforts, a tensorial PT factor was supposed to produce quadratic propagators. As further pointed out in a recent work [34], once the CHY half integrands are decomposed into these tensorial PT factors, one can construct BCJ [35, 36] numerators at one-loop level. Along this line, the critical issue for constructing quadratic propagators becomes decomposing CHY half integrands in terms of tensorial PT factors. Nevertheless, it is still lack of a general way to decompose an arbitrary CHY half integrand into tensorial PT factors.

In this work, we provide a generic approach to converting one-loop CHY formula for YMS (with a pure scalar loop) and YM with linear propagators into expressions with quadratic propagators, by the help of (refined) graphic rule [7, 8, 37]. In particular, since the CHY half integrands at one-loop are expressed by forward limits of  $(n + 2)$ -point half integrands at tree-level, while one of the tree-level YMS half integrands can further be expanded in terms of PT factors according to graphic rule, we express one of the one-loop half integrands as a sum over graphs. Together with the other half integrand of YMS, the previous step in fact expresses the loop integrand as a combination of linear-propagator Feynman diagrams (LPFD), where Berends-Giele (BG) subcurrents of BS are attached to the line with linear propagators. The combination coefficients are determined by graphs, while a LPFD is associated with a partition of external particles which is related to decomposing graphs into subgraphs. For a given LPFD accompanied by a given graph, there may exist subgraphs which are contracted with each other but are separated by linear propagators in the LPFD. Such contraction of subgraphs contribute nonlocal terms. The critical point for extracting quadratic propagators is to achieve the locality. We find that the nonlocal terms can either be canceled out by the help of graph-based identities [7, 8, 38], or be collected into local terms. Once the nonlocality has been treated, the integrand turns into sums of structures where BG subcurrents of YM, YMS, BS and/or contractions of two YM subcurrents are planted to the linear-propagator line. This expression of integrand is further arranged into a formula with quadratic propagators, straightforwardly. We show that the formula of YMS integrand matches the Feynman diagrams with quadratic propagators. As a special case of this approach, contributions of a certain class of graphs, i.e., the graphs with no  $\epsilon \cdot \epsilon$  factor, are written in

terms of the tensorial PT factors, therefore naturally induce quadratic propagators. For the contributions of more general graphs that are treated in this work, our approach does not provide the tensorial PT factor decomposition, but can produce quadratic propagators. The extension to multi-trace YMS amplitudes with pure scalar loop are straightforwardly obtained by involving more types of components in the graphs [8]. Considering the relationship between YMS and YM, we further provide an expansion formula for YM integrand. In the current work, we only study the YMS amplitudes with a scalar loop. *It is worth pointing out that the case considered in this paper does not cover the full single-trace (multi-trace) sector.* There also exist single-trace (multi-trace) integrands which involve gluon propagators on the loop but correspond to different orders of coupling constants. This situation was studied in [33]. The integrands proposed in [33] are reviewed in appendix K. We leave the general discussion on the integrands, which contain gluon propagators on the loop, in a future work.

The structure of this paper is following. In section 2, we review helpful results including tree-level and one-loop CHY formulas, the refined graphic rule as well as properties of off-shell BG current in BS. In section 3, we study the integrand with two scalars and two gluons, and further propose two approaches for treating the nonlocalities. Helpful patterns, X- and BCJ-patterns, are observed in section 3 and are extended to more general cases in section 4. More complicated examples are studied in section 5, where pairs of spurious graphs with opposite signs are introduced to cancel the nonlocalities. A general approach to a quadratic-propagator formula of YMS integrand is presented in section 6. In section 7, we show the formula obtained via graphic rule matches with the result derived from the Feynman diagrams in YMS. We further extend this discussion to multi-trace YMS (with pure scalar loop) and pure YM theory. A summary and further discussions are presented in section 8. Supplements of graphic rule, explicit examples, construction of subgraphs, Feynman rule in YMS and a byproduct identity can be found in the appendix.

## 2 CHY formula, refined graphic rule, tensorial PT factors and properties of BS currents

In this section, we review the main results of the tree-level and one-loop CHY formula, the refined graphic rule, the tensorial PT factors as well as properties of BG current in BS theory. These results provide a preparation for the coming discussions.

### 2.1 Tree-level CHY

CHY formula expresses tree-level amplitude with  $n$  massless external particles by an integral over scattering variables  $\{z_i\}$  ( $i = 1, \dots, n$ ), as follows

$$M_n^{\text{tree}} = \int d\mu_n^{\text{tree}} I_L^{\text{tree}} I_R^{\text{tree}}. \quad (2.1)$$

Theories	BS	YM	YMS	EYM	GR
Amplitudes	$A_{\text{BS}}^{\text{tree}}(\boldsymbol{\sigma} \boldsymbol{\rho})$	$A_{\text{YM}}^{\text{tree}}(\boldsymbol{\sigma})$	$A_{\text{YMS}}^{\text{tree}}(\boldsymbol{\sigma}_1; \dots; \boldsymbol{\sigma}_m    \mathbf{G}   \boldsymbol{\rho}_{\text{SUG}})$	$A_{\text{EYM}}^{\text{tree}}(\boldsymbol{\sigma}_1; \dots; \boldsymbol{\sigma}_m    \mathbf{H})$	$M_{\text{GR}}^{\text{tree}}(1, \dots, n)$
$I_{\text{L}}^{\text{tree}}$	$\text{PT}(\boldsymbol{\sigma})$	$\text{PT}(\boldsymbol{\sigma})$	$\text{PT}(\boldsymbol{\sigma}_1) \dots \text{PT}(\boldsymbol{\sigma}_m) \mathcal{P}$	$\text{PT}(\boldsymbol{\sigma}_1) \dots \text{PT}(\boldsymbol{\sigma}_m) \mathcal{P}$	$\text{Pf}'[\Psi]$
$I_{\text{R}}^{\text{tree}}$	$\text{PT}(\boldsymbol{\rho})$	$\text{Pf}'[\Psi]$	$\text{PT}(\boldsymbol{\rho}_{\text{SUG}})$	$\text{Pf}'[\Psi]$	$\text{Pf}'[\Psi]$

**Table 1.** Tree-level CHY integrands for BS, YM, YMS, EYM and GR. In the single-trace case,  $m = 1$  and the YMS (EYM) half integrand  $I_{\text{L}}^{\text{tree}}$  turns into a single PT factor  $\text{PT}(\boldsymbol{\sigma}_1)$  associated with a Pfaffian  $\text{Pf}[\Psi]_{\mathbf{G};\mathbf{G}} = \text{Pf}[\Psi_{\mathbf{G}}]$  ( $\text{Pf}[\Psi]_{\mathbf{H};\mathbf{H}} = \text{Pf}[\Psi_{\mathbf{H}}]$ ).

The integration measure in the above is given by

$$d\mu_n^{\text{tree}} = \frac{dz_1 \dots dz_n}{\text{vol SL}(2, \mathbb{C})} \prod_{i=1}^{n'} \delta \left( \sum_{j=1, j \neq i}^n \frac{s_{ij}}{z_{ij}} \right), \quad z_{ij} \equiv z_i - z_j, \quad (2.2)$$

where  $s_{ij} \equiv (k_i + k_j)^2 = 2k_i \cdot k_j$  ( $k_i, k_j$  are the momenta of the massless particles  $i$  and  $j$ ). The  $\prod_{i=1}^{n'}$  is defined as

$$\prod_{i=1}^{n'} \delta \left( \sum_{j=1, j \neq i}^n \frac{s_{ij}}{z_{ij}} \right) = \prod_{i \neq a, b, c} z_{ab} z_{bc} z_{ca} \delta \left( \sum_{j=1, j \neq i}^n \frac{s_{ij}}{z_{ij}} \right), \quad (2.3)$$

where  $a, b$  and  $c$  are three arbitrarily chosen particles. The delta functions imposes the scattering equation constraints on the scattering variables

$$\sum_{j=1, j \neq i}^n \frac{s_{ij}}{z_{ij}} = 0. \quad (2.4)$$

External information including the polarization vectors and momenta, is involved in the half integrands  $I_{\text{L}}^{\text{tree}}$  and  $I_{\text{R}}^{\text{tree}}$ , which rely on theory. For BS, YM, YMS, EYM and GR, the half integrands are presented in table 1, where the Parke-Taylor factor  $\text{PT}(\boldsymbol{\sigma})$  ( $\boldsymbol{\sigma} \equiv (\sigma_1 \dots \sigma_n)$  is a permutation of external particles) is defined as follows

$$\text{PT}(\boldsymbol{\sigma}) \equiv \frac{1}{z_{\sigma_1 \sigma_2} z_{\sigma_2 \sigma_3} \dots z_{\sigma_{n-1} \sigma_n} z_{\sigma_n \sigma_1}}. \quad (2.5)$$

The reduced Pfaffian  $\text{Pf}'[\Psi]$  is given by

$$\text{Pf}'[\Psi] \equiv \frac{(-1)^{i+j}}{z_{ij}} \text{Pf} \left[ \Psi_{ij}^{ij} \right], \quad (2.6)$$

Theories	BS	YM	YMS	EYM	GR
Amplitudes	$A_{\text{BS}}^{1\text{-loop}}(\boldsymbol{\sigma} \boldsymbol{\rho})$	$A_{\text{YM}}^{1\text{-loop}}(\boldsymbol{\sigma})$	$A_{\text{YMS}}^{1\text{-loop}}(\boldsymbol{\sigma}_1; \dots; \boldsymbol{\sigma}_m    \mathbf{G}   \boldsymbol{\rho}_{\text{SUG}})$	$A_{\text{EYM}}^{1\text{-loop}}(\boldsymbol{\sigma}_1; \dots; \boldsymbol{\sigma}_m    \mathbf{H})$	$M_{\text{GR}}^{1\text{-loop}}(1, \dots, n)$
$I_L^{1\text{-loop}}$	PT(+, $\boldsymbol{\sigma}$ , -) +cyc( $\boldsymbol{\sigma}$ )	PT(+, $\boldsymbol{\sigma}$ , -) +cyc( $\boldsymbol{\sigma}$ )	PT(+, $\boldsymbol{\sigma}_1$ , -)... PT( $\boldsymbol{\sigma}_m$ ) $\mathcal{P}$ + cyc( $\boldsymbol{\sigma}_1$ )	PT(+, $\boldsymbol{\sigma}_1$ , -)... PT( $\boldsymbol{\sigma}_m$ ) $\mathcal{P}$ + cyc( $\boldsymbol{\sigma}_1$ )	Pf' [ $\Psi_{n+2}$ ]
$I_R^{1\text{-loop}}$	PT(+, $\boldsymbol{\rho}$ , -) +cyc( $\boldsymbol{\rho}$ )	Pf' [ $\Psi_{n+2}$ ]	PT(+, $\boldsymbol{\rho}_{\text{SUG}}$ , -) +cyc( $\boldsymbol{\rho}_{\text{SUG}}$ )	Pf' [ $\Psi_{n+2}$ ]	Pf' [ $\Psi_{n+2}$ ]

**Table 2.** One-loop level CHY integrands for BS, YM, YMS, EYM and GR. Here, we only provide the YMS and EYM half-integrands that result in pure scalar loop and pure gluon loop, respectively.

where  $\Psi$  is a  $2n \times 2n$  antisymmetric matrix

$$\Psi = \begin{pmatrix} A & -C^T \\ C & B \end{pmatrix},$$

where  $\Psi_{ij}^{ij}$  means the  $i$ -,  $j$ -th rows and columns are deleted,  $A$ ,  $B$  and  $C$  are  $n \times n$  matrices which contain the external kinematic data

$$A_{ab} = \begin{cases} \frac{k_a \cdot k_b}{z_{ab}}, & a \neq b \\ 0, & a = b \end{cases}, \quad B_{ab} = \begin{cases} \frac{\epsilon_a \cdot \epsilon_b}{z_{ab}}, & a \neq b \\ 0, & a = b \end{cases}, \quad C_{ab} = \begin{cases} \frac{\epsilon_a \cdot k_b}{z_{ab}}, & a \neq b \\ -\sum_{c \neq a} \frac{\epsilon_a \cdot k_c}{z_{ac}}, & a = b \end{cases}. \quad (2.7)$$

The  $\mathcal{P}$ , which exists in the  $I_L$  for EYM amplitudes, in table 1 is given by

$$\mathcal{P} \equiv \sum_{\substack{a_1 < b_1 \in \mathbf{1} \\ \dots \\ a_{m-1} < b_{m-1} \in \mathbf{m-1}}} \text{sgn}(\{a, b\}) z_{a_1 b_1} \dots z_{a_{m-1} b_{m-1}} \text{Pf}[\Psi]_{\mathbf{H}, a_1, b_1, \dots, a_{m-1}, b_{m-1}; \mathbf{H}}, \quad (2.8)$$

where  $\text{Pf}[\Psi]_{\mathbf{H}, a_1, b_1, \dots, a_{m-1}, b_{m-1}; \mathbf{H}}$  stands for the Pfaffian of a matrix which is obtained from  $\Psi$  in the following way: Keep the rows and columns with respect to (i). elements in the graviton set  $\mathbf{H}$  and  $a_i, b_i$  ( $i = 1, \dots, m-1$ ) pairs for gluon traces, among the first  $n$  rows and columns, (ii). elements in  $\mathbf{H}$ , among the second  $n$  rows and columns. The  $\mathcal{P}$  for YMS has the same expression (2.8) but replacing gluons and the graviton set  $\mathbf{H}$  by scalars and the gluon set  $\mathbf{G}$ , respectively.

## 2.2 One-loop CHY formula from forward limit

The CHY formula for one-loop  $n$ -point amplitudes is obtained from the forward limit of the CHY formula for tree-level  $(n+2)$ -point amplitudes

$$M_n^{1\text{-loop}} = \int \frac{d^D l}{l^2} \lim_{k_{\pm} \rightarrow \pm l} \int d\mu_{n+2}^{\text{tree}} I_L^{1\text{-loop}} I_R^{1\text{-loop}}, \quad (2.9)$$

where  $l^\mu$  denotes the loop momentum in  $D$  dimensions. The above integral is performed under the constraint of the one-loop scattering equations

$$\frac{l \cdot k_i}{z_i} + \sum_{\substack{j=1 \\ j \neq i}} \frac{k_i \cdot k_j}{z_{ij}} = 0, \quad (2.10)$$

in which,  $k_i^\mu$  ( $i = 1, \dots, n$ ) refer to the external momenta. The half integrands  $I_L^{1\text{-loop}}$  and  $I_R^{1\text{-loop}}$  displayed explicitly by table 2, are functions of loop momentum and external data, and are obtained from the forward limits of the  $(n+2)$ -point tree-level half integrands in table 1. A PT factor  $\text{PT}(+, \boldsymbol{\sigma}, -)$  in table 2 is defined by the  $(n+2)$ -point PT factor when  $+$  and  $-$  (which are introduced by forward limit) are considered as the first and the last elements, respectively. The  $\text{cyc}(\boldsymbol{\sigma})$  in table 2 for a given permutation  $\boldsymbol{\sigma}$  stands for all cyclic permutations of  $\boldsymbol{\sigma}$ . As shown in [24, 33], once the half integrands at one-loop level are expanded in terms of PT factors, the full integrand is then expanded as a combination of  $(n+2)$ -point tree-level BS amplitudes with the forward limit  $k_\pm^\mu \rightarrow \pm l^\mu$ . In addition, the polarizations  $\epsilon_-^\mu$  and  $\epsilon_+^\nu$  in the reduced Pfaffian should be replaced according to the following rule

$$\sum_{+,-} \epsilon_-^\mu \epsilon_+^\nu = \Delta^{\mu\nu}, \quad \eta_{\mu\nu} \Delta^{\mu\nu} = D - 2, \quad V_\mu W_\nu \Delta^{\mu\nu} = V \cdot W, \quad (2.11)$$

where  $V^\mu$  and  $W^\nu$  are two vectors.

In the next subsection, we introduce the refined graphic rule for expanding the half integrands, which comes from the expansion formula of tree-level amplitudes.

### 2.3 Expanding the half integrands by refined graphic rule

The expansion formula of the tree-level CHY half integrands totally inherits the expansion of tree amplitudes which was proposed in [7, 8], while the half integrands for  $n$ -point amplitude at one-loop level are obtained from the forward limit of the corresponding  $(n+2)$ -point tree-level half integrands. In the following, we present the refined graphic rules for expanding the  $\text{PT}(+, \boldsymbol{\sigma}, -) \text{Pf}[\Psi_G]$  for single-trace YMS (and EYM), the  $\text{PT}(+, \boldsymbol{\sigma}_1, -) \text{PT}(\boldsymbol{\sigma}_2) \dots \text{PT}(\boldsymbol{\sigma}_m) \mathcal{P}$  for multi-trace YMS (and EYM), and the  $\text{Pf}'[\Psi]$  for YM, EYM and GR. We do not consider the integrands where the forward limit is taken for particles  $+$ ,  $-$  belonging to distinct PT factors, in the current paper.

#### 2.3.1 Expansion of $\text{PT}(+, \boldsymbol{\sigma}, -) \text{Pf}[\Psi_G]$

The  $\text{PT}(+, \boldsymbol{\sigma}, -) \text{Pf}[\Psi_G]$  can be expanded in terms of PT factors in Kleiss-Kuijff (KK) basis [39], where  $+$  and  $-$  play as the first and the last elements, respectively

$$\text{PT}(+, \boldsymbol{\sigma}, -) \text{Pf}[\Psi_G] = \sum_{\mathcal{F}} c^{\mathcal{F}} \left[ \sum_{\boldsymbol{\rho}^{\mathcal{F}}} \text{PT}(+, \boldsymbol{\rho}^{\mathcal{F}}, -) \right]. \quad (2.12)$$

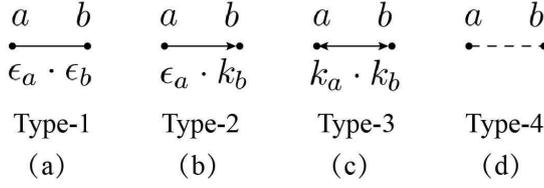


**Figure 1.** Line styles in the refined graphic rule

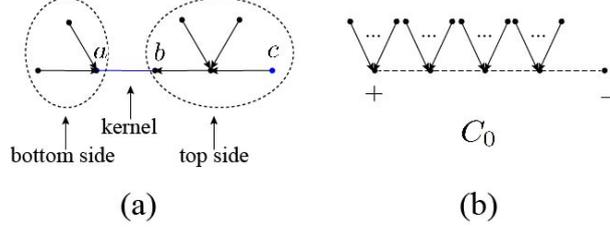


**Figure 2.** Graphs (a) and (b) are typical components in single-trace case. In (a), the kernel is the type-1 line between  $a$  and  $b$ , while the side containing the highest-weight node in this component, say  $c$ , is defined as the top side. The opposite side is the bottom side. Graph (b) is the component  $C_0$  containing scalar trace.

In the above, we have summed over all possible graphs  $\mathcal{F}$  which are generated by considering all external particles as nodes, the Lorentz contractions  $\epsilon_a \cdot \epsilon_b$ ,  $\epsilon_a \cdot k_b$  and  $k_a \cdot k_b$  as lines between nodes (as shown by Fig. 1, the type-4 line with no kinematic factor is introduced for recording the relative order between two nodes), and the set  $\{+, \sigma_1, \dots, \sigma_r\}$  as the root set. Each graph  $\mathcal{F}$  is associated with a kinematic coefficient  $\mathcal{C}^{\mathcal{F}}$  and a set of permutations  $\rho^{\mathcal{F}}$  (where the relative ordering of scalars is  $\sigma$ ). The second summation means that we should sum over all permutations  $\rho^{\mathcal{F}}$ . Now we demonstrate *refined graphic rule* for constructing  $\mathcal{F}$ :

**Step-1** Define a reference order  $\mathbf{R} = \{\gamma_1, \dots, \gamma_s\}$ . Here,  $\gamma$  is a permutation of all  $s$  elements in the set  $\mathbf{G}$ . We define the position of an element of  $\mathbf{G}$  in  $\mathbf{R}$  as its *weight*.

**Step-2** Graphs  $\mathcal{F}$  can be classified according to the number of type-1 lines (which are mentioned as *the kernels*). A graph with  $k$  ( $0 \leq k \leq \lfloor \frac{s}{2} \rfloor$ ) type-1 lines, is constructed by the following steps:

- (i). Pick out  $k$  pairs of elements arbitrarily from the set  $\mathbf{G}$ , and construct  $k$  type-1 lines (kernels) between each pair of nodes. Connect the nodes in the ordered set  $\{+, \sigma, -\}$  (i.e. the trace) by type-4 lines in accordance to the relative order.
- (ii). Connect other elements in  $\mathbf{G}$  towards either the elements in the set  $\{+, \sigma\}$  or the  $2k$  end nodes of the  $k$  kernels which already have been used in the previous step, via type-2 lines. Now we have  $k + 1$  mutually disconnected *components*  $\{C_0, C_1, C_2, \dots, C_k\}$  (structure of components are shown by Fig. 2), where the  $C_0$  refers to the one involving the trace.

**Step-3** Now we connect the components  $C_0, C_1, C_2, \dots, C_k$  together via type-3 lines into a fully connected graph  $\mathcal{F}$  as follows:

- (i). Define the *weight of a component*  $C_i$  (for  $i \neq 0$ ) by the weight of its highest-weight node, and then we arrange the components in the reference order  $R_C = \{C_{\beta_1}, \dots, C_{\beta_k}\}$  as the increasing order of their weights. According to the definition, a component  $C_i$  ( $i \neq 0$ ) is always divided into two parts by the type-1 line. We further define the part which involves the highest-weight node of  $C_i$  as the top side  $C_i^t$ , while the opposite side as the bottom side,  $C_i^b$ . A component  $C_i$  is sometimes presented by the symbol  $C_i = [C_i^b] - [C_i^t]$ , in which a “ $-$ ” is used to denote the type-1 line.
- (ii). Define the root set  $\mathcal{R}_C \equiv C_0$  (Here, the node  $-$  is always excluded from the root set). Construct a *chain of components* (COC) via type-3 lines

$$[C_a^t] - [C_a^b] \leftrightarrow [C_{l_1}^{t(b)}] - [C_{l_1}^{b(t)}] \leftrightarrow [C_{l_2}^{t(b)}] - [C_{l_2}^{b(t)}] \leftrightarrow \dots \leftrightarrow [C_{l_j}^{t(b)}] - [C_{l_j}^{b(t)}] \leftrightarrow C_0. \quad (2.13)$$

which starts from the top side of the highest-weight component  $C_a = C_{\beta_k}$ , passes through some other components  $C_{l_1}, C_{l_2}, \dots, C_{l_j}$  and ends up at  $\mathcal{R}_C$ . In the above expression, the notation “ $\leftrightarrow$ ” denotes a type-3 line. The superscripts in an internal component  $[C_{l_i}^{t(b)}] - [C_{l_i}^{b(t)}]$  mean that once the left side is chosen as the top (bottom) one, the right side is always chosen as the bottom (top) side.

- (iii). Redefine the ordered set  $R_C$  and the root set  $\mathcal{R}_C$  by

$$R_C \rightarrow R_C \setminus \{C_a, C_{l_1}, \dots, C_{l_j}\}, \quad \mathcal{R}_C = C_0 \cup C_a \cup C_{l_1} \cup \dots \cup C_{l_j}. \quad (2.14)$$

Repeat step (ii) until the ordered set  $R_C$  becomes empty, then we get a fully connected refined graph  $\mathcal{F}$  with  $k$  type-1 lines.

**Kinematic coefficients  $\mathcal{C}^{\mathcal{F}}$  and permutations  $\rho^{\mathcal{F}}$**  To each graph  $\mathcal{F}$  constructed by the above steps, we associate a kinematic factor  $\mathcal{C}^{\mathcal{F}}$  which is given by the product of the Lorentz contractions implied by the lines. An extra minus is introduced if there is an arrow pointing away from the direction of roots. Concretely, each type-3 line produces a minus sign, as does each type-2 line pointing away from the root. The possible permutations established by the graph  $\mathcal{F}$  are defined as follows: (i). The first and the last elements in the permutations are always  $+$  and  $-$ . (ii). If two nodes  $a$  and  $b$  live on a same path towards  $+$ , and the node  $a$  is nearer to  $+$  than  $b$ , we have  $a \prec b$  in  $\rho^{\mathcal{F}}$  (the notation  $a \prec b$  means  $a$  appears to the left of  $b$  for a given permutation). (iii). If there are two branches attached to a node, we should shuffle the relative orders corresponding to the two branches together. For example, if we have two branches attached to node  $a$ , one of them contains nodes  $b, c$  in turn, the other has a single node  $d$ , the relative orders between these nodes in  $\rho^{\mathcal{F}}$  are

$$\{a, \{\{b, c\} \sqcup \{d\}\}\} \rightarrow \{a, b, c, d\}, \{a, b, d, c\}, \{a, d, b, c\}. \quad (2.15)$$

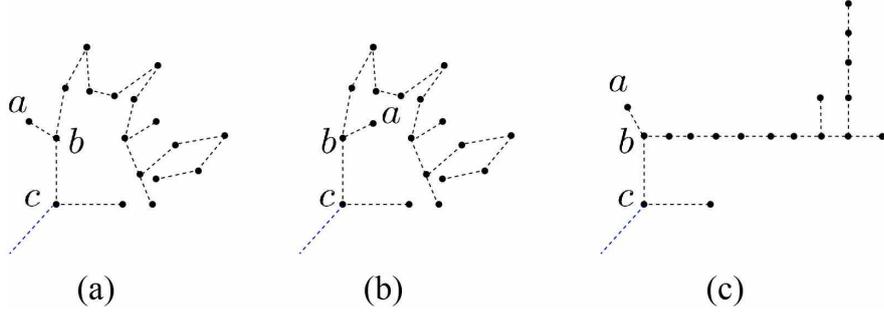


**Figure 3.** The permutations established by a connected tree graph only depend on the topology of a graph and the choice of the nearest-to-root node. Graphs (a), (b) and (c) have the same structure. Once the node  $c$  is chosen as the nearest-to-root one, these graphs correspond to the same set of permutations. Here we should note that two graphs are the same when they are related by exchanging two tree structures attached to a same node. Although, the lines used in these graphs are type-4 ones, those graphs with other line styles but the same topology with (a), (b) and (c) establish the same set of permutations.

Finally, we sum over all possible graphs  $\mathcal{F}$ , which include all possible graphs with  $k$  type-1 lines for  $k = 1, \dots, \lfloor \frac{s}{2} \rfloor$ , then arrive at the expansion of  $\text{PT}(+, \boldsymbol{\sigma}, -) \text{Pf}[\Psi_{\mathbf{G}}]$ . It is clear that the permutations corresponding to the graphs established by the refined graphic rule, which have the same chosen nearest-to-root node, are related only to the topology of the graphs, as shown by Fig. 3. This graphic rule has an equivalent version which is expressed by strength tensors, see appendix A.

### 2.3.2 Expansion of $\text{Pf}'[\Psi_{n+2}]$

As pointed in [12, 16], the reduced Pfaffian  $\text{Pf}'[\Psi_{n+2}]$  (which includes the  $n$  external particles and  $+, -$ ) can be decomposed in terms of  $\text{PT}(+, \dots, -) \text{Pf}[\Psi]$  with less elements in the Pfaffian and more elements in the PT factor. Specifically,

$$\begin{aligned}
\text{Pf}'[\Psi_{n+2}] &= (\epsilon_+ \cdot \epsilon_-) \text{PT}(+, -) \text{Pf}[\Psi_{\{1, \dots, n\}}] \\
&\quad - \sum_i (\epsilon_+ \cdot F_i \cdot \epsilon_-) \text{PT}(+, i, -) \text{Pf}[\Psi_{\{1, \dots, n\} \setminus i}] \\
&\quad + \sum_{\{i_1, i_2\} \in \mathcal{S}_2} (\epsilon_+ \cdot F_{i_1} \cdot F_{i_2} \cdot \epsilon_-) \text{PT}(+, i_1, i_2, -) \text{Pf}[\Psi_{\{1, \dots, n\} \setminus \{i_1, i_2\}}] \\
&\quad - \dots \\
&\quad + (-1)^n \sum_{\{i_1, i_2, \dots, i_n\} \in \mathcal{S}_n} (\epsilon_+ \cdot F_{i_1} \cdot F_{i_2} \cdot \dots \cdot F_{i_n} \cdot \epsilon_-) \text{PT}(+, i_1, i_2, \dots, i_n, -). \tag{2.16}
\end{aligned}$$

where in each summation  $\sum_{\{i_1, i_2, \dots, i_k\} \in \mathcal{S}_k}$ , we have summed over all possible permutations of  $k$  elements  $i_1, i_2, \dots, i_k$  for all possible choices of  $i_1, i_2, \dots, i_k \in \{1, \dots, n\}$ . The  $F_i^{\mu\nu}$  is the strength tensor that is defined by  $k_i^\mu \epsilon_i^\nu - \epsilon_i^\mu k_i^\nu$ . When the rule (2.11) for forward limit is taken into account, the above expansion turns

into

$$\begin{aligned}
\text{Pf}'[\Psi_{n+2}] &= (D-2) \text{PT}(+, -) \text{Pf} [\Psi_{\{1, \dots, n\}}] \\
&+ \sum_{\{i_1, i_2\} \in \mathcal{S}_2 \setminus \mathcal{Z}_2} \text{Tr}[F_{i_1} \cdot F_{i_2}] \left[ \text{PT}(+, i_1, i_2, -) + \text{cyc}(i_1, i_2) \right] \text{Pf} [\Psi_{\{1, \dots, n\} \setminus \{i_1, i_2\}}] \\
&- \dots \\
&+ (-1)^n \sum_{\{i_1, i_2, \dots, i_n\} \in \mathcal{S}_n \setminus \mathcal{Z}_n} \text{Tr}[F_{i_1} \cdot F_{i_2} \cdot \dots \cdot F_{i_n}] \left[ \text{PT}(+, i_1, i_2, \dots, i_n, -) + \text{cyc}(i_1, i_2, \dots, i_n) \right],
\end{aligned} \tag{2.17}$$

where each  $\text{Tr}[F_{i_1} \cdot F_{i_2} \cdot \dots \cdot F_{i_l}]$  is defined by

$$\text{Tr}[F_{i_1} \cdot F_{i_2} \cdot \dots \cdot F_{i_l}] \equiv (F_{i_1})^{\mu_1}_{\mu_2} (F_{i_2})^{\mu_2}_{\mu_3} \dots (F_{i_l})^{\mu_l}_{\mu_1}, \tag{2.18}$$

which has cyclic symmetry with respect to  $i_1, i_2, \dots, i_l$ , and  $\text{Tr}[F_i] = 0$  due to the antisymmetry of the strength tensor  $F_i^{\mu\nu}$ . The property (2.17) will be applied to obtain the quadratic propagator form of YM integrand.

## 2.4 Tensorial PT factors and the problem of quadratic propagators

In the previous section, we have already expanded CHY half integrands in terms of the tree-level PT factors of the form  $\text{PT}(+, \dots, -)$ , thus any one-loop integrand is expressed by a combination of

$$\frac{1}{l^2} \int d\mu_{n+2}^{\text{tree}} \text{PT}(+, \boldsymbol{\sigma}, -) \text{PT}(+, \boldsymbol{\rho}, -), \tag{2.19}$$

where  $\boldsymbol{\sigma}$  and  $\boldsymbol{\rho}$  are two permutations of  $n$  external particles. The above expression, except for the factor  $\frac{1}{l^2}$ , is nothing but a tree-level  $(n+2)$ -point BS amplitude, in which  $+$  and  $-$  are fixed as the two ends. Thus such a term can be rewritten as [24]

$$\frac{1}{l^2} \int d\mu_{n+2}^{\text{tree}} \text{PT}(+, \boldsymbol{\sigma}, -) \text{PT}(+, \boldsymbol{\rho}, -) = \sum_{\substack{(A_1 A_2 \dots A_i) = \boldsymbol{\sigma} \\ (\tilde{A}_1 \tilde{A}_2 \dots \tilde{A}_i) = \boldsymbol{\rho} \\ A_j = \tilde{A}_j}} \frac{1}{l^2} \frac{1}{s_{A_1, l}} \frac{1}{s_{A_1 A_2, l}} \dots \frac{1}{s_{A_1 A_2 \dots A_{i-1}, l}} \phi_{A_1 | \tilde{A}_1} \phi_{A_2 | \tilde{A}_2} \dots \phi_{A_i | \tilde{A}_i}. \tag{2.20}$$

Here, the summation over  $(A_1 A_2 \dots A_i) = \boldsymbol{\sigma}$  and  $(\tilde{A}_1 \tilde{A}_2 \dots \tilde{A}_i) = \boldsymbol{\rho}$  means we sum over all divisions of  $\boldsymbol{\sigma}$  and  $\boldsymbol{\rho}$  including the case  $i = 1$ . The  $\phi_{A_i | \tilde{A}_i}$  is the BG current of BS theory (which will be introduced later). The  $\frac{1}{s_{A_1 \dots A_j, l}}$  is defined by

$$\frac{1}{s_{A_1 \dots A_j, l}} = \frac{1}{2l \cdot (k_{A_1} + \dots + k_{A_j}) + (k_{A_1} + \dots + k_{A_j})^2}. \tag{2.21}$$

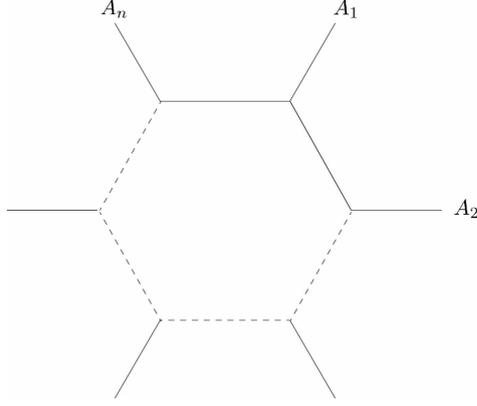


**Figure 4.** An  $n$ -gon diagram with  $n$  subtrees which represent the BG currents  $\phi_{A_i|\widetilde{A}_i}$  ( $i = 1, \dots, n$ ).

Being different from the propagators in traditional Feynman diagrams whose denominator is a quadratic function of  $l^\mu$ , the denominator of the above propagator is a linear function, thus is called *linear propagator*.

In [24], tensorial PT factors  $\text{PT}_t^{\mu_1\mu_2\dots\mu_r}(1, 2, \dots, n)$  were introduced

$$\text{PT}_t^{\mu_1\mu_2\dots\mu_r}(1, 2, \dots, n) \equiv \sum_{i=1}^n \text{PT}(+, i, i+1, \dots, 1, 2, \dots, i-1, -) \prod_{j=1}^r (l^{\mu_j} - k_{1,2,\dots,i-1}^{\mu_j}). \quad (2.22)$$

The subscript “t” of  $\text{PT}_t^{\mu_1\mu_2\dots\mu_r}(1, 2, \dots, n)$  is used to distinguish tensorial PT factors from those PT factors we have used before. When there is no Lorentz index, the tensorial PT factor turns into a sum over cyclic permutations of  $1, \dots, n$  and is called a scalar PT factor

$$\text{PT}_t(1, 2, \dots, n) \equiv \sum_{i=1}^n \text{PT}(+, i, i+1, \dots, i-1, -). \quad (2.23)$$

The product of a scalar PT factor (2.23) and a general tensorial PT factor (2.22) produces quadratic propagators when the integral over scattering variables are performed

$$\begin{aligned} & \frac{1}{l^2} \int d\mu_{n+2}^{\text{tree}} \text{PT}_t^{\mu_1\mu_2\dots\mu_r}(1, \boldsymbol{\rho}(2, \dots, n)) \text{PT}_t(1, \boldsymbol{\sigma}(2, \dots, n)) \\ & \cong \sum_{\substack{(A_1 A_2 \dots A_m) = (1 \boldsymbol{\rho}) \\ (\widetilde{A}_1 \widetilde{A}_2 \dots \widetilde{A}_m) = (1 \boldsymbol{\sigma}) \\ A_j = \widetilde{A}_j \\ 2 \leq m \leq n}} (l + k_A)^{\mu_1} \dots (l + k_A)^{\mu_r} \text{gon}(A_1, A_2, \dots, A_m) \prod_{i=1}^m \phi_{A_i|\widetilde{A}_i}. \end{aligned} \quad (2.24)$$

The  $\cong$  means that the LHS gives the same result with the RHS when the integral over loop momentum  $l^\mu$  is taken. In the above expression,  $(A_1 A_2 \dots A_m)$  and  $(\widetilde{A}_1 \widetilde{A}_2 \dots \widetilde{A}_m)$  are the cyclic partitions of color orderings  $(1 \boldsymbol{\rho})$  and  $(1 \boldsymbol{\sigma})$ , where  $A_1 = A_1 \widetilde{A}$ ,  $A$  and  $\widetilde{A}$  denote the ordered sets of elements in  $A_1$  on the LHS of 1 and

on the RHS of 1, respectively. The  $A_j = \widetilde{A}_j$  implies that  $A_j$  and  $\widetilde{A}_j$  have the same elements but may not be in the same order. The  $m$ -gon,  $gon(A_1, A_2, \dots, A_m)$ , is defined by

$$gon(A_1, A_2, \dots, A_m) \equiv \frac{1}{l^2 l_{A_1}^2 l_{A_{12}}^2 \dots l_{A_{12\dots m-1}}^2}, \quad (2.25)$$

where  $l_{A_{12\dots m-1}}^\mu = l_{A_1 A_2 \dots A_{m-1}}^\mu = l^\mu + k_{A_1}^\mu + k_{A_2}^\mu + \dots + k_{A_{m-1}}^\mu$ ,  $k_A^\mu$  and  $k_{\widetilde{A}}^\mu$  denote the sum of the momenta of the elements in the ordered sets  $A$  and  $\widetilde{A}$ , respectively. The  $\phi_{A_i|\widetilde{A}_i}$  is the BS current which represents the subtree planted on the  $i$ -th corner of the  $m$ -gon, as shown by Fig. 4. The case  $m = 1$  is excluded from the summation since it corresponds to tadpole diagrams which contain a combination of BS currents

$$\phi_{A|\widetilde{A}} + \text{cyclic permutations of } \widetilde{A} \quad (2.26)$$

vanishing due to a U(1)-decoupling identity. There is a crucial relation we used to obtain eq. (2.24)

$$\begin{aligned} & \frac{N(l)}{l^2 s_{A_1, l} s_{A_{12}, l} \dots s_{A_{12\dots m-1}, l}} + \frac{N(l + k_{A_m})}{l^2 s_{A_m, l} s_{A_{m1}, l} \dots s_{A_{m1\dots m-2}, l}} + \dots + \frac{N(l + k_{A_{23\dots m}})}{l^2 s_{A_2, l} s_{A_{23}, l} \dots s_{A_{23\dots m}, l}} \\ & \cong N(l) gon(A_1, A_2, \dots, A_m) \end{aligned} \quad (2.27)$$

where  $N(l)$  is an  $l$ -dependent numerator and the partial fraction identity have been applied.

When the scalar PT factor in eq. (2.24), is replaced by another copy of tensorial PT factor, one arrives a more general result

$$\begin{aligned} & \frac{1}{l^2} \int d\mu_{n+2}^{\text{tree}} \text{PT}_t^{\mu_1 \mu_2 \dots \mu_r} (1, \boldsymbol{\rho} (2, \dots, n)) \text{PT}_t^{\nu_1 \nu_2 \dots \nu_t} (1, \boldsymbol{\sigma} (2, \dots, n)) \\ & \cong l^{\mu_1} \dots l^{\mu_r} \sum_{\substack{(A_1 A_2 \dots A_m) = (1 \boldsymbol{\rho}) \\ (\widetilde{A}_1 \widetilde{A}_2 \dots \widetilde{A}_m) = (1 \boldsymbol{\sigma}) \\ A_j = \widetilde{A}_j \\ 2 \leq m \leq n}} (l - \Delta_{A\widetilde{A}})^{\nu_1} \dots (l - \Delta_{A\widetilde{A}})^{\nu_t} gon^A(A_1, A_2, \dots, A_m) \prod_{i=1}^m \phi_{A_i|\widetilde{A}_i}. \end{aligned} \quad (2.28)$$

The  $\Delta^\mu$  is defined by  $\Delta_{A\widetilde{A}}^\mu \equiv k_A^\mu - k_{\widetilde{A}}^\mu$ , tadpole terms have been removed by hand. The  $gon^A(A_1, A_2, \dots, A_m) \equiv gon(A_1, A_2, \dots, A_m)|_{l^\mu \rightarrow l^\mu - k_A^\mu}$ . Eq. (2.28) also produces quadratic propagators.

We will see later that in some special cases, a CHY integrand can be arranged into a proper format such that it can be decomposed into combinations of (2.24) (as a special case of (2.28)) and thus naturally reproduce quadratic propagators. However, a more general integrand in table 2 may not be directly decomposed into (2.28). In this work, we show that the quadratic propagators arise when the CHY half integrands are decomposed according to the refined graphic rule which has been reviewed in the previous subsection.

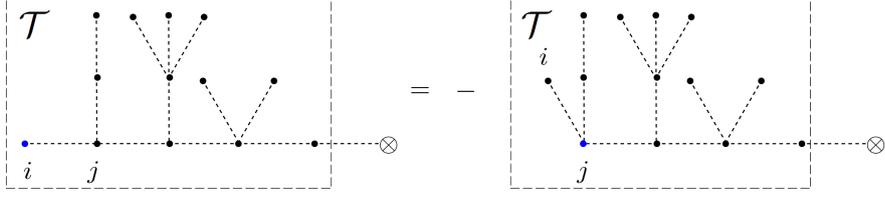


**Figure 5.** A typical graph demonstrating the graph-based identity (2.31) for the BG currents of BS. The cross node  $\otimes$  in each graph is introduced to remind that there exists an off-shell line of the BG current. Assuming  $i, j$  are two adjacent nodes in a connected tree graph  $\mathcal{T}$ , the combination of BS currents with respect to permutations when  $i$  is considered as the leftmost element is the minus of the combination when  $j$  is considered as the leftmost one. Although there are only type-4 lines in the two graphs, we can replace the type-4 lines by any other type of lines and provide the corresponding factors.

## 2.5 Properties of the BG currents in BS theory

In this subsection, we review the definition of the BG [40] currents in BS theory and provide helpful properties of the BG currents.

The tree-level BG current  $\phi_{A|\tilde{A}}$  is recursively defined by [41]

$$\phi_{A|\tilde{A}} = \frac{1}{s_A} \sum_{\substack{A=A_L A_R \\ \tilde{A}=\tilde{A}_L \tilde{A}_R}} \left[ \phi_{A_L|\tilde{A}_L} \phi_{A_R|\tilde{A}_R} - \phi_{A_R|\tilde{A}_L} \phi_{A_L|\tilde{A}_R} \right], \quad (2.29)$$

where  $s_A \equiv k_A^2$  and we have summed over divisions  $A = A_L A_R$ ,  $\tilde{A} = \tilde{A}_L \tilde{A}_R$ . The starting point of this recursion is  $\phi_{a|a} = 1$ ,  $\phi_{a|b} = 0$  ( $a \neq b$ ). If the elements in  $A$  and  $\tilde{A}$  in  $\phi_{A|\tilde{A}}$  are not identical to each other, the current must vanish. The BS current is apparently symmetric under  $A \Leftrightarrow \tilde{A}$  and satisfies the generalized  $U(1)$ -decoupling identity [42]

$$\phi_{A \sqcup B | \tilde{C}} = 0, \quad (2.30)$$

where  $\tilde{C}$  is an arbitrary permutation of elements in  $A \cup B$ , and the summation over all shuffle permutations of  $A$  and  $B$  is implied. Furthermore, as pointed in [37], the BG current (2.29) satisfies relations characterized by graphs. The first graph-based relation is

$$\sum_{\sigma \in \rho^{\mathcal{T}}|_i} \phi_{\sigma|\tilde{A}} = - \sum_{\gamma \in \rho^{\mathcal{T}}|_j} \phi_{\gamma|\tilde{A}}, \quad (2.31)$$

where  $\rho^{\mathcal{T}}|_i$  denotes permutations established by the connected tree graph  $\mathcal{T}$ , with the leftmost element  $i$ . The node  $j$  on the RHS is a node adjacent to  $i$ . The above relation is shown by Fig. 5.

A kind of relation satisfied by the BG currents with more complicated expression is the *off-shell BCJ relation* [37, 38, 42, 43]. These relations have nontrivial kinematic coefficients associating to the BG currents. Each coefficient is a function of  $s_{ij} \equiv 2k_i \cdot k_j$ , where  $k_i^\mu$  and  $k_j^\mu$  are momenta of on-shell external

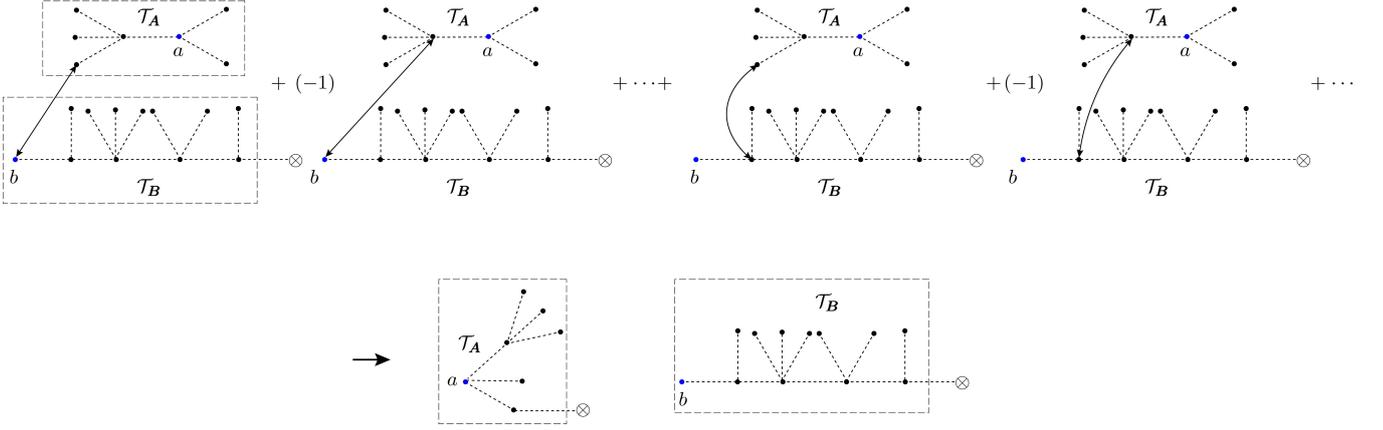


**Figure 6.** Graphs on the first line establish the LHS of the off-shell BCJ relation (2.32). Here, we have two connected tree graphs  $\mathcal{T}_A$  and  $\mathcal{T}_B$ . A graph  $\mathcal{T}_A \oplus \mathcal{T}_B$  is constructed by connecting a pair of nodes in  $\mathcal{T}_A$  and  $\mathcal{T}_B$ , via a type-3 line. The two graphs on the second line define the RHS of off-shell BCJ relation, where  $a$  and  $b$  are chosen as the first elements in the corresponding currents. Similar to Fig. 5, all type-4 lines can be substituted by other types of lines.

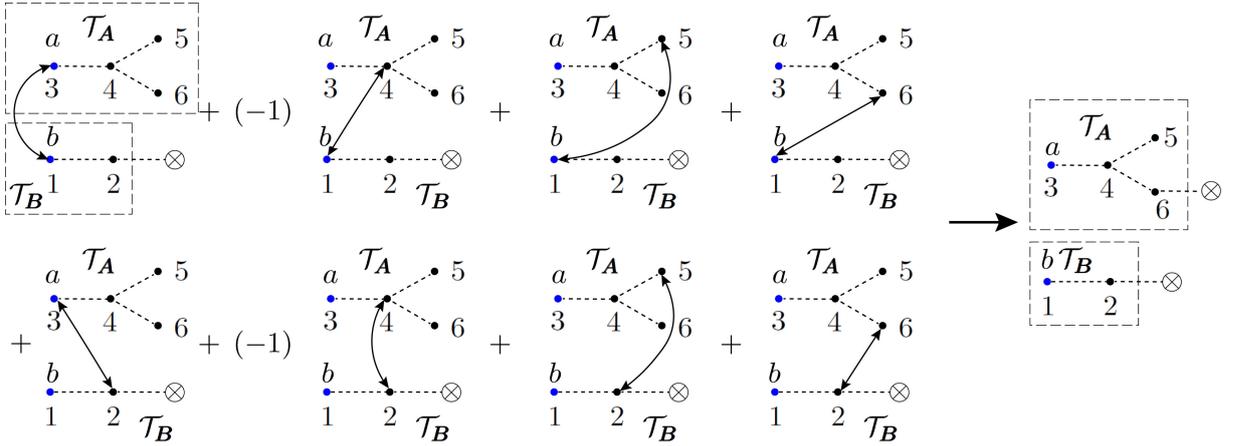


**Figure 7.** An explicit example for the off-shell BCJ relation (2.32), where the two tree graphs  $\mathcal{T}_A$  and  $\mathcal{T}_B$  contain elements 3, 4, 5, 6 and 1, 2, respectively. The nodes  $a \in \mathcal{T}_A$  and  $b \in \mathcal{T}_B$  are chosen as 3 and 1.

particles. The off-shell BCJ relations turn into amplitude relations under the on-shell limit. In [37, 38], the following off-shell BCJ relation based on graphs was proposed

$$\sum_{x \in \mathcal{T}_A, y \in \mathcal{T}_B} (-1)^{|ax|} \sum_{\gamma \in \rho^{(\mathcal{T}_A \oplus \mathcal{T}_B)}|_b} s_{xy} \phi_{\gamma|\sigma} = \sum_{\alpha \in \rho^{\mathcal{T}_A}|_a} \sum_{\beta \in \rho^{\mathcal{T}_B}|_b} [\phi_{\beta|\sigma_{1,i}} \phi_{\alpha|\sigma_{i+1,l}} - \phi_{\alpha|\sigma_{1,l-i}} \phi_{\beta|\sigma_{l-i+1,l}}], \quad (2.32)$$

in which, we have two connected tree graphs  $\mathcal{T}_A$  and  $\mathcal{T}_B$ , as shown by Fig. 6. When connecting two nodes  $x \in \mathcal{T}_A$  and  $y \in \mathcal{T}_B$  by a type-3 line, we get a graph  $\mathcal{T}_A \oplus \mathcal{T}_B$ . The first summation on the LHS means we sum over such graphs  $\mathcal{T}_A \oplus \mathcal{T}_B$  corresponding to all possible choices of  $(x, y)$  pair. The  $a \in \mathcal{T}_A$  and  $b \in \mathcal{T}_B$  are two arbitrarily chosen nodes. Here, the sign  $(-1)^{|ax|}$  depends on the distance  $|ax|$  between

the nodes  $a$  and  $x$ . The second summation is taken over permutations established by the graph  $\mathcal{T}_A \oplus \mathcal{T}_B$ , while  $b$  is considered as the leftmost element. On the RHS,  $\alpha \in \rho^{\mathcal{T}_A}|_a$  and  $\beta \in \rho^{\mathcal{T}_B}|_b$  are the permutations established by  $\mathcal{T}_A$  and  $\mathcal{T}_B$  when  $a$  and  $b$  are considered as the leftmost elements, respectively. Permutation  $\sigma = (\sigma_1 \dots \sigma_l)$  in  $\phi_{\gamma|\sigma}$  on the LHS is divided into two parts  $\sigma_{1,i} = (\sigma_1 \dots \sigma_i)$  and  $\sigma_{i+1,l} = (\sigma_{i+1} \dots \sigma_l)$ , where the number of nodes in  $\mathcal{T}_B$  is assumed to be  $i$  and the number of nodes in  $\mathcal{T}_A \oplus \mathcal{T}_B$  is  $l$ . In the second term on the RHS,  $\sigma$  is divided into  $\sigma_{1,l-i} = (\sigma_1 \dots \sigma_{l-i})$  and  $\sigma_{l-i+1,l} = (\sigma_{l-i+1} \dots \sigma_l)$ . Fig. 7 provides an example of (2.32). Explicitly, this relation is displayed as

$$\begin{aligned}
& s_{13} \phi_{1\{2\}\sqcup\{34\{5\}\sqcup\{6\}\}}|\sigma - s_{14} \phi_{1\{2\}\sqcup\{4\{3\}\sqcup\{5\}\sqcup\{6\}\}}|\sigma + s_{15} \phi_{1\{2\}\sqcup\{54\{3\}\sqcup\{6\}\}}|\sigma + s_{16} \phi_{1\{2\}\sqcup\{64\{3\}\sqcup\{5\}\}}|\sigma \\
& + s_{23} \phi_{1234\{5\}\sqcup\{6\}}|\sigma - s_{24} \phi_{124\{3\}\sqcup\{5\}\sqcup\{6\}}|\sigma + s_{25} \phi_{1254\{3\}\sqcup\{6\}}|\sigma + s_{26} \phi_{1264\{3\}\sqcup\{5\}}|\sigma \\
& = \phi_{12|\sigma_1\sigma_2} \phi_{34\{5\}\sqcup\{6\}}|\sigma_{3\sigma_4\sigma_5\sigma_6} - \phi_{34\{5\}\sqcup\{6\}}|\sigma_1\sigma_2\sigma_3\sigma_4 \phi_{12|\sigma_5\sigma_6},
\end{aligned} \tag{2.33}$$

where the sums over shuffle permutations are implied. We point out that the relation (2.32) is satisfied by off-shell BG currents with nontrivial kinematic coefficients. When we multiply  $k_{123456}^2$  to both sides of the above example and take the on-shell limit  $k_{123456}^2 = 0$ , each BS current on the LHS turns into an on-shell BS amplitude, while the RHS has to vanish. Thus, from this example, we can see the on-shell limit of the off-shell BCJ relation (2.32) gives the corresponding BCJ relation at amplitude level (see [7, 8]).

In the coming sections, (2.29)-(2.32) will be used to extract quadratic propagators from one-loop CHY formula.

### 3 Four-point integrand with two gluons

In this section, we study the single-trace four-point YMS integrands with two external gluons. Inspired by these examples, we find that the crucial point for extracting quadratic propagators is to cancel the nonlocal terms, where two adjacent subgraphs contracted together are separated by linear propagators on the Feynman diagram side. Once this cancellation is achieved, one can always find terms related by cyclic permutations. Therefore, we can extract the quadratic propagators according to eq. (2.27). The examples in this section show two typical approaches to canceling the nonlocalities.

#### 3.1 Four-point integrand with two gluons

As shown by table 2, the CHY half integrands of one-loop single-trace YMS amplitudes with scalar trace  $(x_1 x_2)$  and two gluons  $p, q$  are given by

$$\begin{aligned}
I_L^{1\text{-loop}}(x_1, x_2 || \{p, q\}) &= \text{PT}(+, x_1, x_2, -) \text{Pf}[\Psi_{pq}] + \text{cyc}(x_1 x_2), \\
I_R^{1\text{-loop}}(a_1, a_2, a_3, a_4) &= \text{PT}(+, a_1, a_2, a_3, a_4, -) + \text{cyc}(a_1 a_2 a_3 a_4),
\end{aligned} \tag{3.1}$$

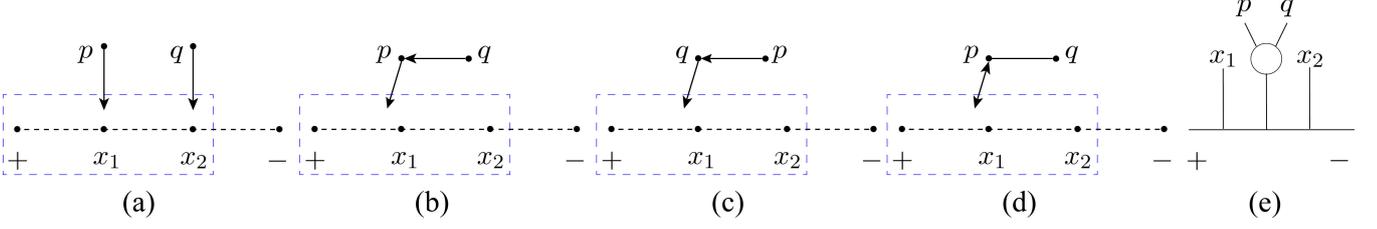


**Figure 8.** All possible graphs for the integrand with two gluons  $p, q$  and two scalars  $x_1, x_2$  are given by (a), (b), (c) and (d). The end node of an arrow inside the boxed region can be any one of  $+, x_1, x_2$ . The reference order is  $p \prec q$  (i.e., the weight of  $p$  is lower than that of  $q$ ). A Feynman diagram with a linear propagator structure  $\frac{1}{s_{x_1,l}} \frac{1}{s_{x_1 p q, l}}$  for the partition  $\{x_1, \{p, q\}, x_2\}$  is given by (e).

where  $(a_1 a_2 a_3 a_4)$  is an arbitrary permutation of  $x_1, x_2, p, q$ . By applying (2.12), the left half integrand in the above expression can further be expanded as

$$I_L^{1\text{-loop}}(x_1, x_2 || \{p, q\}) = \sum_{\mathcal{F}} \mathcal{C}^{\mathcal{F}} \left[ \sum_{\sigma^{\mathcal{F}}} \text{PT}(+, \sigma^{\mathcal{F}}, -) \right] + \text{cyc}(x_1 x_2). \quad (3.2)$$

Here all the graphs  $\mathcal{F}$ , i.e., the graphs Fig. 8 (a), (b), (c) and (d), generated by the refined graphic rule are summed up. The coefficients  $\mathcal{C}^{\mathcal{F}}$  for Fig. 8 (a), (b), (c) and (d) are respectively given by

$$(\epsilon_p \cdot k_i)(\epsilon_q \cdot k_j), \quad (\epsilon_p \cdot k_i)(\epsilon_q \cdot k_p), \quad (\epsilon_q \cdot k_i)(\epsilon_p \cdot k_q), \quad (-k_p \cdot k_i)(\epsilon_p \cdot \epsilon_q), \quad (3.3)$$

where each of  $i$  and  $j$  can be  $x_1, x_2$  or  $+$ . If  $i = x_1, j = x_2$ , permutations  $\sigma^{\mathcal{F}}$  for the graphs Fig. 8 (a), (b), (c) and (d) are presented as

$$\{x_1, \{p\} \sqcup \{x_2, q\}\}, \{x_1, \{p, q\} \sqcup \{x_2\}\}, \{x_1, \{q, p\} \sqcup \{x_2\}\}, \{x_1, \{p, q\} \sqcup \{x_2\}\}. \quad (3.4)$$

When the integral over scattering variables is taken, according to (2.20), the one-loop integrand becomes

$$\begin{aligned} & \frac{1}{l^2} \int d\mu_{\delta}^{\text{tree}} I_L^{1\text{-loop}} I_R^{1\text{-loop}} \\ &= \left[ \sum_{\mathcal{F}} \mathcal{C}^{\mathcal{F}} \sum_{\substack{(A_1 \dots A_i) = \sigma^{\mathcal{F}} \\ (\tilde{A}_1 \dots \tilde{A}_i) = (a_1 a_2 a_3 a_4) \\ |A_j| = |\tilde{A}_j|}} \frac{1}{l^2} \frac{1}{s_{A_1, l}} \dots \frac{1}{s_{A_1 \dots A_{i-1}, l}} \phi_{A_1 | \tilde{A}_1} \dots \phi_{A_i | \tilde{A}_i} + \text{cyc}(x_1 x_2) \right] + \text{cyc}(a_1 a_2 a_3 a_4). \end{aligned} \quad (3.5)$$

In the above expression, we divided each permutation  $\sigma^{\mathcal{F}}$  into nonempty ordered subsets  $A_1, A_2, \dots, A_i$  and then summed over all possible such divisions. The divisions  $(\tilde{A}_1 \tilde{A}_2 \dots \tilde{A}_i)$  of  $(a_1 a_2 a_3 a_4)$  were also summed over. The  $|A_j| = |\tilde{A}_j|$  for each  $j$  means  $A_j$  and  $\tilde{A}_j$  have the same number of elements. Noting that  $\phi_{A_j | \tilde{A}_j} = 0$  when the elements of  $A_j$  and  $\tilde{A}_j$  are not identical to each other, the condition  $|A_j| = |\tilde{A}_j|$  is

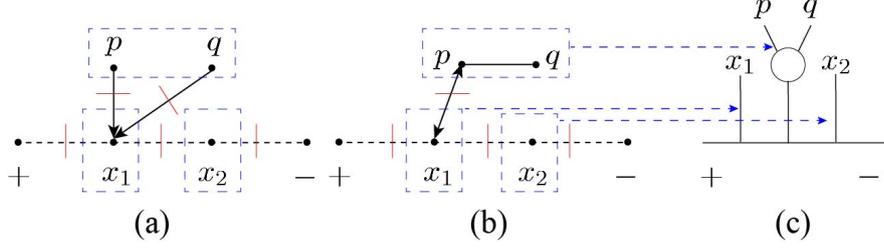


**Figure 9.** In graphs (a) and (b), the red lines separate subgraphs (the boxed regions) from each other. Each subgraph (except for the + and -) is associated with a subcurrent in the Feynman diagram (c). Graph (a) involves a disconnected subgraph that corresponds to a subcurrent  $\phi_{p\sqcup q|\dots}$  on the Feynman diagram side. Thus (a) vanishes due to the  $U(1)$ -decoupling identity (2.30).

equivalent to the condition  $A_j = \tilde{A}_j$  in (2.20).

To transform the linear propagators in (3.5) into quadratic propagators, we may rearrange (3.5) into an expression with a cyclic sum so that (2.27) can be applied. However, the graphs  $\mathcal{F}$  in general do not directly satisfy such cyclic property. To get a cyclic form, we first rewrite (3.5) into the following form by collecting terms corresponding to a given propagator structure:

$$\begin{aligned}
& \frac{1}{l^2} \int d\mu_6^{\text{tree}} I_L^{1\text{-loop}} I_R^{1\text{-loop}} \tag{3.6} \\
& = \left[ \sum_{\substack{\{A_1, A_2, \dots, A_i\} \\ (\tilde{A}_1 \dots \tilde{A}_i) = (a_1 a_2 a_3 a_4) \\ |A_j| = |\tilde{A}_j|}} \frac{1}{l^2} \frac{1}{s_{A_1, l}} \dots \frac{1}{s_{A_1 \dots A_{i-1}, l}} \sum_{\mathcal{F}} \mathcal{C}^{\mathcal{F}} \phi_{\sigma_{\mathcal{F}_1} | \tilde{A}_1} \dots \phi_{\sigma_{\mathcal{F}_i} | \tilde{A}_i} + \text{cyc}(x_1 x_2) \right] + \text{cyc}(a_1 a_2 a_3 a_4).
\end{aligned}$$

In the above expression, for a fixed relative order of scalars  $x_1, x_2$ , we summed over all possible *partitions*  $\{A_1, A_2, \dots, A_i\}$  ( $i \leq 4$ ) of external particles  $x_1, x_2$  and  $p, q$ . Each partition  $\{A_1, A_2, \dots, A_i\}$  corresponds to a given product of linear propagators in the Feynman diagram (as shown by Fig. 8 (e)), and is defined by splitting the external particles into  $i$  disjoint nonempty subsets  $A_1, \dots, A_i$ , which are arranged in a given order such that the relative order between scalars is preserved. For example, in the case with two scalars  $x_1, x_2$  (in the relative order  $(x_1 x_2)$ ) and two gluons  $p, q$ , all possible partitions  $\{A_1, A_2\}$  with two subsets are given by

$$\begin{aligned}
& \{\{x_1\}, \{x_2, p, q\}\}, \{\{x_1, p, q\}, \{x_2\}\}, \{\{x_1, x_2, p\}, \{q\}\}, \{\{q\}, \{x_1, x_2, p\}\}, \{\{x_1, x_2, q\}, \{p\}\}, \\
& \{\{p\}, \{x_1, x_2, q\}\}, \{\{x_1, x_2\}, \{p, q\}\}, \{\{p, q\}, \{x_1, x_2\}\}, \{\{x_1, p\}, \{x_2, q\}\}, \{\{x_1, q\}, \{x_2, p\}\}. \tag{3.7}
\end{aligned}$$

For a given partition  $\{A_1, A_2, \dots, A_i\}$ , we summed over all possible graphs  $\mathcal{F}$  contributing to it. Each  $\mathcal{F}$  can be decomposed into subgraphs  $\mathcal{F}_1, \dots, \mathcal{F}_i$  corresponding to subsets  $A_1, \dots, A_i$  in the partition, which means

- (i). Each subgraph  $\mathcal{F}_j$  contains elements identical to those in a certain subset  $A_j$ .

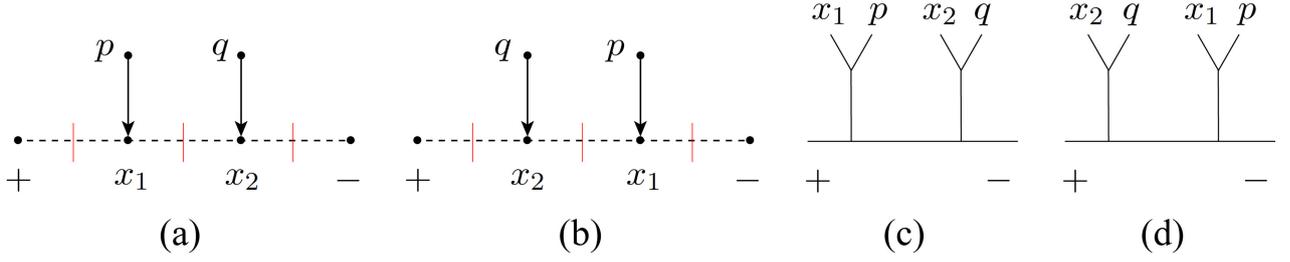


**Figure 10.** Graph (a) is a typical graph whose two subgraphs are interconnected via type-4 lines, and graph (b) is the cyclic form of the two subgraphs in (a). The Feynman diagrams under consideration which accompany to (a) and (b) are respectively (c) and (d), corresponding to partitions of particles  $\{\{x_1, p\}, \{x_2, q\}\}$  and  $\{\{x_2, q\}, \{x_1, p\}\}$ .

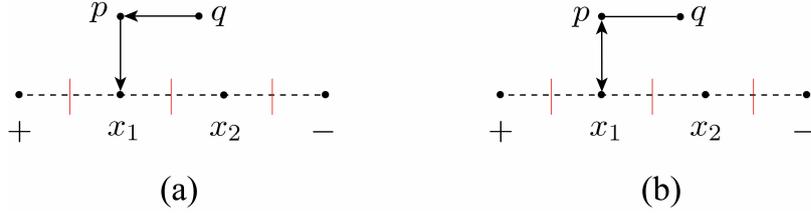


**Figure 11.** In graphs (a) and (b),  $p$ ,  $q$  and  $x_1$  belong to a same subgraph.

- (ii). These subgraphs can be arranged in the same order as subsets, as shown by Fig. 9 (b) and (c).

The  $\sigma^{\mathcal{F}_j}$  ( $j = 1, \dots, i$ ) in (3.6) denotes permutations established by subgraph  $\mathcal{F}_j$ . The summation over all possible  $\sigma^{\mathcal{F}_j}$  is implied. A subgraph  $\mathcal{F}_j$  can either be *connected* or *disconnected*. A *disconnected subgraph*, e.g., Fig. 9 (a) contains disjoint parts  $\mathcal{F}_A, \mathcal{F}_B, \dots$  and produces  $\phi_{\sigma^{\mathcal{F}_A} \sqcup \sigma^{\mathcal{F}_B} \sqcup \dots} \tilde{C}$  which has to cancel out due to the generalized U(1)-decoupling identity (2.30). Thus, *all surviving subgraphs are connected ones*.

In the coming subsections, we show that (3.6) can be rearranged into a cyclic sum in (2.27), thus produces quadratic propagators. Our discussions will be carried out for three classes of graphs, according to the way the subgraphs are interconnected.

### 3.2 The first class of graphs

Graphs of the first class are those with all subgraphs interconnected by type-4 lines. The type-4 line is the line that only records the relative positions between particles and does not provide any kinematic factor. For the two-gluon case, a typical graph that produces subgraphs interconnected via type-4 lines is shown by Fig. 10 (a), and the corresponding linear-propagator contribution (see the Feynman diagram Fig. 10 (c)), can be written as

$$(\epsilon_p \cdot k_{x_1})(\epsilon_q \cdot k_{x_2}) \frac{1}{l^2 s_{x_1 p, l}} \phi_{x_1 p | a_1 a_2} \phi_{x_2 q | a_3 a_4}. \quad (3.8)$$

For the above term, there always exists another graph Fig. 10 (b) which comes from  $\text{cyc}(x_1 x_2)$  in (3.2) and is accompanied by the Feynman diagram Fig. 10 (d). The two subgraphs of Fig. 10 (b) are exactly

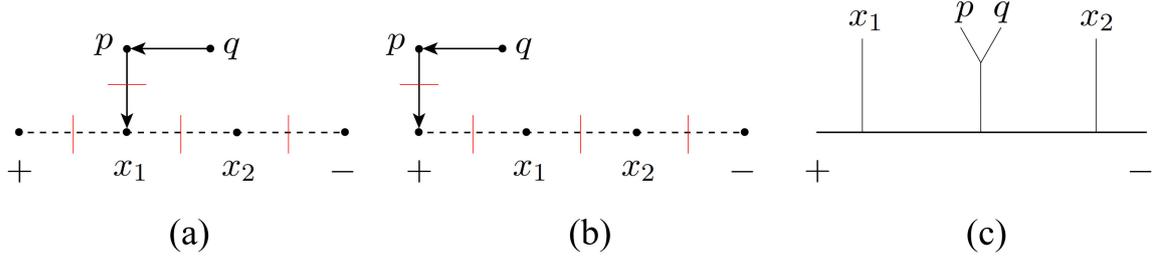


**Figure 12.** Each of the graphs (a) and (b), which involve  $\epsilon_p \cdot k_{x_1}$  and  $\epsilon_p \cdot l$  respectively, provides a nonlocal contribution to the Feynman diagram (c).

the cyclic form of the subgraphs in Fig. 10 (a). Thus we can directly obtain the quadratic propagators by summing the contributions of the two graphs in Fig. 10

$$\begin{aligned}
& (\epsilon_p \cdot k_{x_1})(\epsilon_q \cdot k_{x_2}) \frac{1}{l^2 s_{x_1 p, l}} \phi_{x_1 p | a_1 a_2} \phi_{x_2 q | a_3 a_4} + (\epsilon_p \cdot k_{x_1})(\epsilon_q \cdot k_{x_2}) \frac{1}{l^2 s_{x_2 q, l}} \phi_{x_2 q | a_3 a_4} \phi_{x_1 p | a_1 a_2} \\
& \cong (\epsilon_p \cdot k_{x_1})(\epsilon_q \cdot k_{x_2}) \frac{1}{l^2 l_{x_1 p}^2} \phi_{x_1 p | a_1 a_2} \phi_{x_2 q | a_3 a_4}, \tag{3.9}
\end{aligned}$$

where the RHS permutations of subcurrents in the second term come from the  $\text{cyc}(a_1 a_2 a_3 a_4)$  in (3.1).

This class of graphs always provides quadratic propagators directly, since no kinematic factors are separated by linear propagators, i.e., there is no nonlocal term. Similarly, the graphs in Fig. 11 give the quadratic propagators as follows

$$\text{(a). } (\epsilon_p \cdot k_{x_1})(\epsilon_q \cdot k_p) \frac{1}{l^2 l_{x_1 p q}^2} \phi_{x_1 p q | a_1 a_2 a_3} \phi_{x_2 | a_4}, \quad \text{(b). } (\epsilon_p \cdot \epsilon_q)(-k_p \cdot k_{x_1}) \frac{1}{l^2 l_{x_1 p q}^2} \phi_{x_1 p q | a_1 a_2 a_3} \phi_{x_2 | a_4}. \tag{3.10}$$

### 3.3 The second class of graphs and approach-1 to canceling nonlocal terms

The second class of graphs for the four-point example involves subgraphs  $A$  and  $B$  interconnected via a  $C_a \cdot k_b$  line, where  $C_a^\mu$  can represent the polarization vector or momentum of a node in the subgraph  $A$ , and  $k_b^\mu$  is the momentum of a node in subgraph  $B$ , e.g., Fig. 12 (a). *Nonlocality* arises due to the nontrivial contraction between the kinematic factors of these two subgraphs, which are separated by linear propagators in the corresponding Feynman diagram. *For this class of graphs, we use approach-1 to treat these nonlocal terms: collecting graphs with the coefficients  $C_a \cdot k$  together into  $C_a \cdot X_A$ , where  $X_A^\mu$  is the momentum of the linear propagator to the left of the subcurrent associated with  $A$ . Let us demonstrate this by examples.*

We first take Fig. 12 as an example, where  $p, q$  belong to the same subgraph in Fig. 12 (a), (b) and the same subcurrent in Fig. 12 (c). The graph Fig. 12 (a) together with the Feynman diagram Fig. 12 (c) provide

$$(\epsilon_p \cdot k_{x_1})(\epsilon_q \cdot k_p) \frac{1}{l^2 s_{x_1, l} s_{x_1 p q, l}} \phi_{x_1 | a_1} \phi_{p q | a_2 a_3} \phi_{x_2 | a_4}. \tag{3.11}$$

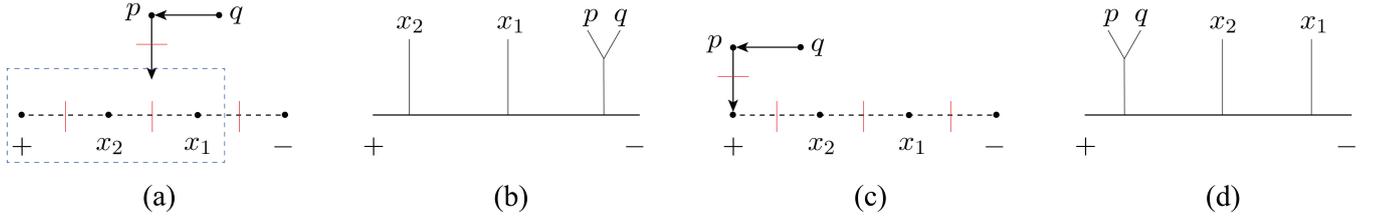


**Figure 13.** Graphs (a), (c) accompanying to the Feynman diagrams (b), (d) provide the cyclic permutations of the subsets in Fig. 12 (c) with graphs Fig. 12 (a), (b).

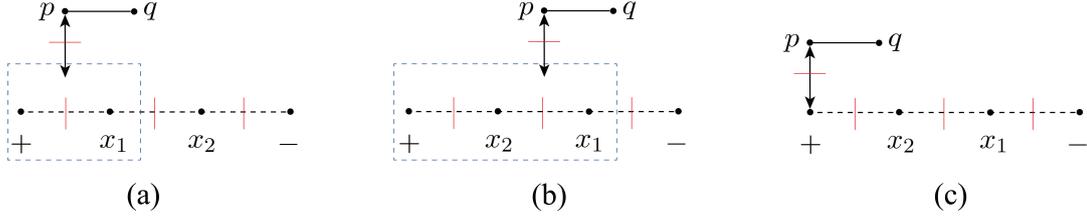


**Figure 14.** Each of the graphs (a), (b) and (c) contains  $p, q$  in a same subgraph and the kinematic factor is given by  $(\epsilon_p \cdot \epsilon_q)(-k_p \cdot X_p)$ . These three graphs contribute to the Feynman diagrams Fig. 12 (c), Fig. 13 (b) and (e), respectively.

Apparently, the subgraph with  $p, q$  is contracted to the subgraph with  $x_1$ , via a type-2 line  $\epsilon_p \cdot k_{x_1}$ . In the Feynman diagram Fig. 12 (c), these two subgraphs are separated by the linear propagator  $\frac{1}{s_{x_1, l}}$ . Thus this is a nonlocal term. To deal with this nonlocality, let us consider Fig. 12 (b) which provides another nonlocal term for the Feynman diagram Fig. 12 (c)

$$(\epsilon_p \cdot l)(\epsilon_q \cdot k_p) \frac{1}{l^2 s_{x_1, l} s_{x_1 p q, l}} \phi_{x_1|a_1} \phi_{p q|a_2 a_3} \phi_{x_2|a_4}. \quad (3.12)$$

The sum of (3.11) and (3.12) becomes

$$(\epsilon_p \cdot X_p)(\epsilon_q \cdot k_p) \frac{1}{l^2 s_{x_1, l} s_{x_1 p q, l}} \phi_{x_1|a_1} \phi_{p q|a_2 a_3} \phi_{x_2|a_4}, \quad (3.13)$$

where  $X_p^\mu = l^\mu + k_{x_1}^\mu$  is the momentum of the linear propagator  $\frac{1}{s_{x_1, l}}$  attached to the subset  $\{p, q\}$ . Thus the nonlocal terms (3.11) and (3.12) have been summed into a local term (3.13). The cyclic permutations of  $(x_1 x_2)$  and  $(a_1 a_2 a_3 a_4)$  allow Fig. 13 (a) and (c) for the Feynman diagrams Fig. 13 (b) and (d). According to (2.27), these contributions together with (3.13) produce a term with quadratic propagators

$$(\epsilon_p \cdot X_p)(\epsilon_q \cdot k_p) \frac{1}{l^2 l_{x_1}^2 l_{x_1 p q}^2} \phi_{x_1|a_1} \phi_{p q|a_2 a_3} \phi_{x_2|a_4}. \quad (3.14)$$

Similarly, the quadratic-propagator contribution of the graphs shown by Fig. 14 (a), (b) and (c) for the

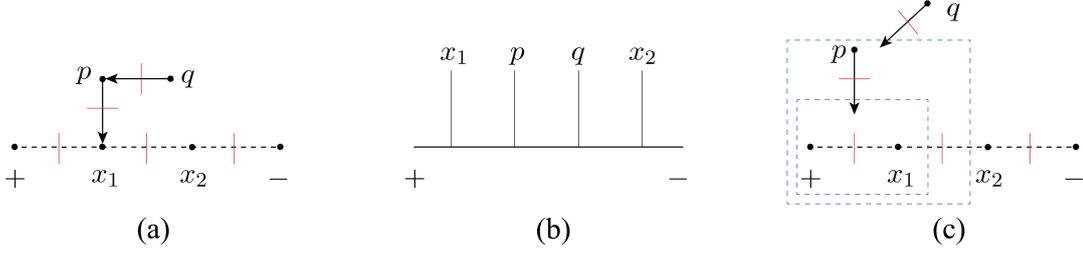


**Figure 15.** Graph (a) which relates to the Feynman diagram (b), contains  $p$  and  $q$  in different subgraphs. The type-2 lines associating to  $p$  and  $q$  induce nonlocalities. These nonlocalities are overcome by collecting all related graphs together, as shown by (c).

Feynman diagrams Fig. 12 (c), Fig. 13 (b) and (d) can be written as

$$(-k_p \cdot X_p)(\epsilon_q \cdot \epsilon_p) \frac{1}{l^2 l_{x_1}^2 l_{x_1 p q}^2} \phi_{x_1|a_1} \phi_{p|a_2 a_3} \phi_{x_2|a_4}. \quad (3.15)$$

The second example is Fig. 15 (a), which is related to the Feynman diagram Fig. 15 (b) and thus contains  $p$  and  $q$  in different subgraphs. For this case, two nonlocal contractions between  $p$  and  $x_1$ ,  $q$  and  $p$  need to be dealt with separately. So for the Feynman diagram Fig. 15 (b), we consider the contribution provided by the graphs in Fig. 15 (c)

$$(\epsilon_p \cdot X_p)(\epsilon_q \cdot X_q) \frac{1}{l^2 s_{x_1, l} s_{x_1 p, l} s_{x_1 p q, l}} \phi_{x_1|a_1} \phi_{p|a_2} \phi_{q|a_3} \phi_{x_2|a_4}, \quad (3.16)$$

where  $X_p^\mu = l^\mu + k_{x_1}^\mu$  and  $X_q^\mu = l^\mu + k_{x_1}^\mu + k_p^\mu$  are the momenta of the propagators attached to the subsets  $\{p\}$  and  $\{q\}$ , respectively. The nonlocal terms are collected to give the local linear-propagator contribution. Thus, after a cyclic summation of the scalar particles, we obtain the quadratic-propagator term

$$(\epsilon_p \cdot X_p)(\epsilon_q \cdot X_q) \frac{1}{l^2 l_{x_1}^2 l_{x_1 p}^2 l_{x_1 p q}^2} \phi_{x_1|a_1} \phi_{p|a_2} \phi_{q|a_3} \phi_{x_2|a_4}. \quad (3.17)$$

For graphs with neither  $\epsilon \cdot \epsilon$  nor  $k \cdot k$  line, the  $p$  and  $q$  can belong to either the same subgraph or distinct subgraphs. These two situations can always be treated following a similar discussion with the first and the second example. The quadratic-propagator contribution of all possible graphs with neither  $\epsilon \cdot \epsilon$  nor  $k \cdot k$  line is given by

$$\begin{aligned} & \frac{(\epsilon_p \cdot l_{x_1})(\epsilon_q \cdot l_{x_1 p x_2})}{l^2 l_{x_1}^2 l_{x_1 p}^2 l_{x_1 p x_2}^2} \phi_{x_1|a_1} \phi_{p|a_2} \phi_{x_2|a_3} \phi_{q|a_4} + \frac{(\epsilon_p \cdot k_{x_1})(\epsilon_q \cdot k_{x_2})}{l^2 l_{x_1 p}^2} \phi_{x_1 p|a_1 a_2} \phi_{x_2 q|a_3 a_4} \\ & + \left[ \frac{(\epsilon_p \cdot l_{x_1 x_2})(\epsilon_q \cdot l_{x_1 x_2 p})}{l^2 l_{x_1}^2 l_{x_1 x_2}^2 l_{x_1 x_2 p}^2} \phi_{x_1|a_1} \phi_{x_2|a_2} \phi_{p|a_3} \phi_{q|a_4} + \frac{(\epsilon_p \cdot l_{x_1 x_2})(\epsilon_q \cdot l_{x_1 x_2 p})}{l^2 l_{x_1 x_2}^2 l_{x_1 x_2 p}^2} \phi_{x_1 x_2|a_1 a_2} \phi_{p|a_3} \phi_{q|a_4} \right] \\ & + \frac{(\epsilon_p \cdot k_{x_1})(\epsilon_q \cdot l_{x_1 p})}{l^2 l_{x_1 p}^2 l_{x_1 p q}^2} \phi_{x_1 p|a_1 a_2} \phi_{q|a_3} \phi_{x_2|a_4} + \frac{(\epsilon_p \cdot k_{x_1})(\epsilon_q \cdot l_{x_1 p x_2})}{l^2 l_{x_1 p}^2 l_{x_1 p x_2}^2} \phi_{x_1 p|a_1 a_2} \phi_{x_2|a_3} \phi_{q|a_4} \end{aligned}$$

$$\begin{aligned}
& + \frac{(\epsilon_p \cdot l_{x_1})(\epsilon_q \cdot k_p)}{l^2 l_{x_1}^2 l_{x_1 p q}^2} \phi_{x_1|a_1} \phi_{pq|a_2 a_3} \phi_{x_2|a_4} + \frac{(\epsilon_p \cdot k_{x_1})(\epsilon_q \cdot l_{x_1 p x_2})}{l^2 l_{x_1 p x_2}^2} \phi_{x_1 p x_2|a_1 a_2 a_3} \phi_{q|a_4} \\
& + \frac{(\epsilon_p \cdot k_{x_1 x_2})(\epsilon_q \cdot l_{x_1 x_2 p})}{l^2 l_{x_1 x_2 p}^2} \phi_{x_1 x_2 p|a_1 a_2 a_3} \phi_{q|a_4} + \frac{(\epsilon_p \cdot k_{x_1})(\epsilon_q \cdot k_{x_1 p})}{l^2 l_{x_1 p q}^2} \phi_{x_1 p q|a_1 a_2 a_3} \phi_{x_2|a_4} \\
& + \left. \frac{(\epsilon_p \cdot l_{x_1 x_2})(\epsilon_q \cdot k_p)}{l^2 l_{x_1 x_2}^2} \phi_{x_1 x_2|a_1 a_2} \phi_{pq|a_3 a_4} + \text{cyc}(x_1 x_2) \right] + (p \leftrightarrow q) + \text{cyc}(a_1 a_2 a_3 a_4), \tag{3.18}
\end{aligned}$$

where the  $\epsilon \cdot k$  factors within each subgraph are preserved, and the  $\epsilon \cdot k$  factors between subgraphs are collected as local factors  $\epsilon \cdot X$ . When  $U(1)$ -decoupling identity<sup>1</sup> and the cyclic sum of  $(x_1 x_2)$  are considered, the terms where two scalars belong to a same subcurrent must vanish. *The sum of  $\text{cyc}(a_1 a_2 a_3 a_4)$  is introduced so that the left and right permutations in a BS subcurrent contain the same particles.* The above result can also be obtained by the tensorial PT-factor (2.22) decomposition of CHY left half integrand

$$\begin{aligned}
I_L^{1\text{-loop}}(x_1, x_2 || \{p, q\}) &= (\epsilon_p \cdot X'_p(\sqcup))(\epsilon_q \cdot X'_q(\sqcup)) \text{PT}_t(x_1, \{x_2\} \sqcup \{p\} \sqcup \{q\}) \\
&+ (\epsilon_p \cdot X'_p(\sqcup))(\epsilon_q)_\mu \text{PT}_t^\mu(x_1, \{x_2\} \sqcup \{p\} \sqcup \{q\}) \\
&+ (\epsilon_q \cdot X'_q(\sqcup))(\epsilon_p)_\mu \text{PT}_t^\mu(x_1, \{x_2\} \sqcup \{p\} \sqcup \{q\}) \\
&+ (\epsilon_p)_\mu (\epsilon_q)_\nu \text{PT}_t^{\mu\nu}(x_1, \{x_2\} \sqcup \{p\} \sqcup \{q\}), \tag{3.19}
\end{aligned}$$

where for a given permutation,  $X'_p(\sqcup)$  is defined by the total momentum of external particles on the left-hand side of  $p$ . This tensorial PT factor can be generalized to half integrand with  $n$  scalars and 2 gluons

$$\begin{aligned}
I_L^{1\text{-loop}}(x_1, x_2, \dots, x_n || \{p, q\}) &= (\epsilon_p \cdot X'_p(\sqcup))(\epsilon_q \cdot X'_q(\sqcup)) \text{PT}_t(x_1, \{x_2, \dots, x_n\} \sqcup \{p\} \sqcup \{q\}) \\
&+ (\epsilon_p \cdot X'_p(\sqcup))(\epsilon_q)_\mu \text{PT}_t^\mu(x_1, \{x_2, \dots, x_n\} \sqcup \{p\} \sqcup \{q\}) \\
&+ (\epsilon_q \cdot X'_q(\sqcup))(\epsilon_p)_\mu \text{PT}_t^\mu(x_1, \{x_2, \dots, x_n\} \sqcup \{p\} \sqcup \{q\}) \\
&+ (\epsilon_p)_\mu (\epsilon_q)_\nu \text{PT}_t^{\mu\nu}(x_1, \{x_2, \dots, x_n\} \sqcup \{p\} \sqcup \{q\}). \tag{3.20}
\end{aligned}$$

According to eq. (2.24), the above expression gives the one-loop quadratic-propagator YMS integrand without  $\epsilon \cdot \epsilon$  factor as follows

$$\begin{aligned}
& I^{1\text{-loop}}(x_1, x_2, \dots, x_n || \{p, q\} | \boldsymbol{\rho}) \tag{3.21} \\
& \cong \sum_{\substack{(A_1 A_2 \dots A_m) = (x_1 \{x_2 \dots x_n\} \sqcup \{p\} \sqcup \{q\}) \\ (\widetilde{A}_1 \widetilde{A}_2 \dots \widetilde{A}_m) = \boldsymbol{\rho} \\ A_j = \widetilde{A}_j \\ 2 \leq m \leq n}} \left[ (\epsilon_p \cdot (X_p(\sqcup) + k_A))(\epsilon_q \cdot (X_q(\sqcup) + k_A)) \text{gon}(A_1, A_2, \dots, A_m) \prod_{i=1}^m \phi_{A_i | \widetilde{A}_i} \right],
\end{aligned}$$

<sup>1</sup>The  $U(1)$ -decoupling identity for scalars can be extended to the subcurrents containing both scalars and gluons because it is essentially determined by the antisymmetry of cubic vertex in the BS current.

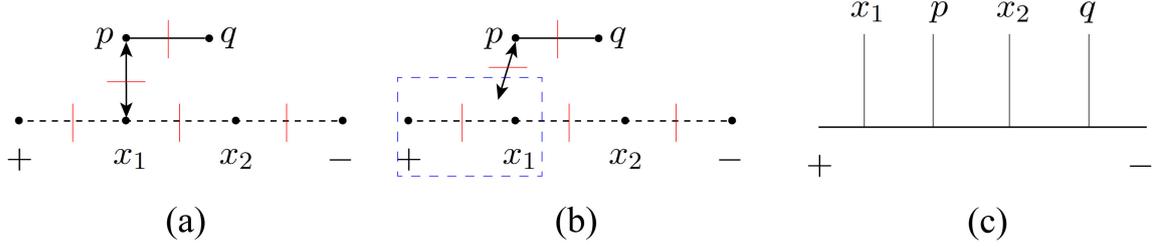


**Figure 16.** In graph (a) associating with the Feynman diagram (c), the subgraph containing node  $p$  is contracted with the one containing  $q$ , but they are separated by linear propagators in the Feynman diagram (c). This nonlocality cannot be treated by approach-1. In fact, when  $p$  is connected to  $+$ , we also have such a nonlocal term with respect to the Feynman diagram (c). The two terms together are presented by (b) which induces an X-pattern by the subgraph  $p$ , since (b) brings a factor  $-k_p \cdot X_p$  to the Feynman diagram (c).

where  $X_p^\mu(\sqcup)$  denotes the sum of the loop momentum  $l^\mu$  and the total momentum of the external particles  $x_1, \dots$ , between  $l^\mu$  and  $p$ . We define  $A, \bar{A}$  as the two parts separated by  $x_1$  in  $A_1 = Ax_1\bar{A}$ . The  $k_A^\mu$  is the total momentum of elements in  $A$ . The expression (3.21) can further be generalized to the case which contains an arbitrary number of gluons and only  $\epsilon \cdot k$  lines

$$I^{1\text{-loop}}(x_1, \dots, x_n | |G|\rho) \cong \sum_{\substack{(A_1 \dots A_m) = (x_1 \{x_2 \dots x_n\} \sqcup \text{perms } G) \\ (A_1 \dots A_m) = \rho \\ A_j = \bar{A}_j \\ 2 \leq m \leq n}} \left[ \prod_{g_k \in G} \epsilon_{g_k} \cdot (X_{g_k}(\sqcup) + k_A) \text{gon}(A_1, \dots, A_m) \prod_{i=1}^m \phi_{A_i | \bar{A}_i} \right], \quad (3.22)$$

where  $G$  is the gluon set and  $\text{perms } G$  denotes all permutations of elements in  $G$ . In the case  $n = 2$  and  $G = \{p, q\}$ , the above expression becomes (3.18).

We conclude that the YMS quadratic-propagator integrands without  $\epsilon \cdot \epsilon$  factor can be obtained by dealing with the graphs coming from refined graphic rules or by expanding the CHY half integrand into tensorial PT factors. Although the tensorial PT-factor approach to quadratic propagators seems straightforward, the CHY half integrand with  $\epsilon \cdot \epsilon$  factors may not be straightforwardly expanded to the tensorial PT factors. Therefore, in the rest of this paper, we still use the graphic expansion method to convert the linear propagators into quadratic ones.

### 3.4 The third class of graphs and approach-2 to canceling the nonlocal terms

In the third class of graphs, some nonlocal contributions cannot be removed by assembling them into  $C \cdot X$  factors. For example, Fig. 16 (a) is a typical graph of this class, due to the nonlocal contraction  $\epsilon_p \cdot \epsilon_q$  between subgraphs  $p$  and  $q$ . For this type of nonlocality, we introduce *approach-2* to deal with it, which relies on two helpful patterns, *BCJ-pattern* and *X-pattern*. Note that the nonlocality in Fig. 16 (a) caused by  $-k_p \cdot k_{x_1}$  can be treated first, by considering the graph where the subgraph  $p$  is connected to  $+$  via  $-k_p \cdot l$ . Thus the factors are summed into a local one  $-k_p \cdot X_p$ , as shown by Fig. 16 (b). The linear-propagator

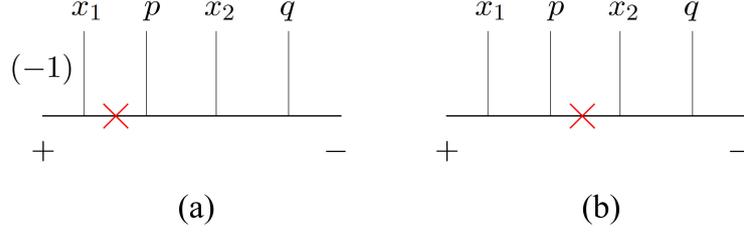


**Figure 17.** The Feynman diagrams (a) and (b) correspond to the two terms on the second line of (3.23).

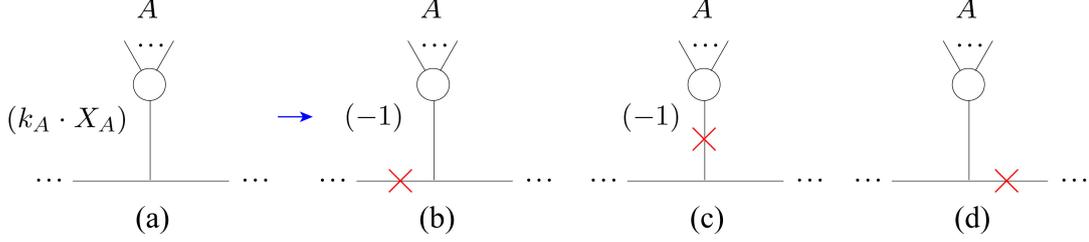


**Figure 18.** When the X-pattern for subgraph  $A$  exists, it can be used to delete the linear propagator to either the left (see (b)) or the right (see (d)) of the subcurrent containing  $A$ , or remove the off-shell line of the subcurrent containing  $A$  (see (c)).

contribution of graph Fig. 16 (b) for Feynman diagram Fig. 16 (c) can be expressed as follows

$$\begin{aligned}
& (-k_p \cdot X_p)(\epsilon_p \cdot \epsilon_q) \frac{1}{l^2} \frac{1}{s_{x_1, l}} \frac{1}{s_{x_1 p, l}} \frac{1}{s_{x_1 p x_2, l}} \phi_{x_1|a_1} \phi_{p|a_2} \phi_{x_2|a_3} \phi_{q|a_4} \\
&= \left(-\frac{1}{2}\right)(\epsilon_p \cdot \epsilon_q) \left[ - \left( \frac{1}{l^2} \frac{1}{s_{x_1 p, l}} \frac{1}{s_{x_1 p x_2, l}} \right) + \left( \frac{1}{l^2} \frac{1}{s_{x_1, l}} \frac{1}{s_{x_1 p x_2, l}} \right) \right] \phi_{x_1|a_1} \phi_{p|a_2} \phi_{x_2|a_3} \phi_{q|a_4},
\end{aligned} \tag{3.23}$$

where we have used the relation

$$k_p \cdot X_p = \frac{1}{2}(l_{x_1 p}^2 - l_{x_1}^2 - k_p^2) = \frac{1}{2}(s_{x_1 p, l} - s_{x_1, l}), \tag{3.24}$$

to cancel out different linear propagators. The on-shell condition  $k_p^2 = 0$  has been used. The two propagator-decreased terms in (3.23) can be characterized by the Feynman diagrams Fig. 17 (a) and (b), respectively<sup>2</sup>. We say a graph has an *X-pattern* if this graph involves a factor  $k_A \cdot X_A$ , where  $k_A^\mu$  denotes the total momentum of particles in subgraph<sup>3</sup>  $A$ ,  $X_A^\mu$  denotes the momentum of the propagator attached to the subcurrent corresponding to the subset  $A$  from left, in the Feynman diagram. Then the relation

$$k_A \cdot X_A = \frac{1}{2} [(k_A + X_A)^2 - X_A^2 - k_A^2] = \frac{1}{2} [((k_A + X_A)^2 - l^2) - (X_A^2 - l^2) - k_A^2], \tag{3.25}$$

<sup>2</sup>An overall factor  $-\frac{1}{2}$  is omitted in each diagram.

<sup>3</sup>Here we use the same notation  $A$  to denote the subset  $A$  and a subgraph corresponding to this subset for convenience. In the general discussions in section 6 and section 7, we introduce different notations for a subset and its corresponding subgraphs.

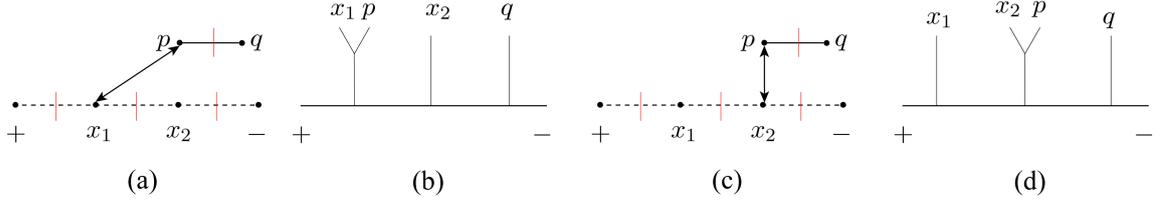


**Figure 19.** Both graphs (a) and (c) contain a BCJ-pattern since they each has a subgraph with  $p$ ,  $x_1$  or  $p$ ,  $x_2$ , which contributes the LHS of off-shell BCJ relation for the corresponding subcurrent in the related Feynman diagram (b) or (d).

can be applied to remove the propagators correspondingly, as shown by Feynman diagrams in Fig. 18. Apparently, Fig. 16 (b) has an X-pattern. More general discussions of X-pattern will be given in the next section.

If there exists a graph with an X-pattern, there also exist some graphs corresponding to it with *BCJ-patterns*, which means the graph has a subgraph that can use the off-shell BCJ relation (2.32). For the graph in Fig. 16 (b), there exists graph Fig. 19 (a) with respect to the Feynman diagram Fig. 19 (b). This graph contains a BCJ-pattern and contributes

$$\begin{aligned}
& (-k_p \cdot k_{x_1})(\epsilon_p \cdot \epsilon_q) \frac{1}{l^2} \frac{1}{s_{x_1 p, l}} \frac{1}{s_{x_1 p x_2, l}} \phi_{x_1 p | a_1 a_2} \phi_{x_2 | a_3} \phi_{q | a_4} \\
& = \left(-\frac{1}{2}\right)(\epsilon_p \cdot \epsilon_q) \left( \frac{1}{l^2} \frac{1}{s_{x_1 p, l}} \frac{1}{s_{x_1 p x_2, l}} \right) \left[ -\phi_{p | a_1} \phi_{x_1 | a_2} \phi_{x_2 | a_3} \phi_{q | a_4} + \phi_{x_1 | a_1} \phi_{p | a_2} \phi_{x_2 | a_3} \phi_{q | a_4} \right],
\end{aligned} \tag{3.26}$$

where the off-shell BCJ relation (2.32) has been applied to rewriting  $(k_p \cdot k_{x_1})\phi_{x_1 p | a_1 a_2}$  as  $\frac{1}{2}\phi_{x_1 | a_1} \phi_{p | a_2} - \frac{1}{2}\phi_{p | a_1} \phi_{x_1 | a_2}$ . A general discussion on BCJ-pattern will be provided in the next section. It can be seen that the second term of the above expression is canceled out by the first term of (3.23). This cancellation between BCJ-pattern and X-pattern is not occasional, we can find another graph with X-pattern to cancel out the first term of (3.26) and another graph with BCJ-pattern to cancel out the second term of (3.23). More precisely, the latter graph containing  $x_2$  and  $p$  in the same subgraph, as shown by Fig. 19 (c), provides the linear-propagator contribution with respect to the Feynman diagram Fig. 19 (d)

$$\left(-\frac{1}{2}\right)(\epsilon_p \cdot \epsilon_q) \left( \frac{1}{l^2} \frac{1}{s_{x_1, l}} \frac{1}{s_{x_1 x_2 p, l}} \right) \left[ -\phi_{x_1 | a_1} \phi_{p | a_2} \phi_{x_2 | a_3} \phi_{q | a_4} + \phi_{x_1 | a_1} \phi_{x_2 | a_2} \phi_{p | a_3} \phi_{q | a_4} \right], \tag{3.27}$$

where the off-shell BCJ relation (2.32) has also been applied to  $(k_p \cdot k_{x_2})\phi_{x_2 p | a_2 a_3}$ . Thus, the first term of the above expression actually cancels out the second term of (3.23). The complete cancellation map is given by Fig. 46 in appendix D. The BCJ-patterns and the X-patterns cancel out each other until reaching the boundary case, where no scalar subcurrent is located between subcurrents  $p$  and  $q$  in the Feynman

diagram, as shown by Fig. 46 (c1). The contribution obtained by this boundary case can be written as

$$\begin{aligned}
& (-k_p \cdot X_p)(\epsilon_p \cdot \epsilon_q) \frac{1}{l^2} \frac{1}{s_{x_1,l}} \frac{1}{s_{x_1x_2,l}} \frac{1}{s_{x_1x_2p,l}} \phi_{x_1|a_1} \phi_{x_2|a_2} \phi_{p|a_3} \phi_{q|a_4} \\
&= \left(-\frac{1}{2}\right)(\epsilon_p \cdot \epsilon_q) \left[ -\left(\frac{1}{l^2} \frac{1}{s_{x_1,l}} \frac{1}{s_{x_1x_2p,l}}\right) + \left(\frac{1}{l^2} \frac{1}{s_{x_1,l}} \frac{1}{s_{x_1x_2,l}}\right) \right] \phi_{x_1|a_1} \phi_{x_2|a_2} \phi_{p|a_3} \phi_{q|a_4},
\end{aligned} \tag{3.28}$$

with respect to the Feynman diagrams Fig. 46 (c2) and (c3). Although the first term from the X-pattern also cancels out with the term from a certain BCJ-pattern, the second term is retained with the factor  $\epsilon_p \cdot \epsilon_q$  local. After the cyclic summations of  $(x_1x_2)$  and  $(a_1a_2a_3a_4)$ , we finally get the quadratic-propagator contribution

$$\begin{aligned}
& \left(-\frac{1}{2}\right)(\epsilon_p \cdot \epsilon_q) \left[ \frac{1}{l^2} \frac{1}{s_{x_1,l}} \frac{1}{s_{x_1x_2,l}} + \frac{1}{l^2} \frac{1}{s_{pq,l}} \frac{1}{s_{ppq_{x_1,l}}} + \frac{1}{l^2} \frac{1}{s_{x_2,l}} \frac{1}{s_{x_2pq,l}} \right] \phi_{x_1|a_1} \phi_{x_2|a_2} \phi_{p|a_3} \phi_{q|a_4} \\
&= \left(-\frac{1}{2}\right)(\epsilon_p \cdot \epsilon_q) \left[ \frac{1}{l^2} \frac{1}{l_{x_1}^2} \frac{1}{l_{x_1x_2,l}^2} \right] \phi_{x_1|a_1} \phi_{x_2|a_2} \phi_{p|a_3} \phi_{q|a_4}.
\end{aligned} \tag{3.29}$$

In general, when other Feynman diagrams are considered, the BCJ-patterns and the X-patterns where  $p$  and  $q$  are separated by other subcurrents have to cancel out. The only surviving terms are those Feynman diagrams where  $p, q$  are adjacent to each other and the linear propagator between them is removed. All such surviving terms are collected as

$$\begin{aligned}
& \left(-\frac{1}{2}\right)(\epsilon_p \cdot \epsilon_q) \left[ \frac{1}{l^2} \frac{1}{l_{x_1}^2} \frac{1}{l_{x_1pq,l}^2} \phi_{x_1|a_1} \phi_{p|a_2} \phi_{q|a_3} \phi_{x_2|a_4} + \frac{1}{l^2} \frac{1}{l_{x_1}^2} \frac{1}{l_{x_1x_2,l}^2} \phi_{x_1|a_1} \phi_{x_2|a_2} \phi_{p|a_3} \phi_{q|a_4} \right. \\
& \left. + \frac{1}{l^2} \frac{1}{l_{x_1x_2}^2} \phi_{x_1x_2|a_1a_2} \phi_{p|a_3} \phi_{q|a_4} + \frac{1}{l^2} \frac{1}{l_{x_2x_1}^2} \phi_{x_2x_1|a_1a_2} \phi_{p|a_3} \phi_{q|a_4} \right] + \text{cyc}(a_1a_2a_3a_4).
\end{aligned} \tag{3.30}$$

When the U(1)-decoupling identity (2.30) is applied, the last two terms cancel out, the above expression gets a further simplification

$$\left(-\frac{1}{2}\right)(\epsilon_p \cdot \epsilon_q) \left[ \frac{1}{l^2} \frac{1}{l_{x_1}^2} \frac{1}{l_{x_1pq,l}^2} \phi_{x_1|a_1} \phi_{p|a_2} \phi_{q|a_3} \phi_{x_2|a_4} + \frac{1}{l^2} \frac{1}{l_{x_1}^2} \frac{1}{l_{x_1x_2,l}^2} \phi_{x_1|a_1} \phi_{x_2|a_2} \phi_{p|a_3} \phi_{q|a_4} \right] + \text{cyc}(a_1a_2a_3a_4). \tag{3.31}$$

### 3.5 Compact expression of the four-point integrand with two gluons

In the previous discussions, we have shown how to extract the quadratic propagators in the four-point example with two gluons. Our starting point is the linear-propagator-expressed Feynman diagrams (LPFD), whose coefficients are expressed by the refined graphs. When the nonlocalities are canceled out and the cyclic permutations of scalars are considered, we get the expressions with quadratic propagators. In this

subsection, we assemble all results corresponding to any given structure of quadratic propagators (i.e., a given *cyclic partition*<sup>4</sup> of external particles) and provide a compact formula of the result.

First, partitions in which each subset contains only one element provide box diagrams. The first term in (3.18) and the first term in the square brackets of (3.18),

$$\frac{(\epsilon_p \cdot l_{x_1})(\epsilon_q \cdot l_{x_1 p x_2})}{l^2 l_{x_1}^2 l_{x_1 p}^2 l_{x_1 p x_2}^2} \phi_{x_1|a_1} \phi_{p|a_2} \phi_{x_2|a_3} \phi_{q|a_4}, \quad \frac{(\epsilon_p \cdot l_{x_1 x_2})(\epsilon_q \cdot l_{x_1 x_2 p})}{l^2 l_{x_1}^2 l_{x_1 x_2}^2 l_{x_1 x_2 p}^2} \phi_{x_1|a_1} \phi_{x_2|a_2} \phi_{p|a_3} \phi_{q|a_4} \quad (3.32)$$

correspond to such partitions  $\{x_1, p, x_2, q\}$  and  $\{x_1, x_2, p, q\}$ , respectively. If the subset has only one scalar, e.g.,  $x_1$  for partition  $\{x_1, x_2, p, q\}$ , it supplies a scalar subcurrent  $\phi_{x_1|a_1}$ . If the subset contains only one gluon, e.g.,  $p$  for partition  $\{x_1, x_2, p, q\}$ , it provides  $(\epsilon_p \cdot l_{x_1 x_2}) \phi_{x_1|a_1} = \tilde{J}(p) \cdot X_p$ . The effective current  $\tilde{J}^\mu(p) = \epsilon_p^\mu \phi_{x_1|a_1}$  is defined by refined graphic rule when the Lorentz index (associated with off-shell line) is considered as the root. The momentum  $X_p^\mu = l_{x_1 x_2}^\mu$  is just the momentum of the (quadratic) propagator to the left of the subcurrent  $\tilde{J}^\mu(p)$ . The contributions of all box diagrams can be collected as

$$\begin{aligned} & \frac{(\epsilon_p \cdot l_{x_1 x_2})(\epsilon_q \cdot l_{x_1 x_2 p})}{l^2 l_{x_1}^2 l_{x_1 x_2}^2 l_{x_1 x_2 p}^2} \phi_{x_1|a_1} \phi_{x_2|a_2} \phi_{p|a_3} \phi_{q|a_4} + \frac{(\epsilon_p \cdot l_{x_1})(\epsilon_q \cdot l_{x_1 p x_2})}{l^2 l_{x_1}^2 l_{x_1 p}^2 l_{x_1 p x_2}^2} \phi_{x_1|a_1} \phi_{p|a_2} \phi_{x_2|a_3} \phi_{q|a_4} \\ & + \frac{(\epsilon_p \cdot l_{x_1})(\epsilon_q \cdot l_{x_1 p})}{l^2 l_{x_1}^2 l_{x_1 p}^2 l_{x_1 p q}^2} \phi_{x_1|a_1} \phi_{p|a_2} \phi_{q|a_3} \phi_{x_2|a_4} + (p \leftrightarrow q) + \text{cyc}(a_1 a_2 a_3 a_4) \\ = & \frac{(\tilde{J}(p) \cdot X_p)(\tilde{J}(q) \cdot X_q)}{l^2 l_{x_1}^2 l_{x_1 x_2}^2 l_{x_1 x_2 p}^2} \phi_{x_1|a_1} \phi_{x_2|a_2} + \frac{(\tilde{J}(p) \cdot X_p)(\tilde{J}(q) \cdot X_q)}{l^2 l_{x_1}^2 l_{x_1 p}^2 l_{x_1 p x_2}^2} \phi_{x_1|a_1} \phi_{x_2|a_3} \\ & + \frac{(\tilde{J}(p) \cdot X_p)(\tilde{J}(q) \cdot X_q)}{l^2 l_{x_1}^2 l_{x_1 p}^2 l_{x_1 p q}^2} \phi_{x_1|a_1} \phi_{x_2|a_4} + (p \leftrightarrow q) + \text{cyc}(a_1 a_2 a_3 a_4) \end{aligned} \quad (3.33)$$

where we don't have term  $\text{cyc}(x_1 x_2)$ , since partition  $\{x_2, x_1, p, q\}$  is the same as  $\{x_1, p, q, x_2\}$  at the loop level.

Second, partitions involving only one two-element subset provide triangle diagrams. There are three types of such partitions which correspond to the two-element subset containing (i). two scalars, (ii). a scalar and a gluon, (iii). two gluons:

- For the case (i), consider the partitions  $\{\{x_1, x_2\}, p, q\}$  and  $\{\{x_2, x_1\}, p, q\}$ , whose contribution are given by the second term in the square brackets and  $\text{cyc}(x_1 x_2)$  term of (3.18)

$$\frac{(\epsilon_p \cdot l_{x_1 x_2})(\epsilon_q \cdot l_{x_1 x_2 p})}{l^2 l_{x_1 x_2}^2 l_{x_1 x_2 p}^2} \phi_{x_1 x_2|a_1 a_2} \phi_{p|a_3} \phi_{q|a_4}, \quad \frac{(\epsilon_p \cdot l_{x_2 x_1})(\epsilon_q \cdot l_{x_2 x_1 p})}{l^2 l_{x_2 x_1}^2 l_{x_2 x_1 p}^2} \phi_{x_2 x_1|a_1 a_2} \phi_{p|a_3} \phi_{q|a_4}. \quad (3.34)$$

The numerator in the above expression can be rewritten as  $\phi_{x_1 x_2|a_1 a_2}(\tilde{J}(p) \cdot X_p)(\tilde{J}(q) \cdot X_q)$  and  $\phi_{x_2 x_1|a_1 a_2}(\tilde{J}(p) \cdot X_p)(\tilde{J}(q) \cdot X_q)$ . Due to the  $U(1)$ -decoupling identity, the sum of these two partitions

---

<sup>4</sup>Partitions associating with quadratic propagators in the final result are cyclic partitions which means  $\{A_1, A_2, \dots, A_i\} = \{A_2, \dots, A_i, A_1\}$ , while the partitions accompanied to LPFD are not cyclic ones.

vanishes.

- For the case (ii), consider the partition  $\{\{x_1, p\}, x_2, q\}$ , whose contribution is the fourth term in the square brackets of (3.18)

$$\frac{(\epsilon_p \cdot k_{x_1})(\epsilon_q \cdot l_{x_1 p x_2})}{l^2 l_{x_1 p}^2 l_{x_1 p x_2}^2} \phi_{x_1 p | a_1 a_2} \phi_{x_2 | a_3} \phi_{q | a_4}. \quad (3.35)$$

The numerator is given by  $\tilde{J}(x_1, p) \phi_{x_2 | a_3} (\tilde{J}(q) \cdot X_q)$ , where  $\tilde{J}(x_1, p)$  is the effective current generated by refined graph about  $x_1$  and  $p$ . We choose the scalar  $x_1$  as the root of graph, rather than the off-shell line which is the root for subset with only gluons.

- The case (iii) reveals a new feature. For example, the partition  $\{x_1, \{p, q\}, x_2\}$  gets contributions from (3.15), the fifth term in the square brackets of (3.18), as well as the  $p \leftrightarrow q$  term of (3.18), and explicitly provides

$$\left[ (-k_p \cdot X_p)(\epsilon_q \cdot \epsilon_p) \phi_{p q | a_2 a_3} + (\epsilon_p \cdot X_p)(\epsilon_q \cdot k_p) \phi_{p q | a_2 a_3} + (\epsilon_q \cdot X_q)(\epsilon_p \cdot k_p) \phi_{q p | a_2 a_3} \right] \frac{\phi_{x_1 | a_1} \phi_{x_2 | a_4}}{l^2 l_{x_1}^2 l_{x_1 p q}^2} \quad (3.36)$$

The expression inside the square brackets is just  $\tilde{J}(p, q) \cdot X_{\{p, q\}}$ , where the effective current  $\tilde{J}^\mu(p, q)$  corresponds to the sum of refined graphs with the reference order  $p \prec q$ . In addition, when the cancellation between X-pattern and BCJ-pattern has been considered, the graph with  $\epsilon_p \cdot \epsilon_q$  line also provides a nontrivial term (the first term of (3.30)) for the partition  $\{x_1, \{p, q\}, x_2\}$

$$\left(-\frac{1}{2}\right) (\epsilon_p \cdot \epsilon_q) \frac{1}{l^2} \frac{1}{l_{x_1}^2} \frac{1}{l_{x_1 p q}^2} \phi_{x_1 | a_1} \phi_{p | a_2} \phi_{q | a_3} \phi_{x_2 | a_4}. \quad (3.37)$$

This term merged  $\{p\}$  and  $\{q\}$  into a single subset  $\{p, q\}$ , and its numerator can be expressed as  $(-\frac{1}{2}) \phi_{x_1 | a_1} (\tilde{J}(p) \cdot \tilde{J}(q)) \phi_{x_2 | a_4}$ . Thus the final expression for the partition  $\{x_1, \{p, q\}, x_2\}$  is given by

$$\phi_{x_1 | a_1} \left[ \tilde{J}(p, q) \cdot X_{\{p, q\}} + \left(-\frac{1}{2}\right) (\tilde{J}(p) \cdot \tilde{J}(q)) \right] \phi_{x_2 | a_4} \frac{1}{l^2} \frac{1}{l_{x_1}^2} \frac{1}{l_{x_1 p q}^2}. \quad (3.38)$$

The contributions of all triangle diagrams can then be collected as

$$\begin{aligned} & \left[ \tilde{J}(p, q) \cdot X_{\{p, q\}} + \left(-\frac{1}{2}\right) (\tilde{J}(p) \cdot \tilde{J}(q)) \right] \frac{\phi_{x_1 | a_1} \phi_{x_2 | a_4}}{l^2 l_{x_1}^2 l_{x_1 p q}^2} + \left[ \tilde{J}(p, q) \cdot X_{\{p, q\}} + \left(-\frac{1}{2}\right) (\tilde{J}(p) \cdot \tilde{J}(q)) \right] \frac{\phi_{x_1 | a_1} \phi_{x_2 | a_2}}{l^2 l_{x_1}^2 l_{x_1 x_2}^2} \\ & + \left[ \frac{(\tilde{J}(p) \cdot X_p)(\tilde{J}(q) \cdot X_q)}{l^2 l_{x_1 x_2}^2 l_{x_1 x_2 p}^2} \phi_{x_1 x_2 | a_1 a_2} + \frac{(\tilde{J}(p) \cdot X_p)(\tilde{J}(q) \cdot X_q)}{l^2 l_{x_2 x_1}^2 l_{x_2 x_1 p}^2} \phi_{x_2 x_1 | a_1 a_2} + \frac{\tilde{J}(x_1, p)(\tilde{J}(q) \cdot X_q)}{l^2 l_{x_1 p}^2 l_{x_1 p x_2}^2} \phi_{x_2 | a_3} \right. \\ & \left. + \frac{\tilde{J}(x_1, p)(\tilde{J}(q) \cdot X_q)}{l^2 l_{x_1 p}^2 l_{x_1 p q}^2} \phi_{x_2 | a_4} + \frac{\tilde{J}(x_2, p)(\tilde{J}(q) \cdot X_q)}{l^2 l_{x_1}^2 l_{x_1 x_2 p}^2} \phi_{x_1 | a_1} + (p \leftrightarrow q) \right] + \text{cyc}(a_1 a_2 a_3 a_4), \quad (3.39) \end{aligned}$$

where the  $X_{\{p,q\}}^\mu$  denote the momentum of the propagator attached to the subset  $\{p, q\}$  from left. Particularly,  $X_{\{p,q\}}^\mu = l_{x_1}^\mu$  and  $X_{\{p,q\}}^\mu = l_{x_1 x_2}^\mu$  for the first and the second squarebrackets. The first two terms on the second line cancel out due to the  $U(1)$ -decoupling identity.

Third, partitions containing two subsets provide bubble diagrams. There are also three possibilities here and the final results can be collected following discussions similar to the above:

- There exists a three-element subset which contains both gluons and scalars. For example, the contribution of the partition  $\{\{x_1, p, q\}, x_2\}$  is

$$\begin{aligned} \tilde{J}(x_1, p, q) \phi_{x_2|a_4} \frac{1}{l_{x_1 p q}^2} = & \left[ (-k_p \cdot k_{x_1})(\epsilon_q \cdot \epsilon_p) \phi_{x_1 p q|a_1 a_2 a_3} + (\epsilon_p \cdot k_{x_1})(\epsilon_q \cdot k_p) \phi_{x_1 p q|a_1 a_2 a_3} \right. \\ & \left. + (\epsilon_q \cdot k_{x_1})(\epsilon_p \cdot k_q) \phi_{x_1 q p|a_1 a_2 a_3} + (\epsilon_p \cdot k_{x_1})(\epsilon_q \cdot k_{x_1}) \phi_{x_1 \{p\} \sqcup \{q\}|a_1 a_2 a_3} \right] \frac{\phi_{x_2|a_4}}{l_{x_1 p q}^2}. \end{aligned} \quad (3.40)$$

The effective current  $\tilde{J}(x_1, p, q)$  is generated by the refined graphic rule where  $x_1$  plays as root. Another example is given by the sum of terms with respect to partitions  $\{\{x_1, x_2, p\}, q\}$ ,  $\{\{x_2, x_1, p\}, q\}$

$$\tilde{J}(x_1, x_2, p) \phi_{q|a_4} \frac{1}{l_{x_1 x_2 p}^2} + \tilde{J}(x_2, x_1, p) \phi_{q|a_4} \frac{1}{l_{x_1 x_2 p}^2} \quad (3.41)$$

which vanishes due to  $U(1)$ -decoupling identity.

- There exist two-element subsets, one containing two scalars and one containing two gluons, i.e., the partition  $\{\{x_1, x_2\}, \{p, q\}\}$ . Although the contribution of this partition has to vanish due to the  $U(1)$ -decoupling identity, we express it formally as

$$\left( \sum_{\text{cyc}(x_1 x_2)} \phi_{x_1 x_2|a_1 a_2} \right) \left[ \tilde{J}(p, q) \cdot X_{\{p,q\}} + \left( -\frac{1}{2} \right) (\tilde{J}(p) \cdot \tilde{J}(q)) \right] \frac{1}{l^2} \frac{1}{l_{x_1 x_2}^2}. \quad (3.42)$$

- There exist two-element subsets, each containing a scalar and a gluon. For instance the partition  $\{\{x_1, p\}, \{x_2, q\}\}$  gives the quadratic-propagator term

$$\tilde{J}(x_1, p) \tilde{J}(x_2, q) \frac{1}{l^2} \frac{1}{l_{x_1 p}^2}. \quad (3.43)$$

The nonvanishing contribution of all bubble diagrams is given by

$$\tilde{J}(x_1, p, q) \phi_{x_2|a_4} \frac{1}{l_{x_1 p q}^2} + \tilde{J}(x_2, p, q) \phi_{x_1|a_4} \frac{1}{l_{x_1 p}^2} + \left[ \tilde{J}(x_1, p) \tilde{J}(x_2, q) \frac{1}{l^2} \frac{1}{l_{x_1 p}^2} + (p \leftrightarrow q) \right] + \text{cyc}(a_1 a_2 a_3 a_4). \quad (3.44)$$

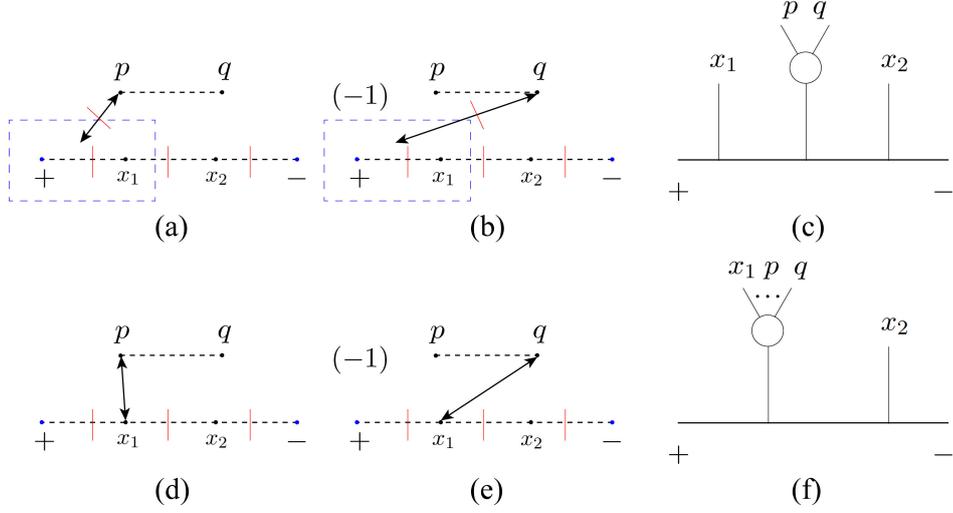


**Figure 20.** The graphs (a) and (b) together provide an X-pattern with respect to the Feynman diagram (c). The graphs (d) and (e) together provide a BCJ-pattern with respect to the Feynman diagram (f).

Last, the partition with all particles involved in a single subset corresponds to a tadpole diagram. Although the tadpole diagram has to vanish due to  $U(1)$ -decoupling identity, we also display the explicit quadratic-propagator expression along our approach

$$\tilde{J}(x_1, x_2, p, q) \frac{1}{l^2} + \text{cyc}(x_1 x_2) + \text{cyc}(a_1 a_2 a_3 a_4). \quad (3.45)$$

Here the effective current  $\tilde{J}(x_1, x_2, p, q)$  is generated by graphs where scalars  $x_1$  and  $x_2$  are considered as roots.

Now let us summarize the final expression:

$$I^{1\text{-loop}}(x_1, x_2 || \{p, q\}) \cong \sum_{\{A_1, A_2, \dots, A_I\}} \frac{1}{l^2} J[A_1] \frac{1}{l_{A_1}^2} J[A_2] \cdots \frac{1}{l_{A_1 \dots A_{I-1}}^2} J[A_I] + \text{cyc}(a_1 a_2 a_3 a_4), \quad (3.46)$$

where we summed over all possible cyclic partitions  $\{A_1, A_2, \dots, A_I\}$  ( $I = 1, \dots, 4$ ) of external particles  $x_1, x_2, p, q$ . The subcurrent  $J[A_i]$  is given by

$$\begin{aligned} J[A_i] &= \tilde{J}(A_i), & (\text{if } A_i \text{ contains scalars}) \\ J[A_i] &= \tilde{J}(A_i) \cdot X_{A_i} + \left(-\frac{1}{2}\right) \left[ \tilde{J}(A_{iL}) \cdot \tilde{J}(A_{iR}) \right], & (\text{if } A_i \text{ contains only gluons}) \end{aligned} \quad (3.47)$$

where  $\tilde{J}(A_i)$  (or  $\tilde{J}^\mu(A_i)$ ) denotes the effective current generated by the refined graphic rule,  $X_{A_i}^\mu$  is the momentum of the loop propagator to the left of the subset  $A_i$ . When  $A_i$  contains only scalars,  $\tilde{J}(A_i)$  becomes a pure scalar current  $\phi_{A_i|\tilde{A}_i}$ . The effective currents  $\tilde{J}^\mu(A_{iL})$  and  $\tilde{J}^\mu(A_{iR})$  denote the polarizations  $\epsilon_p^\mu$  and  $\epsilon_q^\mu$ , respectively.

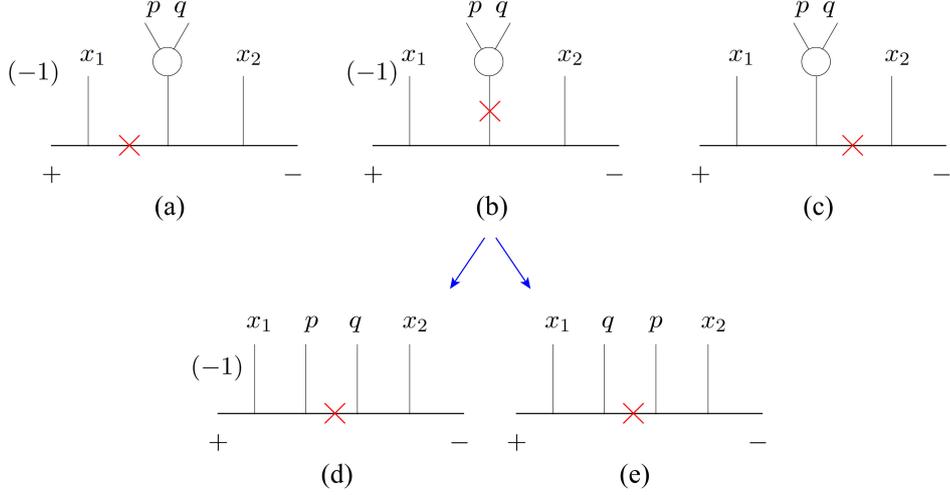


**Figure 21.** The X-pattern Fig. 20 (a), (b) reduces the Feynman diagram Fig. 20 (c) to (a), (b) and (c) by deleting the corresponding propagators. The diagram (b) is further reduced into (d) and (e), when the BG recursion for tree-level BS current is considered.

## 4 X-pattern and BCJ-pattern

In the previous section, we have defined X-pattern and BCJ-pattern, which respectively contain a  $k_A \cdot X_A$  factor and a substructure of off-shell BCJ relation (2.32). In the example, we have already seen that the subgraph with node  $p$  in Fig. 16 (b) (for the Feynman diagram Fig. 16 (c)), and the subgraphs with nodes  $p, x_1$  in Fig. 19 (a) and  $p, x_2$  in Fig. 19 (c) (for the Feynman diagrams Fig. 19 (b) and (d)) are respectively X-pattern and BCJ-patterns. The cancellations between X- and BCJ-patterns in the example play a crucial role for treating the nonlocal terms. In the current section, we show more examples and summarize the general features of graphs corresponding to X- and BCJ-pattern.

### 4.1 Example-1

The first example is shown by Fig. 20. In Fig. 20, both graphs (a) and (b) contain a subgraph with  $p$  and  $q$ , which correspondingly provide factors  $(-k_p \cdot X_p)\phi_{pq|a_2a_3}$ ,  $(k_q \cdot X_q)\phi_{qp|a_2a_3}$  for the Feynman diagram Fig. 20 (c). When the graph-based relation (2.31) is applied, the factor for Fig. 20 (b) turns into  $(-k_q \cdot X_{\{p,q}\})\phi_{pq|a_2a_3}$ , noting that  $X_{\{p,q}}$  which denotes the momentum of the linear propagator attached to the subset  $\{p, q\}$  from left is the same with the  $X_p$  and  $X_q$  for Fig. 20 (a) and (b). Thus the total factor of Fig. 20 (a) and (b) becomes  $[-(k_p + k_q) \cdot X_{\{p,q}\}]\phi_{pq|a_2a_3}$  accompanying to the subcurrent containing  $p, q$  in the Feynman diagram Fig. 20 (c). This agrees with the definition of X-pattern. According to (3.25) (or equivalently Fig. 18), Fig. 20 (c) is reduced into the three diagrams Fig. 21 (a), (b) and (c), in which, we have correspondingly deleted the linear propagator to the left of  $\{p, q\}$ , the propagator of the tree structure containing  $\{p, q\}$  and the linear propagator to the right of  $\{p, q\}$ . When the definition of the BG current for BS (2.29) is considered, Fig. 21 (b) is further reduced into Fig. 21 (d) and (e). The sum of diagrams

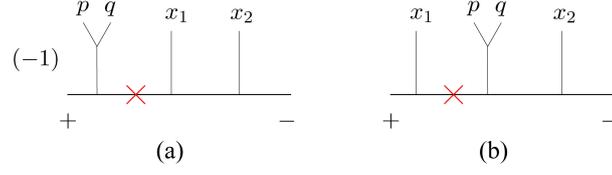


**Figure 22.** When the off-shell BCJ relation is applied, the diagram Fig. 20 (f) accompanied by the BCJ-pattern Fig. 20 (d), (e) is further reduced into graphs (a) and (b).

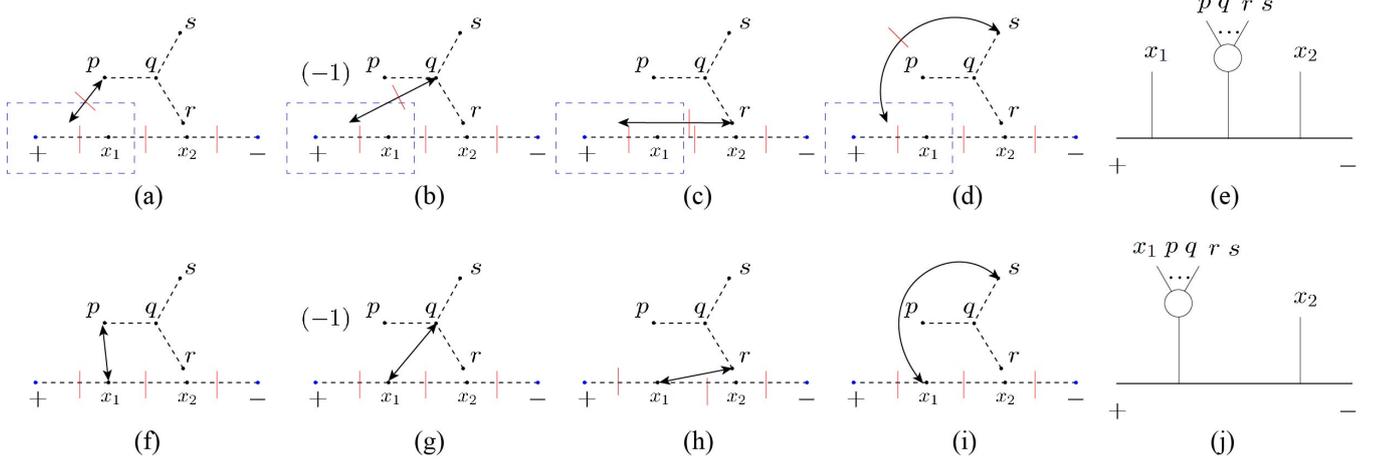


**Figure 23.** Graphs (a)-(d) provide an X-pattern for the Feynman diagram (e), while graphs (f)-(i) provide a BCJ-pattern for the diagram (j).

Fig. 21 (a), (c), (d), (e) is then given by

$$\left(-\frac{1}{2}\right) \left[ (-1) \frac{1}{l^2} \frac{1}{s_{x_1 p q, l}} \phi_{x_1|a_1} \phi_{p q|a_2 a_3} \phi_{x_2|a_4} + \frac{1}{l^2} \frac{1}{s_{x_1, l}} \phi_{x_1|a_1} \phi_{p q|a_2 a_3} \phi_{x_2|a_4} \right. \\ \left. + (-1) \frac{1}{l^2} \frac{1}{s_{x_1, l}} \frac{1}{s_{x_1 p q, l}} \phi_{x_1|a_1} \phi_{p|a_2} \phi_{q|a_3} \phi_{x_2|a_4} + \frac{1}{l^2} \frac{1}{s_{x_1, l}} \frac{1}{s_{x_1 p q, l}} \phi_{x_1|a_1} \phi_{q|a_2} \phi_{p|a_3} \phi_{x_2|a_4} \right]. \quad (4.1)$$

Associating with the X-pattern shown by Fig. 20 (a), (b), the graphs Fig. 20 (d), (e), (each of which involves a subgraph where  $p$  or  $q$  is connected to scalar  $x_1$ ) together provide a BCJ-pattern since the sum of these contributions is the LHS of the off-shell BCJ relation (2.32):

$$(-k_p \cdot k_{x_1}) \phi_{x_1 p q|a_1 a_2 a_3} - (-k_q \cdot k_{x_1}) \phi_{x_1 q p|a_1 a_2 a_3}. \quad (4.2)$$

According to the off-shell BCJ relation (2.32), the above expression becomes

$$\left(-\frac{1}{2}\right) [-\phi_{p q|a_1 a_2} \phi_{x_1|a_3} + \phi_{x_1|a_1} \phi_{p q|a_2 a_3}]. \quad (4.3)$$

The two terms can be expressed by Fig. 22 (a) and (b), respectively.

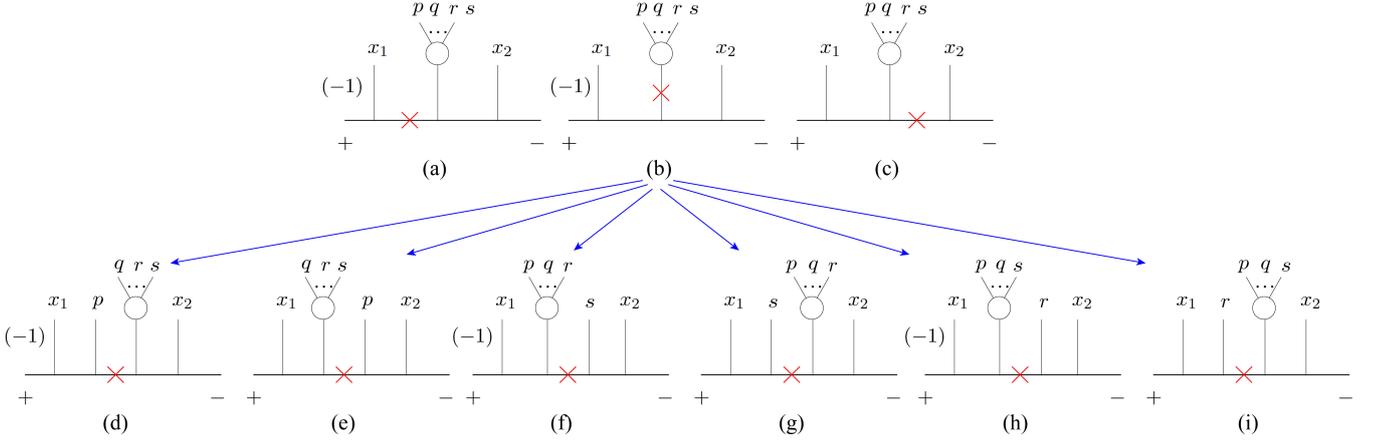


**Figure 24.** The property Fig. 18, together with the X-pattern Fig. 23 (a)-(d) reduces the Feynman diagram Fig. 23 (e) into (a), (b) and (c). The BG recursion for BS current further reduces the diagram (b) into diagrams (d)-(i).

## 4.2 Example-2

The second example is presented by Fig. 23. The graphs Fig. 23 (a), (b), (c) and (d), associating with the subcurrent containing  $p, q, r, s$  in the Feynman diagram Fig. 23 (e) respectively contribute

$$\begin{aligned}
& (-k_p \cdot X_{\{p,q,r,s\}}) \phi_{pq\{s\}\sqcup\{r\}|a_2a_3a_4a_5}, \quad -(-k_q \cdot X_{\{p,q,r,s\}}) \phi_{q\{p\}\sqcup\{s\}\sqcup\{r\}|a_2a_3a_4a_5}, \\
& (-k_r \cdot X_{\{p,q,r,s\}}) \phi_{rq\{p\}\sqcup\{s\}|a_2a_3a_4a_5}, \quad (-k_s \cdot X_{\{p,q,r,s\}}) \phi_{sq\{p\}\sqcup\{r\}|a_2a_3a_4a_5},
\end{aligned} \tag{4.4}$$

where  $X_{\{p,q,r,s\}}^\mu = l^\mu + k_{x_1}^\mu$  is the momentum of the linear propagator attached to the subcurrent containing  $p, q, r, s$  from left. When the graph-based relation (2.31) is applied to Fig. 23 (b), (c) and (d), the four terms can be collected into

$$-(k_p + k_q + k_r + k_s) \cdot X_{\{p,q,r,s\}} \phi_{pq\{s\}\sqcup\{r\}|a_2a_3a_4a_5}, \tag{4.5}$$

therefore agrees with the definition of X-pattern. Once the property of X-pattern (as shown by Fig. 18) is considered, the Feynman diagram Fig. 23 (e) turns into the three diagrams Fig. 24 (a), (b), (c). In the diagram Fig. 24 (b), the off-shell line of the subcurrent is deleted, hence it further splits into products of two subcurrents. This can be represented by the diagrams Fig. 24 (d)-(i), whose expressions respectively contain

$$\begin{aligned}
& \frac{1}{2} \phi_{p|a_2} \phi_{q\{r\}\sqcup\{s\}|a_3a_4a_5}, & \left(-\frac{1}{2}\right) \phi_{q\{r\}\sqcup\{s\}|a_2a_3a_4} \phi_{p|a_5}, \\
& \frac{1}{2} \phi_{pqr|a_2a_3a_4} \phi_{s|a_5}, & \left(-\frac{1}{2}\right) \phi_{s|a_2} \phi_{pqr|a_3a_4a_5}, \\
& \frac{1}{2} \phi_{pqs|a_2a_3a_4} \phi_{r|a_5}, & \left(-\frac{1}{2}\right) \phi_{r|a_2} \phi_{pqs|a_3a_4a_5}.
\end{aligned} \tag{4.6}$$

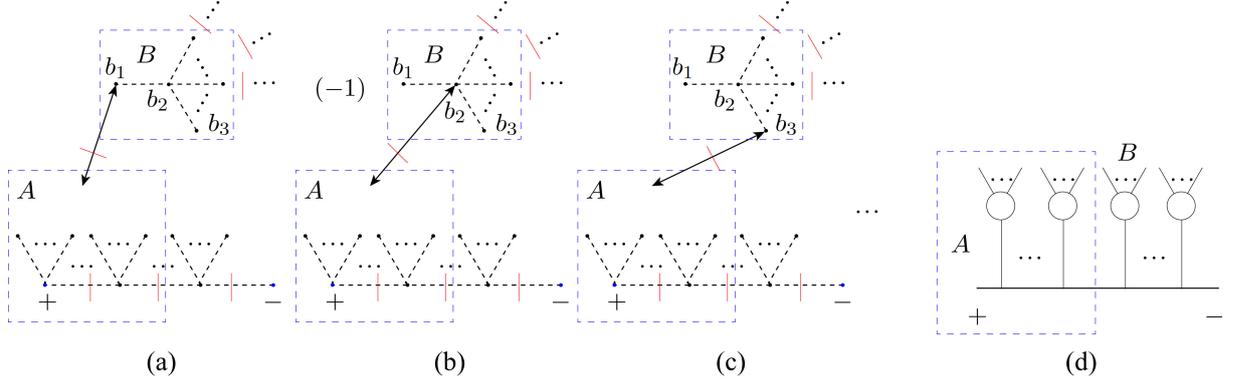


**Figure 25.** Graphs (a), (b), (c), ... together provide an X-pattern, associating with the Feynman diagram (d) where all elements in  $B$  are contained in a single subcurrent.

Note that there also exist terms  $\frac{1}{2}\phi_{pq|a_2a_3}\phi_{\{r\}\sqcup\{s\}|a_4a_5}$ , and  $(-\frac{1}{2})\phi_{\{r\}\sqcup\{s\}|a_2a_3}\phi_{pq|a_4a_5}$ , but these two terms have to vanish due to  $U(1)$ -decoupling identity. The graphs Fig. 23 (f)-(i) provide the LHS of off-shell BCJ relation for the subcurrent involving  $x_1, p, q, r, s$  in Fig. 23 (j):

$$\begin{aligned}
& (-k_p \cdot k_{x_1})\phi_{x_1pq\{r\}\sqcup\{s\}|a_1a_2a_3a_4a_5} - (-k_q \cdot k_{x_1})\phi_{x_1q\{p\}\sqcup\{r\}\sqcup\{s\}|a_1a_2a_3a_4a_5} \\
& + (-k_r \cdot k_{x_1})\phi_{x_1rq\{p\}\sqcup\{s\}|a_1a_2a_3a_4a_5} + (-k_s \cdot k_{x_1})\phi_{x_1sq\{p\}\sqcup\{r\}|a_1a_2a_3a_4a_5}.
\end{aligned} \tag{4.7}$$

According to the off-shell BCJ relation (2.32), the above expression is given by

$$\left(-\frac{1}{2}\right) [\phi_{x_1|a_2}\phi_{pq\{r\}\sqcup\{s\}|a_2a_3a_4a_5} - \phi_{pq\{r\}\sqcup\{s\}|a_1a_2a_3a_4}\phi_{x_1|a_5}]. \tag{4.8}$$

### 4.3 General X- and BCJ-pattern

Now we are ready for extracting the general features of X- and BCJ-patterns from the two examples.

In general, an *X-pattern* occurs in a set of graphs  $\{\mathcal{F}_i\}$  if the following conditions are satisfied:

- (i). All graphs in  $\{\mathcal{F}_i\}$  contain two *connected subtree structures*  $A$  and  $B$  which are interconnected via a type-3 (i.e.,  $k_a \cdot k_b$ ) line for all  $(a, b)$  ( $a \in A, b \in B$ ) pairs, as shown by Fig. 25 (a), (b), (c), ... The node  $+$  belongs to the subtree structure  $A$ .
- (ii). Each graph is associated with a sign which relies on the choice of node  $b \in B$ . Particularly, the relative signs for two graphs  $\mathcal{F}_i$  and  $\mathcal{F}_j$  is given by  $(-1)^d$ , where  $d$  is the distance between nodes  $b_i$  and  $b_j$  (which are the choices of nodes  $b \in B$  in graphs  $\mathcal{F}_i$  and  $\mathcal{F}_j$ , respectively).
- (iii). All graphs in  $\{\mathcal{F}_i\}$  are identical when the line between  $A, B$  in each graph is removed. Each graph corresponds to a choice of  $(a, b)$  pair, and graphs for all choices of  $(a, b)$  pairs form the full set  $\{\mathcal{F}_i\}$ .

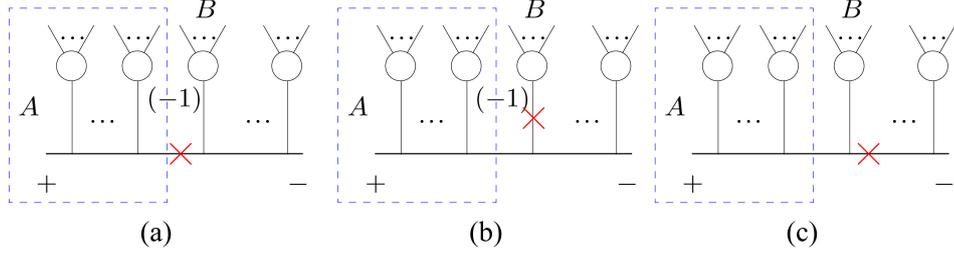


**Figure 26.** When the property of X-pattern shown by Fig. 18 is applied, Fig. 25 (d) splits into three diagrams (a), (b) and (c).

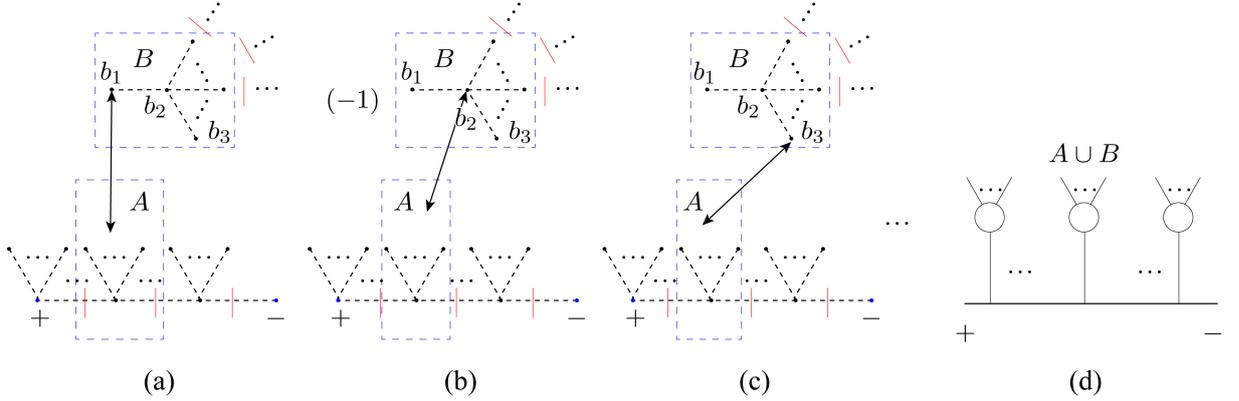


**Figure 27.** The graphs (a), (b), (c)... provide a BCJ-pattern for the Feynman diagram (d), in which elements in  $A \cup B$  are contained by a single subcurrent.

Now we associate each graph  $\mathcal{F}_i$  with the Feynman diagram Fig. 25 (d), where all elements in  $B$  are contained by a subcurrent  $\phi_{(\sigma^B|_{b_i})|\tilde{B}}$  ( $\sigma^B|_{b_i}$  denotes the permutations established by graph  $B$  when the node  $b_i \in B$  is chosen as the leftmost element in  $B$ ), and all elements in  $A$  are contained by the full subtree structure to the left of  $B$ . For a given choice of  $b = b_i \in B$ , the graphs with different choices of  $a \in A$  can be collected together to produce a factor  $-k_{b_i} \cdot X_B$  (where  $X_B^\mu$  is the total momentum of nodes in the region  $A$ , in each of Fig. 25 (a), (b), (c)...), or in other words, the momentum of the linear propagator attached to  $B$  in the Feynman diagram Fig. 25 (d) from left). When the graph-based relation (2.31) is further applied, the sum of these terms (up to an overall sign) can be transformed as follows

$$\begin{aligned}
& (-k_{b_1} \cdot X_B) \phi_{(\sigma^B|_{b_1})|\tilde{B}} + (-1)^{d_2} (-k_{b_2} \cdot X_B) \phi_{(\sigma^B|_{b_2})|\tilde{B}} + (-1)^{d_3} (-k_{b_3} \cdot X_B) \phi_{(\sigma^B|_{b_3})|\tilde{B}} + \dots \\
& = \left[ -(k_{b_1} + k_{b_2} + k_{b_3} + \dots) \cdot X_B \right] \phi_{(\sigma^B|_{b_1})|\tilde{B}}, \tag{4.9}
\end{aligned}$$

where  $d_2, d_3, \dots$  are distances between  $b_2, b_3, \dots$  and  $b_1$ , respectively. On the second line, all subcurrents with permutations  $\sigma^B|_{b_i}$  are transformed into the subcurrent with permutation  $\sigma^B|_{b_1}$ , and the coefficients are precisely collected as  $-k_B \cdot X_B$ . This agrees with the definition of X-pattern. Hence, the Feynman diagram further splits into Fig. 26 (a), (b) and (c).

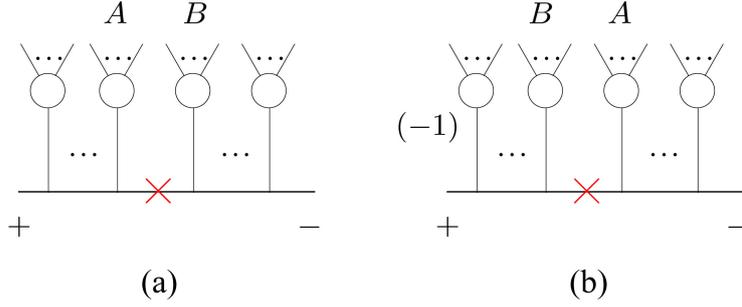


**Figure 28.** Off-shell BCJ relation further reduces Fig. 27 (d) into the two diagrams (a) and (b).

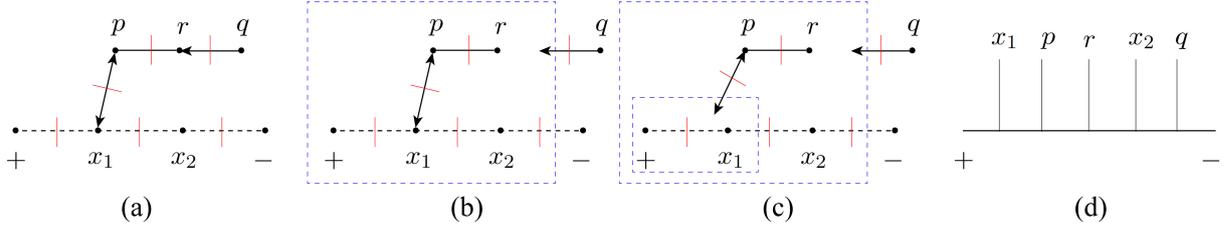


**Figure 29.** Graph (a) induces nonlocalities by the line between nodes  $q, r$ , nodes  $p, x_1$  as well as the nodes  $p, r$ , for the Feynman diagram (d). The nonlocality caused by the line between  $q, r$  can be overcome by collecting all related contributions as shown by (b), while the nonlocality caused by the line between  $p$  and  $x_1$  is further treated in a similar way, as shown by (c). These treatments follow from approach-1.

The general BCJ-pattern is characterized by Fig. 27. Concretely, each graph Fig. 27 (a), (b), (c)... contains a subgraph where  $A$  is connected with  $B$  via a type-3 line. If  $b_i$  and  $b_j$  are two adjacent nodes (e.g. the  $b_1$  and  $b_2$ ), the signs associating with graphs  $b = b_i$  and  $b = b_j$  must be opposite. When the kinematic coefficient  $-k_a \cdot k_b$  and the relative sign are dressed, the sum of all such graphs produce the LHS of the off-shell BCJ relation (2.32). Then we arrive at

$$\left(-\frac{1}{2}\right) \left[ \phi_{\sigma^A} | \tilde{C}_L \phi_{(\sigma^B|_{b_1})} | \tilde{C}_R - \phi_{(\sigma^B|_{b_1})} | \tilde{C}_L \phi_{\sigma^A} | \tilde{C}_R \right], \quad (4.10)$$

where  $\tilde{C} = \tilde{C}_L \tilde{C}_R$  denotes a fixed permutation of elements in  $A \cup B$  for the right side. The above two terms are respectively characterized by the diagrams Fig. 28 (a) and (b).

## 5 Spurious graphs and five-point integrand with three gluons

In the YMS amplitudes with more than two gluons, the two approaches in section 3.3 and section 3.4 can be combined to cancel nonlocal terms. However, these approaches are not sufficient for treating all nonlocal terms produced by graphic rule in the cases with more than two gluons. To complete the cancellation of nonlocalities, we have to introduce pairs of *spurious graphs* with opposite signs. Once the spurious graphs are included, the nonlocal terms can always be arranged into forms that can further be treated via approach-1 and -2. In this section, we use five-point example with three gluons  $p, q, r$  (with the

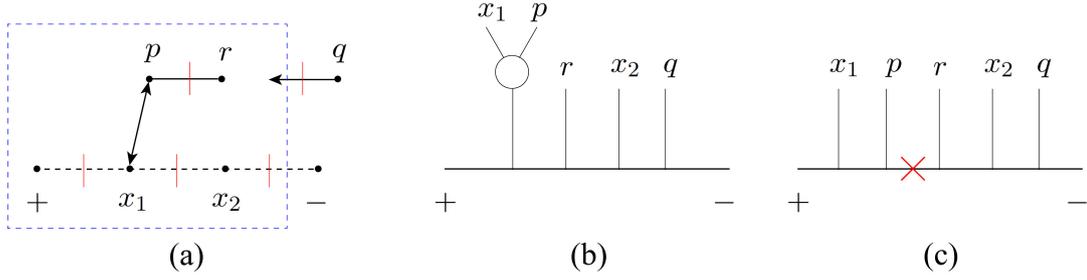


**Figure 30.** Graph (a) contains a BCJ-pattern, the subgraph with  $x_1$  and  $p$ , for the diagram (b). When the cancellation between the X-pattern Fig. 29 (c) and the BCJ-pattern (a) is performed, we get the diagram (c) which comes from the X-pattern in Fig. 29 (c).

reference order  $p \prec q \prec r$ ) and two scalars  $x_1, x_2$  to demonstrate this new mechanism. We further collect terms corresponding to a given partition of external particles, and propose a compact formula expressed by effective currents.

### 5.1 Five-point example and spurious graphs

The first example for combining the two approaches is the graph Fig. 29 (a) accompanied to the Feynman diagram Fig. 29 (d) with the partition  $\{x_1, p, r, x_2, q\}$ . The subgraphs  $q$  and  $r$  in Fig. 29 (a) are contracted via a line  $\epsilon_q \cdot k_r$ , but they are separated by the linear propagators between them in Fig. 29 (d), thus this contribution is exactly a nonlocal one. Nevertheless, one can follow *approach-1*, by collecting other corresponding contributions with  $\epsilon_q \cdot k$ , all graphs together (as shown by Fig. 29 (b)) produce a total factor  $\epsilon_q \cdot X_q = \epsilon_q \cdot (l + k_{x_1} + k_p + k_r + k_{x_2})$ . This factor is expressed by the contraction of  $\epsilon_q^\mu$  with the momentum of the linear propagator  $\frac{1}{s_{x_1 p r x_2, l}}$  attached to the subcurrent  $q$ , hence this nonlocality has been canceled. Similarly, for the graph Fig. 29 (b), the nonlocality caused by  $-k_p \cdot k_{x_1}$  can also be treated by considering the graph where  $p$  is connected to  $+$  via  $-k_p \cdot l$ . Thus the factors are summed into  $-k_p \cdot X_p$ , as shown by Fig. 29 (c).

Though the nonlocalities caused by  $-k_p \cdot k$  and  $\epsilon_q \cdot k$  have already been rearranged into local contributions, the nonlocality caused by the type-1 line between  $p$  and  $q$  cannot be dealt with in this way. We have to follow *approach-2*. To see this, we find that the factor  $-k_p \cdot X_p$  in Fig. 29 (c) also indicates an X-pattern for the gluon  $p$ . The corresponding BCJ-pattern is shown by Fig. 30 (a), associated with the diagram Fig. 30 (b). When the cancellation between X- and BCJ-pattern has been carried out, the surviving term of X-pattern reads

$$\left(-\frac{1}{2}\right) \frac{1}{l^2} \frac{1}{s_{x_1, l}} \frac{1}{s_{x_1 p r, l}} \frac{1}{s_{x_1 p r x_2, l}} (\epsilon_p \cdot \epsilon_r) (\epsilon_q \cdot X_q) \phi_{x_1|a_1} [\phi_{p|a_2} \phi_{r|a_3}] \phi_{x_2|a_4} \phi_{q|a_5}, \quad (5.1)$$

which is expressed by the diagram Fig. 30 (c) and does not have any nonlocality. The cyclic permutations of  $(a_1 a_2 a_3 a_4 a_5)$  and  $(x_1 x_2)$  together with graphic rule allow the cyclic summation of the subcurrents separated by the linear propagators in the above expression. Using (2.27), we get the final expression with quadratic

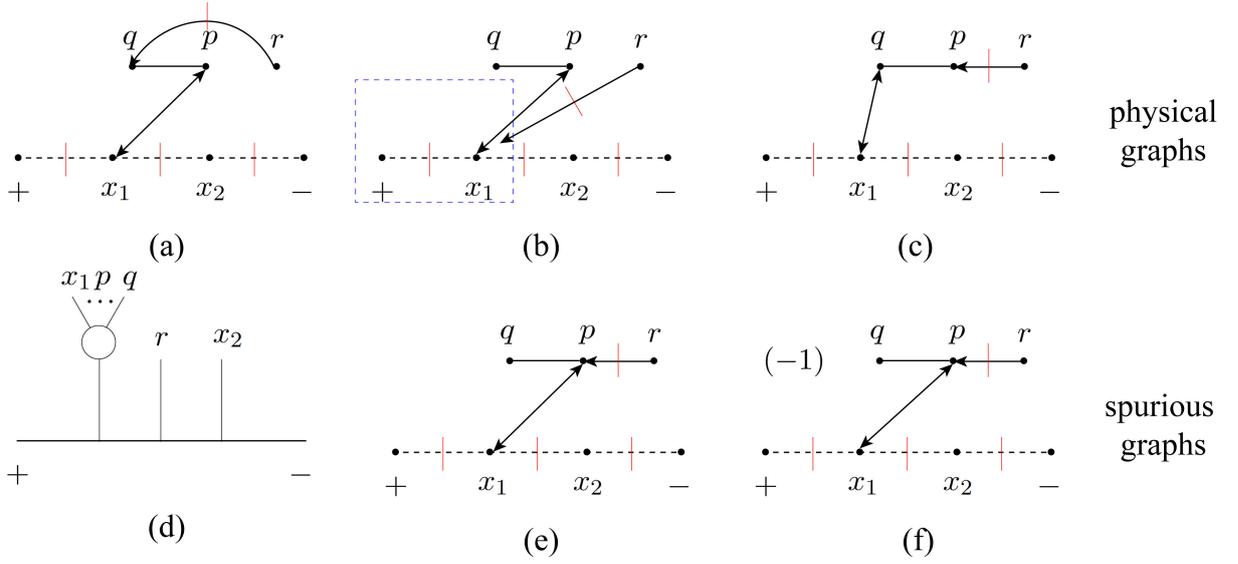


**Figure 31.** The nonlocalities of graphs (a), (b) and (c), accompanied to the diagram (d), cannot be treated via approach-1 or -2. This is a consequence of the graphic rule with reference order. To remedy this shortcoming, we introduce a pair of spurious graphs (e) and (f) with opposite signs.

propagators

$$\left(-\frac{1}{2}\right) \frac{1}{l^2} \frac{1}{l_{x_1}^2} \frac{1}{l_{x_1 p r}^2} \frac{1}{l_{x_1 p r x_2}^2} (\epsilon_p \cdot \epsilon_r) (\epsilon_q \cdot X_q) \phi_{x_1|a_1} [\phi_{p|a_2} \phi_{r|a_3}] \phi_{x_2|a_4} \phi_{q|a_5}. \quad (5.2)$$

The above approach cannot always be applied straightforwardly. In some situations, the physical graphs (graphs defined by the graphic rule) may neither be collected together to cancel the nonlocality, nor contain complete BCJ- or X-pattern. Thus their nonlocal contributions cannot be canceled by directly combining the two approaches. To treat this new situation, we should introduce *spurious graphs*. Let us begin with the graphs Fig. 31 (a), (b) and (c) which associate to the Feynman diagram with linear propagators Fig. 31 (d). Fig. 31 (a) and (b) provide nonlocal terms since each includes a factor  $\epsilon_r \cdot k_i$  but  $r$  and  $i$  ( $q$  for (a),  $+$ ,  $x_1$  for (b)) are separated by the linear propagator  $\frac{1}{s_{x_1 p q, l}}$ . One may try to collect such nonlocal contributions to get an  $\epsilon_r \cdot X_r$ , but the graphic rule does not allow Fig. 31 (e) which contains the factor  $\epsilon_r \cdot k_p$ . On the other hand, one may try to cancel the nonlocality accompanied to Fig. 31 (c) following the approach-2: the cancellation between BCJ-pattern and X-pattern (apparently approach-1 is ineffective for this graph because the subgraph containing  $x_1$ ,  $p$ ,  $q$  is not a physical graph defined by graphic rule). However, it is still lack of a graph Fig. 31 (f) for a complete BCJ-pattern. To overcome the obstacles mentioned above, we add a pair of graphs Fig. 31 (e) and (f), which are the same spurious graphs but have opposite signs. Though these graphs are not allowed by graphic rule, they cancel each

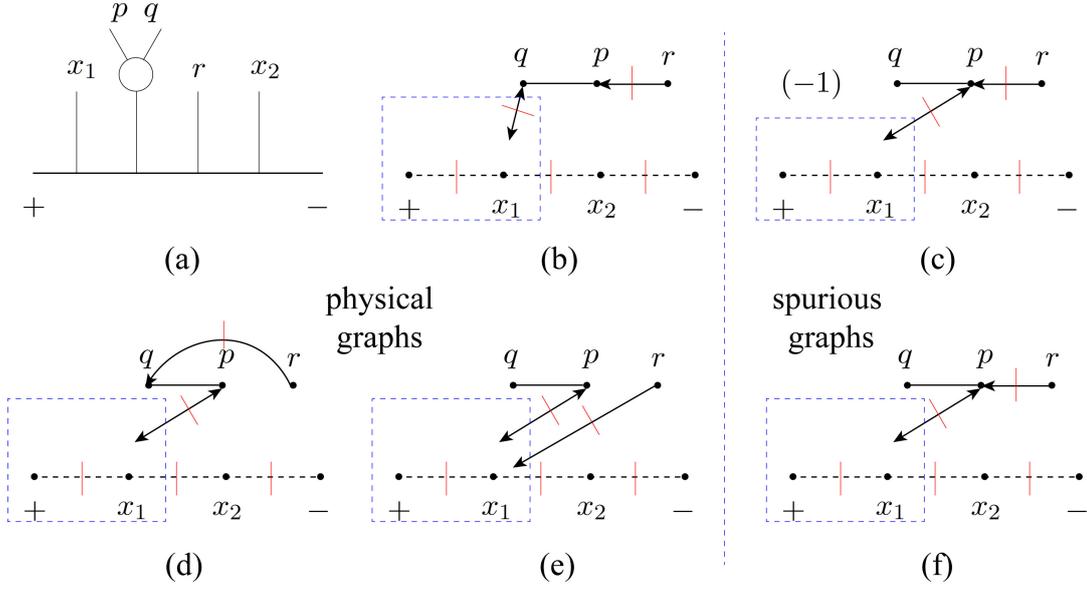


**Figure 32.** Graphs (b), (d) and (e) are physical graphs for diagram (a). A pair of spurious graphs (c) and (f) are introduced. Graphs (b) and (c) provide an X-pattern for (a), thus the nonlocality can be treated according to approach-2. Graphs (d), (e) and (f) can be collected together so that a factor  $\epsilon_r \cdot X_r$  arises and cancels the related nonlocality according to approach-1.

other. Now the sum of graphs Fig. 31 (a), (b) and (e) provides

$$\frac{1}{l^2} \frac{1}{s_{x_1 p q, l}} \frac{1}{s_{x_1 p q r, l}} (\epsilon_p \cdot \epsilon_q) (-k_p \cdot k_{x_1}) (\epsilon_r \cdot X_r) \phi_{x_1 p q | a_1 a_2 a_3} \phi_{r | a_4} \phi_{x_2 | a_5}, \quad (5.3)$$

where  $X_r^\mu = l^\mu + k_{x_1}^\mu + k_p^\mu + k_q^\mu$  which is the momentum of the linear propagator  $\frac{1}{s_{x_1 p q, l}}$  to the left of  $r$ . Hence we have obtained a local expression. The cyclic permutations of  $(x_1 x_2)$  and  $(a_1 a_2 a_3 a_4 a_5)$  allow those terms obtained by acting cyclic permutations of the subsets. Altogether provides the quadratic propagator expression

$$\frac{1}{l^2} \frac{1}{l_{x_1 p q}^2} \frac{1}{l_{x_1 p q r}^2} (\epsilon_p \cdot \epsilon_q) (-k_p \cdot k_{x_1}) (\epsilon_r \cdot X_r) \phi_{x_1 p q | a_1 a_2 a_3} \phi_{r | a_4} \phi_{x_2 | a_5}. \quad (5.4)$$

The sum of graphs Fig. 31 (c) and (f) involves a BCJ-pattern. We therefore can find the corresponding X-pattern, the subgraphs consisting of  $q$  and  $p$  in the graphs Fig. 32 (b) and (c) accompanied to the Feynman diagram Fig. 32 (a). The graph Fig. 32 (b) is a physical graph, but Fig. 32 (c) is a spurious one. In fact, the spurious graph Fig. 32 (c) with opposite sign (see Fig. 32 (f)) is also introduced for treating the nonlocalities in Fig. 32 (d) and (e). According to the approach-2, the Feynman diagram Fig. 31 (d) with the BCJ-pattern from graphs Fig. 31 (c) and (f), has to cancel with a part of Fig. 32 (a) accompanied by the X-pattern in Fig. 32 (b) and (c), when Fig. 28 and Fig. 26 are considered. After this step, the

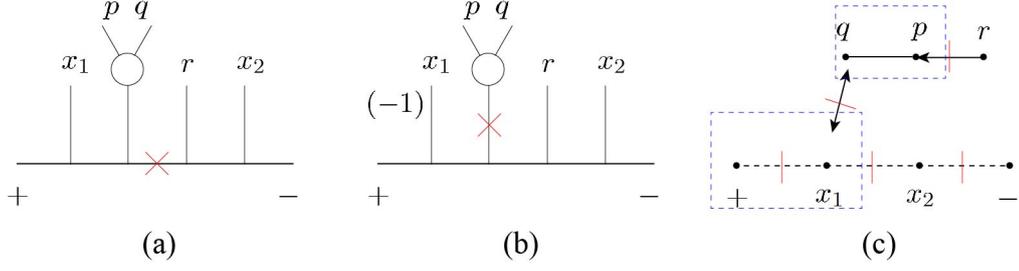


**Figure 33.** When the property Fig. 18 of X-pattern is applied, the X-pattern Fig. 32 (b) and (c) reduces the diagram Fig. 32 (a) into three terms. One of them is canceled with the BCJ-pattern Fig. 31 (c) and (f) (with respect to diagram Fig. 31 (d)), the remaining two terms are given by diagrams (a) and (b), with the coefficient  $(\epsilon_q \cdot \epsilon_p)(\epsilon_r \cdot k_p)$  coming from (c).

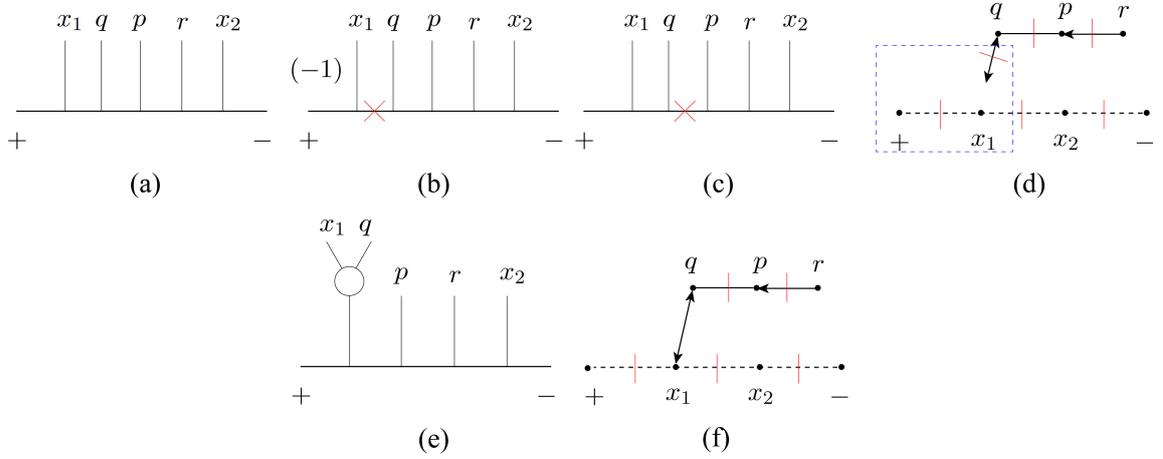


**Figure 34.** The X-pattern for the partition  $\{x_1, q, p, r, x_2\}$  is given by graph (d) for the Feynman diagram (a). This diagram splits into diagrams (b) and (c). Diagram (b) cancels with (e) accompanied by the BCJ-pattern (f).

remaining part of the diagram Fig. 32 (a) becomes the sum of diagrams Fig. 33 (a) and (b) with the coefficient defined by graph Fig. 33 (c) where the type-3 line is removed. Fig. 33 (a) produces

$$\left(-\frac{1}{2}\right) \frac{1}{l^2} \frac{1}{s_{x_1, l}} \frac{1}{s_{x_1 p q r, l}} (\epsilon_q \cdot \epsilon_p)(\epsilon_r \cdot k_p) \phi_{x_1|a_1} \left[ \phi_{q p|a_2 a_3} \phi_r|a_4 \right] \phi_{x_2|a_5}, \quad (5.5)$$

which has no nonlocal contribution now. When the cyclic permutations of  $(x_1 x_2)$  and  $(a_1 a_2 a_3 a_4 a_5)$  are considered, we get a quadratic-propagator form

$$\left(-\frac{1}{2}\right) \frac{1}{l^2} \frac{1}{l_{x_1}^2} \frac{1}{l_{x_1 p q r}^2} (\epsilon_q \cdot \epsilon_p)(\epsilon_r \cdot k_p) \phi_{x_1|a_1} \left[ \phi_{q p|a_2 a_3} \phi_r|a_4 \right] \phi_{x_2|a_5}. \quad (5.6)$$

One may notice that there remains a diagram Fig. 33 (b) which still has nonlocality. This diagram, actually cancels with Fig. 34 (c), Fig. 35 (c) which come from other two Feynman diagrams Fig. 34 (a), Fig. 35 (a) with respect to the partitions  $\{x_1, q, p, r, x_2\}$ ,  $\{x_1, p, q, r, x_2\}$  accompanied by the X-patterns

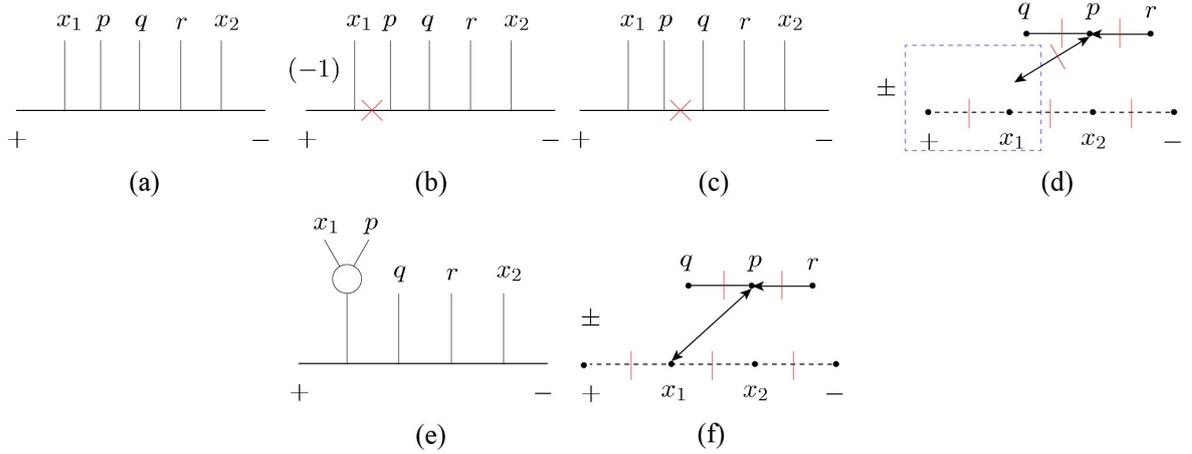


**Figure 35.** The X-pattern for the partition  $\{x_1, p, q, r, x_2\}$  is given by the spurious graph (d) (with a minus sign) for the Feynman diagram (a). This diagram splits into diagrams (b) and (c). Diagram (b) cancels with (e) accompanied by the BCJ-pattern in the spurious graph (f) (with a minus sign).

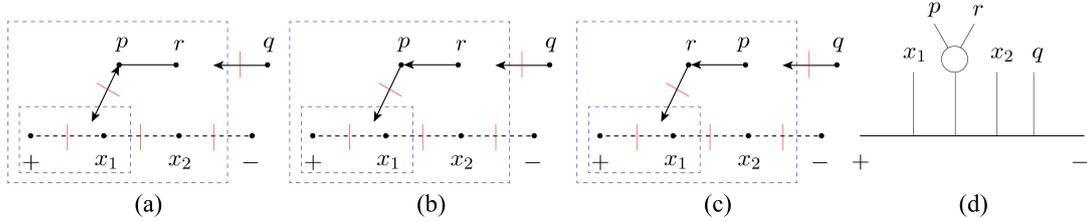


**Figure 36.** Graphs (a), (b) and (c) with respect to the Feynman diagram (d) and the graph Fig. 29 (c) with respect to diagram Fig. 30 (c) together provide all contributions to the partition  $\{x_1, \{p, r\}, x_2, q\}$ .

Fig. 34 (d) and Fig. 35 (d). The remaining parts of Fig. 34 (a), Fig. 35 (a) (i.e., Fig. 34 (b), Fig. 35 (b)), finally cancel against the diagrams Fig. 34 (e), Fig. 35 (e) with the BCJ-patterns Fig. 34 (f), Fig. 35 (f), respectively. Noting that graphs Fig. 35 (d) and (f) are spurious ones, in the above cancellations, we have used Fig. 35 (d) and (f) with minus signs. The remaining two spurious graphs with positive signs are used to cancel the nonlocalities with other graphs.

To sum up, the nonlocalities can be canceled by introducing spurious graphs and combining approach-1 and -2.

## 5.2 Compact expression of the five-point integrand with three gluons

In the previous subsection, we began with graphs associated with LPFD for a given partition of external particles, and arrived at quadratic-propagator Feynman diagrams, without nonlocality. We can always collect all contributions corresponding to a same cyclic partition in the final results. Now we demonstrate this by explicit examples.

*The first example* is the partition  $\{x_1, \{p, r\}, x_2, q\}$ , which gets contributions from (5.2) and Fig. 36 (a), (b), (c) with the Feynman diagram Fig. 36 (d). The local expression (5.2) which comes from the

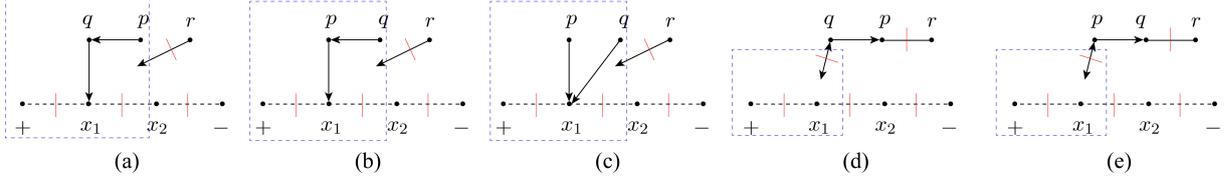


**Figure 37.** Graphs (a), (b) and (c), together with Fig. 31 (a), (b) and (e), provide all contributions to the partition  $\{\{x_1, p, q\}, r, x_2\}$ . Graphs (d) and (e) together with Fig. 33 (c) provide a contribution to the partition  $\{x_1, \{p, q, r\}, x_2\}$ , corresponding to the case with contraction  $\tilde{J}(p, q) \cdot \tilde{J}(r)$ .

cancellations between X- and BCJ-patterns have already been discussed. Fig. 36 (a), (b) and (c) with the diagram Fig. 36 (d) are collected as

$$\frac{1}{l^2} \frac{1}{l_{x_1}^2} \frac{1}{l_{x_1 p r}^2} \frac{1}{l_{x_1 p r x_2}^2} \left[ ((-k_p \cdot X_p)(\epsilon_p \cdot \epsilon_r) + (\epsilon_r \cdot k_p)(\epsilon_p \cdot X_p)) \phi_{pr|a_2 a_3} + (\epsilon_p \cdot k_r)(\epsilon_r \cdot X_r) \phi_{rp|a_2 a_3} \right] (\epsilon_q \cdot X_q) \times \phi_{x_1|a_1} \phi_{x_2|a_4} \phi_{q|a_5}. \quad (5.7)$$

In the above expression, the terms inside the square brackets can be collected as  $\tilde{J}(p, r) \cdot X_{\{p, r\}}$ , where  $\tilde{J}^\mu(p, r)$  is the effective current [37] constructed by the graphic rule, under the reference order  $p \prec r$ . The  $X_{\{p, r\}}^\mu$  is the momentum of the quadratic propagator attached to  $\tilde{J}^\mu(p, r)$  from left. The sum of (5.2) and (5.7) together provides

$$\frac{1}{l^2} \frac{1}{l_{x_1}^2} \frac{1}{l_{x_1 p r}^2} \frac{1}{l_{x_1 p r x_2}^2} \left[ \tilde{J}(p, r) \cdot X_{\{p, r\}} + \left( -\frac{1}{2} \tilde{J}(p) \cdot \tilde{J}(r) \right) \right] (\tilde{J}(q) \cdot X_q) \phi_{x_1|a_1} \phi_{x_2|a_4}, \quad (5.8)$$

where  $\epsilon_p^\mu \phi(p|a_2)$ ,  $\epsilon_r^\mu \phi(r|a_3)$  and  $\epsilon_q^\mu \phi(q|a_5)$  are also absorbed into the corresponding subcurrents  $\tilde{J}^\mu(p)$ ,  $\tilde{J}^\mu(q)$  and  $\tilde{J}^\mu(r)$ , respectively.

The second example is given by the partition  $\{\{x_1, p, q\}, r, x_2\}$ . The expression (5.4) makes a contribution to this partition, while other contributions are collected as

$$\frac{1}{l^2} \frac{1}{l_{x_1 p q}^2} \frac{1}{l_{x_1 p q r}^2} \left[ (\epsilon_p \cdot k_q)(\epsilon_q \cdot k_{x_1}) \phi_{x_1 q p|a_1 a_2 a_3} + (\epsilon_q \cdot k_p)(\epsilon_p \cdot k_{x_1}) \phi_{x_1 p q|a_1 a_2 a_3} + (\epsilon_p \cdot k_{x_1})(\epsilon_q \cdot k_{x_1}) \phi_{x_1 \{q\} \sqcup \{p\} | a_1 a_2 a_3} \right] (\epsilon_r \cdot X_r) \phi_{r|a_4} \phi_{x_2|a_5}, \quad (5.9)$$

in which, the three terms come from Fig. 37 (a), (b) and (c), respectively. The expressions (5.4) and (5.9) sum into

$$\frac{1}{l^2} \frac{1}{l_{x_1 p q}^2} \frac{1}{l_{x_1 p q r}^2} \tilde{J}(x_1, p, q) (\tilde{J}(r) \cdot X_r) \phi_{x_2|a_5}, \quad (5.10)$$

which is given by the effective subcurrent  $\tilde{J}(x_1, p, q)$  with the scalar  $x_1$  and gluons  $p, q$ , and the subcurrent  $\tilde{J}^\mu(r)$ .

The last example is the partition  $\{x_1, \{p, q, r\}, x_2\}$ , which contains the term (5.6) already induced by the graph Fig. 33 (c) with corresponding diagram Fig. 33 (a). The terms induced by graphs Fig. 37 (d) and (e) further provide

$$\left(-\frac{1}{2}\right) \frac{1}{l^2} \frac{1}{l_{x_1}^2} \frac{1}{l_{x_1 p q r}^2} \phi_{x_1|a_1} \left[ (-\epsilon_q \cdot k_p)(\epsilon_p \cdot \epsilon_r) \phi_{q p|a_2 a_3} \phi_{r|a_4} + (-\epsilon_p \cdot k_q)(\epsilon_q \cdot \epsilon_r) \phi_{p q|a_2 a_3} \phi_{r|a_4} \right] \phi_{x_2|a_5}. \quad (5.11)$$

The total contribution of (5.6) and (5.11) is given by

$$\left(-\frac{1}{2}\right) \frac{1}{l^2} \frac{1}{l_{x_1}^2} \frac{1}{l_{x_1 p q r}^2} \left[ \tilde{J}(p, q) \cdot \tilde{J}(r) \right] \phi_{x_2|a_5}. \quad (5.12)$$

Other contributions for this partition can also be obtained as

$$\left(-\frac{1}{2}\right) \frac{1}{l^2} \frac{1}{l_{x_1}^2} \frac{1}{l_{x_1 p q r}^2} \left[ \tilde{J}(p) \cdot \tilde{J}(q, r) \right] \phi_{x_2|a_5}, \quad (5.13)$$

$$\left(-\frac{1}{2}\right) \frac{1}{l^2} \frac{1}{l_{x_1}^2} \frac{1}{l_{x_1 p q r}^2} \left[ \tilde{J}(q) \cdot \tilde{J}(p, r) \right] \phi_{x_2|a_5}, \quad (5.14)$$

$$\frac{1}{l^2} \frac{1}{l_{x_1}^2} \frac{1}{l_{x_1 p q r}^2} \left[ \tilde{J}(p, q, r) \cdot X_{\{p, q, r\}} \right] \phi_{x_2|a_5}. \quad (5.15)$$

The sum of (5.12), (5.13), (5.14) and (5.15) gives rise to

$$\frac{1}{l^2} \frac{1}{l_{x_1 p q}^2} \frac{1}{l_{x_1 p q r}^2} \left[ \tilde{J}(p, q, r) \cdot X_{\{p, q, r\}} + \left(-\frac{1}{2}\right) \left( \tilde{J}(p, q) \cdot \tilde{J}(r) + \tilde{J}(p) \cdot \tilde{J}(q, r) + \tilde{J}(q) \cdot \tilde{J}(p, r) \right) \right] \phi_{x_2|a_5}. \quad (5.16)$$

The  $\tilde{J}^\mu(a, b)$  and  $\tilde{J}^\mu(p, q, r)$  are the effective currents [37] constructed via the graphic rule (see appendix C), where the off-shell node (the Lorentz index  $\mu$ ) is considered as the root. The reference order of gluons in each effective current inherits the relative reference order of the full graph.

The contributions of other partitions in the final result can be assembled in an analogue way. When all possible partitions are considered, we get a compact expression for the final reduction result of the five-point integrand with three gluons

$$I^{1\text{-loop}}(x_1, x_2 || \{p, q, r\}) \cong \sum_{\{A_1, A_2, \dots, A_I\}} \frac{1}{l^2} J[A_1] \frac{1}{l_{A_1}^2} J[A_2] \cdots \frac{1}{l_{A_1 \dots A_{I-1}}^2} J[A_I] + \text{cyc}(a_1 a_2 a_3 a_4 a_5), \quad (5.17)$$

in which, all possible cyclic partitions  $\{A_1, A_2, \dots, A_I\}$  of external particles  $x_1, x_2, p, q, r$ , where the relative cyclic order of  $x_1, x_2$  is always kept, have been summed over. The  $J[A_i]$  are defined as

$$J[A_i] = \tilde{J}(A_i), \quad (\text{if } A_i \text{ contains scalars})$$

$$J[A_i] = \tilde{J}(A_i) \cdot X_{A_i} + \left(-\frac{1}{2}\right) \left[ \sum_{A_i \rightarrow A_{iL}, A_{iR}} \tilde{J}(A_{iL}) \cdot \tilde{J}(A_{iR}) \right], \quad (\text{if } A_i \text{ contains only gluons}) \quad (5.18)$$

where  $A_i \rightarrow A_{iL}, A_{iR}$  stands for splitting  $A_i$  into two nonempty subsets such that the highest-weight element in  $A_i$  belongs to  $A_{iR}$ . Concretely, if  $A_i$  contains only two elements  $a$  and  $b$  with reference order  $a \prec b$ , the splitting is  $\{a, b\} \rightarrow \{a\} \{b\}$ . If  $A_i$  contains three elements  $p, q$  and  $r$ , the possible splittings are

$$\{p, q\} \{r\}, \quad \{p\} \{q, r\}, \quad \{q\} \{p, r\}, \quad (5.19)$$

corresponding to (5.12), (5.13), (5.14).

## 6 General discussions and the final result for single-trace YMS

In section 3 and section 5, explicit examples for extracting quadratic propagators have been provided. We have seen that the cancellation of nonlocalities played a crucial way and the final result had compact expressions in these examples. In this section, we provide a general approach to the cancellation of nonlocal terms and the compact formula of the final quadratic-propagator result. We begin with the following expression of YMS integrand

$$\begin{aligned} \frac{1}{l^2} \int d\mu_{n+2}^{\text{tree}} I_L^{1\text{-loop}} I_R^{1\text{-loop}} &= \sum_{\mathcal{F}} \mathcal{C}^{\mathcal{F}} \left[ \sum_{\substack{(A_1 A_2 \dots A_i) = \sigma^{\mathcal{F}} \\ (\tilde{A}_1 \tilde{A}_2 \dots \tilde{A}_i) = \gamma \\ A_j = \tilde{A}_j}} \frac{1}{l^2} \frac{1}{s_{A_1, l}} \frac{1}{s_{A_1 A_2, l}} \cdots \frac{1}{s_{A_1 A_2 \dots A_{i-1}, l}} \phi_{A_1 | \tilde{A}_1} \phi_{A_2 | \tilde{A}_2} \cdots \phi_{A_i | \tilde{A}_i} \right. \\ &\quad \left. + \text{cyc}(x_1 x_2 \dots x_r) \right] + \text{cyc}(\gamma), \end{aligned} \quad (6.1)$$

which is obtained by substituting (2.12) and (2.20) into (2.9), directly. Here,  $\sigma^{\mathcal{F}}$  denotes permutations established by the graph  $\mathcal{F}$ ,  $x_1, \dots, x_r$  are the scalars,  $\gamma$  is a permutation of all scalars and gluons in the right half integrand. This expression turns back to eq. (3.5) if the integrand involves two scalars and two gluons.

To collect the coefficients corresponding to a Feynman diagram, we arrange the two summations in the above expression as follows

$$\sum_{\mathcal{F}} \mathcal{C}^{\mathcal{F}} \sum_{\substack{(A_1 A_2 \dots A_i) = \sigma \omega \rho^{\mathcal{F}} \\ (\tilde{A}_1 \tilde{A}_2 \dots \tilde{A}_i) = \gamma \\ A_j = \tilde{A}_j}} \rightarrow \sum_{\substack{\text{partitions} \\ \{A_1, A_2, \dots, A_i\}}} \left[ \sum_{\substack{\text{topologies of subsets} \\ \text{for a given partition}}} \sum_{\substack{\text{configurations of} \\ \text{subgraphs for a topology}}} \text{Contractions} [\mathcal{C}^{\mathcal{F}_j}] \right]. \quad (6.2)$$

This means we can collect contributions of *all partitions* (or in other words LPFD) instead of contributions of *all graphs*. For a given partition  $\{A_1, \dots, A_i\}$  of external particles, one can establish the possible topologies

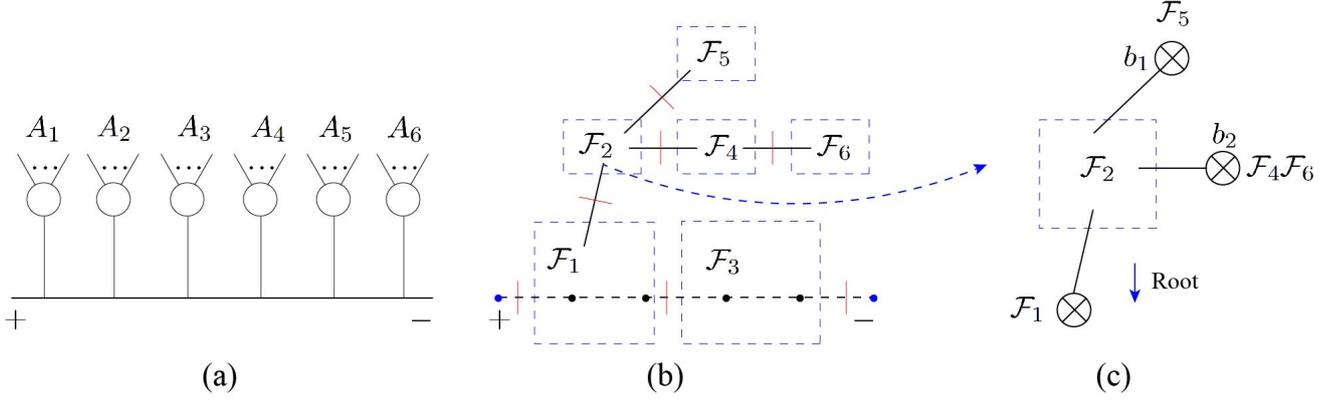


**Figure 38.** The LPFD for partition  $\{A_1, A_2, A_3, A_4, A_5, A_6\}$  is given by diagram (a). Assume that  $A_1$  and  $A_3$  contain scalars, while  $A_2, A_4, A_5, A_6$  are pure gluon subsets. Graph (b), where  $\mathcal{F}_1, \dots, \mathcal{F}_6$  stand for the subgraphs corresponding to subsets  $A_1, \dots, A_6$ , is a possible topology for this partition. The subgraphs containing scalars are interconnected via type-4 lines to record the relative order between scalars. Other lines between subgraphs can be of other three types and are expressed by solid lines with no arrow. When other subgraphs connected to a given subgraph are considered as off-shell nodes, the subgraph under consideration can be regarded as a graph with both on-shell and off-shell nodes, e.g., (c). In (c), the off-shell node below  $\mathcal{F}_2$  stands for the subgraph  $\mathcal{F}_1$ , while the off-shell nodes  $b_1$  and  $b_2$  (which locate above  $\mathcal{F}_2$ ) respectively represent the subtree  $\mathcal{F}_5$  and the subtree consisting of  $\mathcal{F}_4, \mathcal{F}_6$ .

by connecting lines (with ignoring the types of these lines) between these subsets and sum over all such topologies. Fixing a partition and a topology, one determines the possible configurations of subgraphs by graphic rule when the tree structures attached to this subset are regarded as off-shell nodes. When we contract the Lorentz indices between coefficients  $\mathcal{C}^{\mathcal{F}_j}$  for subgraphs  $\mathcal{F}_j$  corresponding to the subset  $A_j$ , the full coefficient for this LPFD is obtained. Therefore, the integrand turns into

$$\begin{aligned}
& \frac{1}{l^2} \int d\mu_{n+2}^{\text{tree}} I_L^{1\text{-loop}} I_R^{1\text{-loop}} \\
&= \sum_{\substack{\text{partitions} \\ \{A_1, A_2, \dots, A_i\}}} \left[ \sum_{\substack{\text{topologies of subsets} \\ \text{for a partition}}} \sum_{\substack{\text{configurations of} \\ \text{subgraphs for a topology}}} \text{Contractions} [\mathcal{C}^{\mathcal{F}_j}] \right. \\
& \quad \left. \times \frac{1}{l^2} \frac{1}{s_{A_1, l}} \frac{1}{s_{A_1 A_2, l}} \cdots \frac{1}{s_{A_1 A_2 \cdots A_{i-1}, l}} \phi_{A_1 | \tilde{A}_1} \phi_{A_2 | \tilde{A}_2} \cdots \phi_{A_i | \tilde{A}_i} + \text{cyc}(x_1 x_2 \dots x_r) \right] + \text{cyc}(\boldsymbol{\gamma}). \quad (6.3)
\end{aligned}$$

Generally speaking, in (6.3), there exist terms containing contractions between subgraphs corresponding to distinct subsets. Since these subsets are separated by linear propagators in the Feynman diagram, such terms are nonlocal ones. These nonlocalities have to be canceled. Actually, we can reconstruct the subgraphs by adjusting the refined graphic rule in a proper way so that (i). the X- and BCJ- patterns arise and/or (ii). the  $C \cdot X$  factor can be collected. Hence the cancellations of nonlocalities can also be achieved, following the same approaches in section 3 and section 5. When the cyclic permutations of  $(x_1 x_2 \dots x_r)$  and  $\boldsymbol{\gamma}$  are considered, we finally get a compact formula with quadratic propagators.

In the remaining part of this section, we demonstrate the above general approach in more detail, including generating topologies for a partition, the construction rule for a subgraph and the cancellation between X- and BCJ-patterns. After that, we provide the final compact expression for single-trace YMS integrand (which contains a pure scalar loop) with quadratic propagators.

### 6.1 Topologies for a given partition

When a partition of external particles has been given, e.g., the partition  $\{A_1, A_2, A_3, A_4, A_5, A_6\}$  which corresponds to the LPFD Fig. 38 (a), one can easily find out all possible topologies for these subsets that agree with the graphic rule:

- Subsets containing scalars are interconnected according to their relative order in the partition, via type-4 lines. The leftmost (rightmost) subset containing scalars is further connected to  $+$  ( $-$ ) via a type-4 line.
- If a subset  $A_i$  contains only gluons, one can connect (i). a line between  $A_i$  and any subset, say  $A_j$ , which locates on the left of  $A_i$  in the partition, or (ii). a line between  $A_i$  and the node  $+$ . The line style is not fixed.

A typical topology for the Feynman diagram Fig. 38 (a), is presented by Fig. 38 (b) which encodes relative positions of subgraphs.

In appendix E and appendix F, we provide systematic rules (which are equivalent to each other as pointed in [7]) for constructing subgraphs with proper spurious graphs in a given topology. The key result following the construction in appendix F is that a subgraph consists of an upper and a lower block  $\mathcal{U}$  and  $\mathcal{L}$ , which are (i). connected via a type-3 line if both blocks has on-shell nodes (see Fig. 49 (a)), or (ii). connected via a half-arrow line if one of the block has no on-shell node (see Fig. 49 (b) and (c)). According to appendix F, a subgraph may (a). contain a BCJ-pattern (whose two subgraphs are  $\mathcal{U}$  and  $\mathcal{L}$ ) or an X-pattern (only occurs in the case where the lower block has no on-shell node), (b). play as a physical subgraph when cross nodes are extracted out (in the case where the upper block has no on-shell node), (c). be neither the case (a) nor (b) and relies on the subgraph above it (in the case where the lower block has no on-shell node). In the coming subsections, we provide a general discussion on the cancellations between X- and BCJ-patterns and summarize the final expression with no nonlocal term.

### 6.2 General cancellation between X- and BCJ-patterns

Now, let us demonstrate the general cancellation between X- and BCJ-patterns. We begin with the typical graph Fig. 39 (a) (which may contribute to different partitions), where each subgraph is considered as any graph constructed by combining version-1 and -2 rules when the partition and topology have been fixed. We will show that the cancellations occur among graphs with respect to different topologies and different partitions.

**Cancellations of BCJ-patterns** Without loss of generality, we concentrate on the subgraph  $\mathcal{F}_1$  and suppose that it is a subgraph with BCJ-pattern. In other words, it consists of upper and lower blocks  $\mathcal{U}_1$ ,

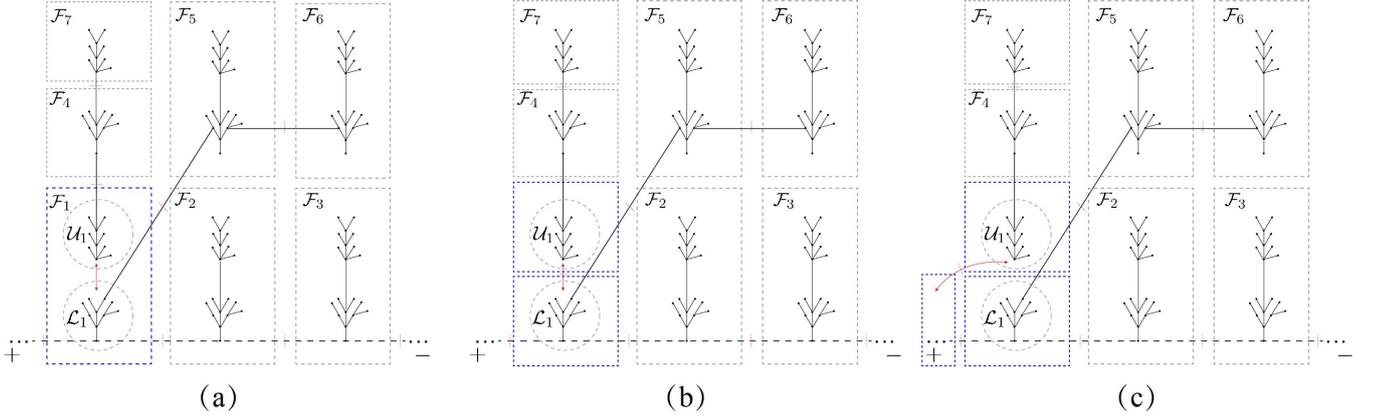


**Figure 39.** Three typical graphs which are decomposed into subgraphs. The subgraph  $\mathcal{F}_1$  in graph (a) is a BCJ-pattern whose upper and lower blocks are  $\mathcal{U}_1$  and  $\mathcal{L}_1$ . Graph (b) is obtained by decomposing  $\mathcal{F}_1$  in (a) into two subgraphs  $\mathcal{U}_1$  and  $\mathcal{L}_1$ . When the  $\mathcal{U}_1$  in (b) is connected to the substructure below  $\mathcal{L}_1$  via a type-3 line, we get graph (c). Graph (b) and (c) provide an X-pattern with  $\mathcal{U}_1$ .

$\mathcal{L}_1$ , which are connected via a type-3 line, as shown by Fig. 39 (a). We further assume that the partition under consideration for this graph has the form  $\{\dots, A_1, \dots\}$ . This graph then provides

$$\left(-\frac{1}{2}\right) \left[ \dots (\mathcal{C}^{\mathcal{L}_1} \mathcal{C}^{\mathcal{U}_1} \phi_{[\mathcal{L}_1, \mathcal{U}_1]}) \dots \right] \dots \frac{1}{s_{A_0, l}} \frac{1}{s_{A_0 A_1, l}} \dots, \quad (6.4)$$

where the off-shell BCJ relation has been applied. In the above, the  $A_0$  denotes the set of all elements on the left of  $A_1$  in the partition. The right permutation in a BS current was omitted for short. The  $\phi_{[A_L, A_R]}$  stands for

$$\phi_{A_L | \tilde{A}_L} \phi_{A_R | \tilde{A}_R} - \phi_{A_R | \tilde{A}'_L} \phi_{A_L | \tilde{A}'_R} \quad (6.5)$$

where  $\tilde{A}_L \tilde{A}_R = \tilde{A}'_L \tilde{A}'_R$ . The subscripts  $\mathcal{U}_1$  and  $\mathcal{L}_1$  in  $\phi_{\mathcal{U}_1}$  and  $\phi_{\mathcal{L}_1}$  stand for permutations established by the corresponding subgraphs.

For Fig. 39 (a) with the partition  $\{\dots, A_1, \dots\}$ , one can always find other graphs (with other topologies) Fig. 39 (b) and (c). Fig. 39 (b) can be considered as the graph obtained by dividing the upper and lower blocks of  $\mathcal{F}_1$  in Fig. 39 (a) into two subgraphs. Fig. 39 (c) can be obtained by connecting a type-3 line between  $\mathcal{U}_1$  and the subsets to the left of  $\mathcal{U}_1$  instead of  $\mathcal{L}_1$  in Fig. 39 (b). These two graphs contribute X-patterns, i.e., the subgraph with  $\mathcal{U}_1$ . Particularly, for partition  $\{\dots, \mathcal{L}_1, \mathcal{U}_1, \dots\}$ , both Fig. 39 (b) and (c) produce an X-pattern, while for partition  $\{\dots, \mathcal{U}_1, \mathcal{L}_1, \dots\}$ , the graph Fig. 39 (c) has an X-pattern. The explicit expression for partition  $\{\dots, \mathcal{L}_1, \mathcal{U}_1, \dots\}$  (with graphs Fig. 39 (b), (c)) is given by

$$\left[ \dots (\mathcal{C}^{\mathcal{L}_1} \phi_{\mathcal{L}_1}) (\mathcal{C}^{\mathcal{U}_1} \phi_{\mathcal{U}_1}) \dots \right] \dots [-k_{\mathcal{U}_1} \cdot (l + k_{A_0 \mathcal{L}_1})] \frac{1}{s_{A_0 \mathcal{L}_1, l}} \frac{1}{s_{A_0 A_1, l}} \dots \quad (6.6)$$

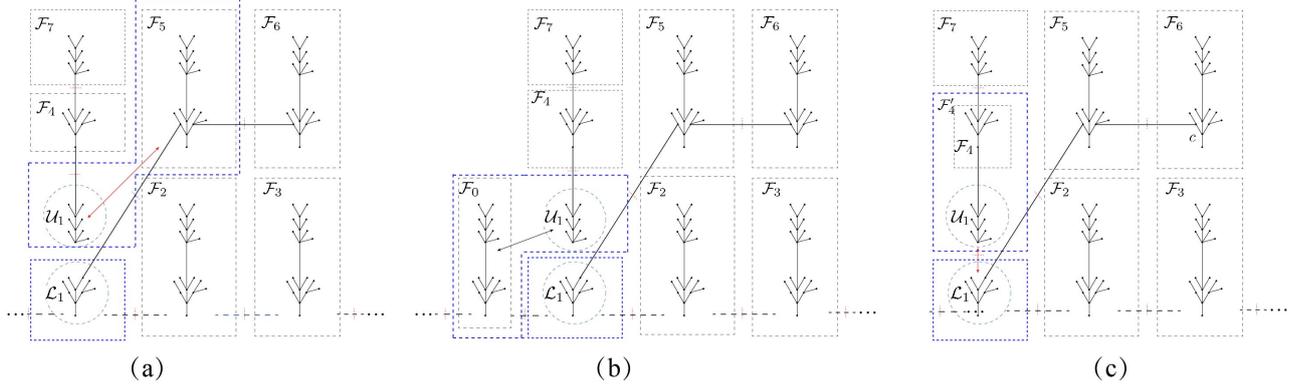


**Figure 40.** Graphs (a), (b) and (c) provide further cancellations with the remaining contributions of the X-pattern in Fig. 39 (b) and (c). Graphs (a) and (b) contain BCJ-patterns whose upper block is  $\mathcal{U}_1$  and lower blocks are  $\mathcal{F}_5$  and  $\mathcal{F}_0$ , respectively. In graph (c),  $\mathcal{F}_4$  and  $\mathcal{U}_1$  are merged into a larger X-pattern.

$$= \left[ \dots (\mathcal{C}^{\mathcal{L}_1} \phi_{\mathcal{L}_1}) (\mathcal{C}^{\mathcal{U}_1} \phi_{\mathcal{U}_1}) \dots \right] \dots \left( -\frac{1}{2} \right) \left[ -\frac{1}{s_{A_0 A_1, l}} + \frac{1}{s_{A_0 \mathcal{L}_1, l}} - \frac{k_{\mathcal{U}_1}^2}{s_{A_0 \mathcal{L}_1, l} s_{A_0 A_1, l}} \right] \dots$$

The definition of X-pattern and the property (3.25) have been used. Analogously, the contribution of Fig. 39 (c) for the partition  $\{\dots, \mathcal{U}_1, \mathcal{L}_1, \dots\}$  is given by

$$\begin{aligned} & \left[ \dots (\mathcal{C}^{\mathcal{L}_1} \phi_{\mathcal{L}_1}) (\mathcal{C}^{\mathcal{U}_1} \phi_{\mathcal{U}_1}) \dots \right] \dots [-k_{\mathcal{U}_1} \cdot (l + k_{A_0})] \frac{1}{s_{A_0, l}} \frac{1}{s_{A_0 \mathcal{U}_1, l}} \dots \\ & = \left[ \dots (\mathcal{C}^{\mathcal{L}_1} \phi_{\mathcal{L}_1}) (\mathcal{C}^{\mathcal{U}_1} \phi_{\mathcal{U}_1}) \dots \right] \dots \left( -\frac{1}{2} \right) \left[ -\frac{1}{s_{A_0 \mathcal{U}_1, l}} + \frac{1}{s_{A_0, l}} - \frac{k_{\mathcal{U}_1}^2}{s_{A_0, l} s_{A_0 \mathcal{U}_1, l}} \right] \dots \end{aligned} \quad (6.7)$$

When we expand the ‘commutator’ in (6.4), the first and the second terms of (6.4) respectively cancel against the first term of (6.6) and the second term of (6.7). Hence the full BCJ-pattern has been canceled.

**Further cancellations of X-patterns** When the BCJ-pattern in Fig. 39 (a) has been canceled out, there are remaining contributions of X-patterns in Fig. 39 (b) and (c), i.e., the second and the third terms in (6.6), the first and the third terms in (6.7). Now we concentrate on these terms and further classify our discussions by distinct partitions for Fig. 39 (b) and (c):

- **The subset next to  $\mathcal{U}_1$  in the partition for Fig. 39 (b) is not involved by a cross node above  $\mathcal{U}_1$ ,** e.g., the partition  $\{\dots, \mathcal{L}_1, \mathcal{U}_1, A_5, \dots\}$ . For this case, one can always find a BCJ-pattern Fig. 40 (a), whose upper and lower blocks are  $\mathcal{U}_1$  and  $\mathcal{F}_5$ , respectively. When the off-shell BCJ relation is applied, this graph provides

$$\left( -\frac{1}{2} \right) \left[ \dots (\mathcal{C}^{\mathcal{L}_1} \phi_{\mathcal{L}_1}) (\mathcal{C}^{\mathcal{U}_1} \mathcal{C}^{\mathcal{F}_5} \phi_{[\mathcal{U}_1, \mathcal{F}_5]}) \dots \right] \dots \frac{1}{s_{A_0 \mathcal{L}_1, l}} \frac{1}{s_{A_0 A_1 A_5, l}} \dots, \quad (6.8)$$

whose first term cancel out the second term of (6.6) (where  $(\mathcal{C}^{\mathcal{F}_5} \phi_{\mathcal{F}_5}) \frac{1}{s_{A_0 A_1 A_5, l}}$  is absorbed by the

dots), according to the cancellation of BCJ-pattern with the partition  $\{\dots, \mathcal{L}_1, \{\mathcal{U}_1, A_5\}, \dots\}$ . Similarly, the first term of (6.7) (for the partition  $\{\dots, \mathcal{F}_0, \mathcal{U}_1, \mathcal{L}_1, \dots\}$  where  $\mathcal{F}_0$  refers to the subset near to  $\mathcal{U}_1$  from left and the corresponding subgraph) is canceled by one term of the BCJ-pattern in Fig. 40 (b) with the partition  $\{\dots, \{\mathcal{F}_0, \mathcal{U}_1\}, \mathcal{L}_1, \dots\}$ .

- **The subset next to  $\mathcal{U}_1$  in the partition for Fig. 39 (b) is contained by a cross node above  $\mathcal{U}_1$ , e.g., the partition  $\{\dots, \mathcal{L}_1, \mathcal{U}_1, A_4, \dots\}$ <sup>5</sup>. If the lower block of  $\mathcal{F}_4$  does not contain on-shell node, one can always find a graph with a larger X-pattern  $\mathcal{F}'_4$ , which is obtained from Fig. 39 (b) by merging  $\mathcal{U}_1$  and  $A_4$  into a single X-pattern, as shown by Fig. 40 (c). Explicitly, this graph provides**

$$\begin{aligned} & \left[ \dots (\mathcal{C}^{\mathcal{L}_1} \phi_{\mathcal{L}_1}) (\mathcal{C}^{\mathcal{F}'_4} \phi_{\mathcal{F}'_4}) \dots \right] [-k_{A_4 \mathcal{U}_1} \cdot (l + k_{A_0} + k_{\mathcal{L}_1})] \frac{1}{s_{A_0 \mathcal{L}_1, l}} \frac{1}{s_{A_0 A_1 A_4, l}} \dots \quad (6.9) \\ & = \left( -\frac{1}{2} \right) \left[ \dots (\mathcal{C}^{\mathcal{L}_1} \phi_{\mathcal{L}_1}) (\mathcal{C}^{\mathcal{F}'_4} \phi_{\mathcal{F}'_4}) \dots \right] \left[ -\frac{1}{s_{A_0 A_1 A_4, l}} + \frac{1}{s_{A_0 \mathcal{L}_1, l}} - \frac{(k_{\mathcal{U}_1} + k_{A_4})^2}{s_{A_0 A_1 A_4, l} s_{A_0 \mathcal{L}_1, l}} \right] \dots \end{aligned}$$

The third term on the last line in the above expression involves

$$- \left( -\frac{1}{2} \right) \mathcal{C}^{\mathcal{F}'_4} \frac{(k_{\mathcal{U}_1} + k_{A_4})^2}{s_{A_0 A_1 A_4, l} s_{A_0 \mathcal{L}_1, l}} \phi_{\mathcal{F}'_4}. \quad (6.10)$$

According to the BG recursion (2.29) of the BS currents, the numerator together with the current  $\phi$  produces a combination of product of two subcurrents, which contains the following term

$$\frac{1}{2} \frac{1}{s_{A_0 A_1 A_4, l} s_{A_0 \mathcal{L}_1, l}} (\mathcal{C}^{\mathcal{F}'_4} \phi_{[\mathcal{U}_1, \mathcal{F}_4]}) = \frac{1}{2} \frac{1}{s_{A_0 A_1 A_4, l} s_{A_0 \mathcal{L}_1, l}} (\mathcal{C}^{\mathcal{U}_1} \mathcal{C}^{\mathcal{F}_4} \phi_{[\mathcal{U}_1, \mathcal{F}_4]}), \quad (6.11)$$

where  $\mathcal{C}^{\mathcal{F}'_4}$  has been rewritten as the contraction between  $\mathcal{C}^{\mathcal{U}_1}$  and  $\mathcal{C}^{\mathcal{F}_4}$ . Noting that the expression  $\mathcal{C}^{\mathcal{F}_4} \phi_{\mathcal{F}_4} \frac{1}{s_{A_0 A_1 A_4, l}}$  is absorbed by dots in (6.6), once the commutator is expanded, we find the first term cancels with the second term on the last line of (6.6). Following a similar discussion, the last terms of (6.6), (6.7) cancel with the X-patterns which come from subdivisions of  $\mathcal{U}_1$ . If the lower block of  $\mathcal{F}_4$  in Fig. 39 (b) involves on-shell nodes, the second term of (6.6) survives because one cannot find a larger X-pattern to cancel it. In this case, when the first and the last terms are canceled out, (6.6) becomes

$$\left[ \dots (\mathcal{C}^{\mathcal{L}_1} \phi_{\mathcal{L}_1}) (\mathcal{C}^{\mathcal{U}_1} \phi_{\mathcal{U}_1}) (\mathcal{C}^{\mathcal{F}_4} \phi_{\mathcal{F}_4}) \dots \right] \dots \left( -\frac{1}{2} \right) \frac{1}{s_{A_0 \mathcal{L}_1, l}} \frac{1}{s_{A_0 A_1 A_4, l}} \dots \quad (6.12)$$

If the  $\mathcal{F}_4$  further involves a BCJ-pattern, it has to cancel out. *If the upper block of  $\mathcal{F}_4$  has no on-shell node, the above expression finally survives and provides a contraction between  $(\mathcal{C}^{\mathcal{U}_1} \phi_{\mathcal{U}_1})$  and  $(\mathcal{C}^{\mathcal{F}_4} \phi_{\mathcal{F}_4})$  ( $\mathcal{F}_4$  is a physical graph constructed by graphic rule), with the linear propagator between them deleted.*

<sup>5</sup>In this example, there is only one cross node above  $\mathcal{U}_1$ . For cases with more cross nodes above  $\mathcal{U}_1$ , the subset next to  $\mathcal{U}_1$  may belong to any one of these cross nodes. However, the discussion in this part is also effective.

There is a boundary case that  $\mathcal{U}_1$  in (6.6) contains only one node. In this case, the on-shell condition gives  $k_{\mathcal{U}_1}^2 = 0$ , and  $\mathcal{U}_1$  cannot further be divided. Therefore, the third term in (6.6) itself vanishes but do not cancel with a further division.

### 6.3 From linear to quadratic propagators

We now summarize what we have learnt in the previous subsections and then provide the general expression with quadratic propagators.

- For a given partition and a topology, if a subgraph contains a BCJ-pattern, one can always find the corresponding graph with an X-pattern to cancel it. Therefore, the surviving graphs cannot involve any subgraph with BCJ-pattern.
- If a subgraph contains an X-pattern (the on-shell nodes in this subgraph can only be gluons), the corresponding Feynman diagram further splits into three terms, as shown by Fig. 26, in which, (a) cancels with a BCJ-pattern, (c) may cancel with either a BCJ-pattern or a larger X-pattern, while (b) may cancel with an X-pattern (which can be considered as a subdivision of the original X-pattern). The only possible nonvanishing term from this subgraph (which corresponds to a subset say,  $A_{iL}$ ) is given by the contraction between  $\mathcal{F}_{iL}$  and another subgraph, say  $\mathcal{F}_{iR}$  whose upper block has no on-shell node (in other words, a subgraph constructed by version-1 rule). On the LPDF side, this structure exists in the diagram where  $\mathcal{F}_{iR}$  is adjacent to the  $\mathcal{F}_{iL}$  from right. The linear propagator between them is deleted. Such contraction provides a factor  $(-\frac{1}{2}) \left[ \tilde{J}(A_{iL}) \cdot \tilde{J}(A_{iR}) \right]$ , where  $\tilde{J}_\mu(A_{iL}) = \sum_{\mathcal{F}_{iL}} \mathcal{C}_\mu^{\mathcal{F}_{iL}} \phi_{\mathcal{F}_{iL}}$  and  $\tilde{J}_\mu(A_{iR}) = \sum_{\mathcal{F}_{iR}} \mathcal{C}_\mu^{\mathcal{F}_{iR}} \phi_{\mathcal{F}_{iR}}$  are the effective currents defined by graphic rule with an off-shell node.
- For a given partition and a given topology, if a cross node, say  $b_i$ , of a subgraph  $\mathcal{F}_j$  itself plays as the upper block (in other words, the upper block of this subgraph contains no on-shell node), one can find out other related topologies for the same partition, where the full substructure involved by  $b_i$  plays as the upper block of other subgraphs to the left of  $A_j$  in the partition. The leftmost subset  $A_k$  involved in  $b_i$  for the partition then produces a factor  $(\mathcal{C}^{\mathcal{F}_k} \cdot X_{A_k}) \phi_{\mathcal{F}_k} = \tilde{J}(A_k) \cdot X_{A_k}$ .
- For a subset which contains scalars (and maybe gluons), the only surviving subgraphs are the ones whose upper block does not contain on-shell node. In this case, all on-shell nodes (scalars and possible gluons) are used to construct the lower blocks. These subgraphs are just physical graphs constructed by version-1 rule and all together provide a  $\tilde{J}(A_j)$ .

When all possibilities are considered, we get a local expression of integrand

$$I^{\text{1-loop}}(x_1, x_2, \dots, x_r || G | \rho) \cong \left[ \sum_{\{A_1, A_2, \dots, A_I\}} \frac{1}{l^2} J[A_1] \frac{1}{s_{A_1, l}} J[A_2] \cdots \frac{1}{s_{A_1 \dots A_{I-1}, l}} J[A_I] + \text{cyc}(x_1 x_2 \dots x_r) \right]$$

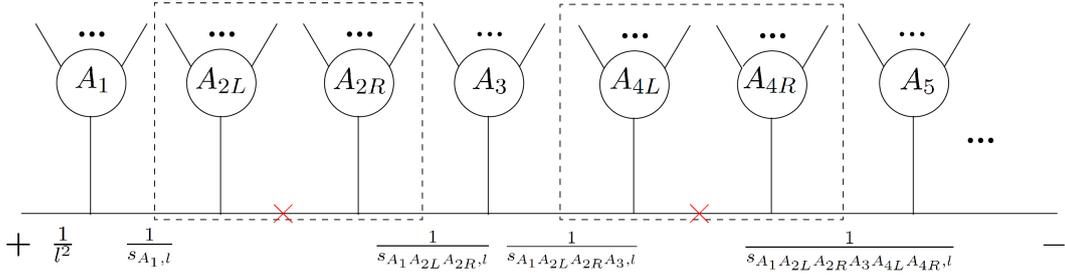


**Figure 41.** A typical diagram with surviving terms, where  $A_1, A_3, A_5$  are the (YMS or pure gluon) subcurrents corresponding to the physical subgraphs. The substructures containing  $A_{2L}, A_{2R}$  and  $A_{4L}, A_{4R}$  provide contractions between pure gluon effective subcurrents  $\tilde{J}(A_{2L}) \cdot \tilde{J}(A_{2R})$  and  $\tilde{J}(A_{4L}) \cdot \tilde{J}(A_{4R})$ .

$$+ \text{cyc}(a_1 a_2 \dots a_{r+s}). \quad (6.13)$$

In the first term, we summed over all possible partitions  $\{A_1, A_2, \dots, A_I\}$  of external particles (including  $r$  scalars  $x_1, x_2, \dots, x_r$  and  $s$  gluons). The relative order of  $x_1, x_2, \dots, x_r$  in the partition  $\{A_1, A_2, \dots, A_I\}$  is always kept. Terms related by cyclic permutations of scalars and terms related by the cyclic permutations of all elements on the right side  $\boldsymbol{\rho} = (a_1 a_2 \dots a_{r+s})$  are also taken into account. The  $J[A_i]$  are defined as

$$J[A_i] = \tilde{J}(A_i), \quad (\text{if } A_i \text{ contains scalars}) \quad (6.14)$$

$$J[A_i] = \tilde{J}(A_i) \cdot X_{A_i} + \left(-\frac{1}{2}\right) \left[ \sum_{A_i \rightarrow A_{iL}, A_{iR}} \tilde{J}(A_{iL}) \cdot \tilde{J}(A_{iR}) \right]. \quad (\text{if } A_i \text{ contains only gluons}) \quad (6.15)$$

A typical diagram of (6.13) is shown by Fig. 41.

The cyclic permutations of  $(x_1 x_2 \dots x_r)$  and  $(a_1 a_2 \dots a_{r+s})$  in (6.13) together with graphic rule allow the cyclic summation of the subcurrents  $J[A_1], \dots, J[A_I]$ . Using (2.27), we finally conclude that the integrand with quadratic propagators is expressed by

$$I^{1\text{-loop}}(x_1, x_2, \dots, x_r | G | \boldsymbol{\rho}) \cong \sum_{\substack{\{A_1, A_2, \dots, A_I\} \\ (\tilde{A}_1 \tilde{A}_2 \dots \tilde{A}_I) \\ A_i = \tilde{A}_i}} \frac{1}{l^2} J[A_1] \frac{1}{l^2_{A_1}} J[A_2] \cdots \frac{1}{l^2_{A_1 \dots A_{I-1}}} J[A_I], \quad (6.16)$$

where  $\{A_1, A_2, \dots, A_I\}$  are possible cyclic partitions of external particles, while  $(\tilde{A}_1 \tilde{A}_2 \dots \tilde{A}_I)$  are possible divisions of the cyclic permutation of  $(a_1 a_2 \dots a_{r+s})$  such that the elements in  $\tilde{A}_i$  ( $i = 1, \dots, I$ ), which are hidden inside  $\tilde{J}[A_i]$ , are identical with those in  $A_i$ . Each subset  $\tilde{A}_i$  cannot contain all scalars, because this case has to vanish due to the  $U(1)$ -decoupling identity under the cyclic sum of scalars in (6.13). The four-point and the five-point examples precisely agree with this general expression. More detail about (6.13) are demonstrated by YMS integrand with four gluons in appendix I.

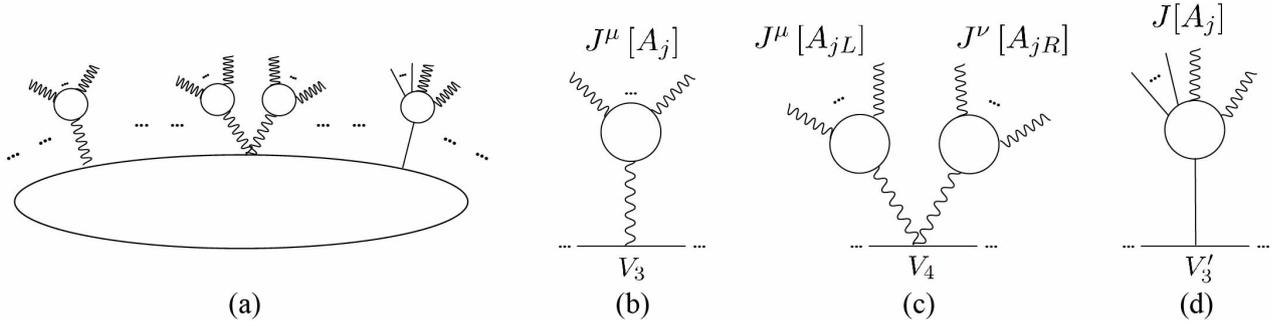


**Figure 42.** Traditional Feynman diagrams for single-trace YMS in general can be packaged into (a), where tree structures are collected as BG currents which are further attached to the loop with quadratic propagators via the vertices Fig. 58 (c), (d) and/or (e). Thus there are three types of such substructures, as shown by (b), (c) and (d) (the vertices Fig. 58 (c), (d) and (e) are respectively denoted by  $V_3$ ,  $V'_3$  and  $V_4$ ), where  $J^\mu[A_j]$ 's in (b) and (c) are pure gluon BG currents,  $J[A_j]$  in (d) is a YMS BG current with both scalar and gluon external lines.

## 7 Traditional Feynman diagrams and the extension to multi-trace YMS and YM

In this section, we reveal the relationship between the main result (6.16) that was derived from one-loop CHY formula, and the direct analysis from Feynman diagrams of single-trace YMS. We further extend these results straightforwardly to multi-trace YMS amplitudes (with a pure scalar loop) and pure YM amplitudes.

### 7.1 The relationship with traditional Feynman diagrams

Now we demonstrate the explicit relationship between the quadratic propagator form (6.16) and the Feynman diagrams. To achieve this, we display the expressions of vertices in traditional Feynman rule for single-trace YMS in Fig. 58 and then package the Feynman diagrams by attaching tree-level BG currents to the loop with quadratic propagators, via vertices in Fig. 58. The sum of all Feynman diagrams becomes the sum of diagrams with structures like Fig. 42 (a). The BG currents in general can be planted to the quadratic-propagator scalar loop via three types of vertices, as shown by Fig. 42 (b), (c), (d). Each  $J^\mu$  in Fig. 42 (b) and (c) is a BG current for gluons. Upto an overall factor, this current has been proven to

satisfy the off-shell decomposition formula [37] (also see [44, 45])<sup>6</sup>:

$$J^\mu = \tilde{J}^\mu + K^\mu + L^\mu, \quad (7.1)$$

in which the first term  $\tilde{J}^\mu$  can be decomposed into a combination of BS currents, according to the refined graphic rule while all external momenta in the numerator are rescaled as  $k^\mu \rightarrow 2k^\mu$ . The second term,  $K^\mu$  is proportional to the total momentum of external gluons in the current. The third term  $L^\mu$  contains substructures which are obtained via replacing subcurrents by objects proportional to the total momentum of these subcurrents.

Note that the *three-point vertex* Fig. 58 (c) with two scalar lines and one gluon line is proportional to  $\delta^{ab}2k_1^\mu$ <sup>7</sup>, due to the Ward identity  $k_{A_j} \cdot J(A_j) = 0$  where  $J^\mu(A_j)$  is the subcurrent contracted with this vertex. When the color factor is extracted out, the substructure Fig. 42 (b), together with  $\tilde{J}^\mu$  produces  $2\tilde{J}[A_j] \cdot X_{A_j}$ , where  $X_{A_j}^\mu$  denotes the momentum of the propagator attached to  $J^\mu(A_j)$  from left. In Fig. 42 (c), the *four-point vertex*, together with the  $\tilde{J}^\mu$  contributes a  $-\tilde{J}[A_{jL}] \cdot \tilde{J}[A_{jR}]$ .

The *remaining terms* resulted from the  $K^\mu$  and  $L^\mu$  can be collected as

$$V_3 \sim [(X_{A_j} - (-X_{A_j} - k_{A_j})) - k_{A_j}] \cdot (K[A_j] + L[A_j]), \quad (7.2)$$

$$V_4 \sim -(L[A_{jL}] + K[A_{jL}]) \cdot J[A_{jR}] - J[A_{jL}] \cdot (L[A_{jR}] + K[A_{jR}]) + (L[A_{jL}] + K[A_{jL}]) \cdot (L[A_{jR}] + K[A_{jR}]).$$

In the above expression, the first line comes from the three-point vertex with the new expression  $\delta^{ab}2k_1^\mu$ , where  $2k_1^\mu$  (from the vertex Fig. 58 (c)) in this case is  $2X_{A_j}^\mu$ . Terms in (7.2) can be treated as follows. (i). The term  $(X_{A_j} - (-X_{A_j} - k_{A_j})) \cdot (K[A_j] + L[A_j])$  on the first line and all terms on the second line can be collected into a sum of Feynman diagrams, where some subcurrents are replaced by their total momenta (This discussion follows from section 5.1 in [37]). This part, together with the corresponding part in YMS currents (see Fig. 58 (d)), has to vanish due to Ward identity. (ii). The term  $-k_{A_j} \cdot L[A_j]$  in (7.2) is proportional to the sum of tree-level Feynman diagrams where some of the subcurrents are replaced by their total momenta, hence also vanishes. (iii). Following discussions parallel with [37], we find that the

---

<sup>6</sup>Here we make some clarifications about the result in [37]: (i). In [37], the reference order was fixed as the inverse of the right permutation of the BS amplitude. However, this result can be generalized to the cases with other reference orders by changing the particular expressions of the  $K^\mu$  term and  $L^\mu$  term. (ii). In [37], the expansion of  $\tilde{J}^\mu$  is expressed by summing over permutations, but in this paper, we sum over graphs. In fact they are equivalent to each other as pointed out in [7]. (iii). In [37], there are two equivalent decompositions of  $\tilde{J}^\mu$ : (a) The first is choosing the off-shell line as the last element, and an on-shell line as the first. Assuming that there are  $m$  external on-shell particles, this is an  $(m-1)!$ -decomposition and the coefficients were mentioned as type-A numerators. (b). The second is to choose the off-shell element as the first one but the last element is not fixed. This is an  $m!$ -decomposition and the coefficients are mentioned as type-B numerators in [37]. In this work, the  $\tilde{J}$  in eq. (7.1) is considered as the second decomposition. (iv). When extracting a factor  $\frac{i}{\sqrt{2}}$ ,  $\frac{i}{2}$  and  $-i$  from each three-point vertex, four-point vertex and gluon propagator in standard Feynman diagrams, we get an overall factor  $(1/\sqrt{2})^{N_g-1}$ , where  $N_g$  denotes the total number of external gluons in the current. This factor does not affect our discussions and is not included in (7.1).

<sup>7</sup>For each two-scalar one-gluon vertex, two-scalar two-gluon vertex and each scalar propagator, we extract a factor  $-i/\sqrt{2}$ ,  $-i/2$  and  $i$ , respectively. These factors only contribute to an overall factor and do not affect our discussions.

$K^\mu$  has the form

$$K^\mu = \frac{1}{k_{A_j}^2} k_{A_j}^\mu \sum_{A_j \rightarrow A_{jL}, A_{jR}} \tilde{\mathcal{J}}[A_{jL}] \cdot \tilde{\mathcal{J}}[A_{jR}], \quad (7.3)$$

when the reference order for expanding  $\tilde{\mathcal{J}}^\mu$  in (7.1) is chosen as the same with the right permutation in the BS currents. Consequently, the term  $-k_{A_j} \cdot K[A_j]$  can further be rewritten as

$$-k_{A_j} \cdot K[A_j] = - \sum_{A_j \rightarrow A_{jL}, A_{jR}} \tilde{\mathcal{J}}[A_{jL}] \cdot \tilde{\mathcal{J}}[A_{jR}]. \quad (7.4)$$

To sum up, the total contribution of Fig. 42 (b) and (c) is

$$2\tilde{\mathcal{J}}[A_j] \cdot X_{A_j} - 2 \sum_{A_j \rightarrow A_{jL}, A_{jR}} \tilde{\mathcal{J}}[A_{jL}] \cdot \tilde{\mathcal{J}}[A_{jR}]. \quad (7.5)$$

The prefactors of the two terms above are 2 and  $-2$ , respectively. On another hand, we choose the reference order in (6.1) as the permutation in the right half integrand, then multiply each external momentum and the loop momentum in the coefficients in (6.1) by 2 (thus all the momenta in numerators of  $\tilde{\mathcal{J}}^\mu$  are rescaled by a factor 2). The prefactors of the two terms in (6.15) respectively become 2 and  $-2$ . Thus, the two terms in (6.15) precisely agree with the two terms in (7.5), which are derived from Feynman diagrams.

Although the decomposition formula of the YMS BG current has not been explicitly given, it is natural to expect that the current mixing scalars and gluons can also split into the part decomposing according to the graphic rule, and another part which has to vanish in the on-shell limit. When the current is attached to the loop via three-scalar vertex as shown by Fig. 58 (d), the former part matches with (6.14), while the latter part, in general can be expanded into terms, in which some YM subcurrents are replaced by objects proportional to their total momenta. The sum of this part and the (i) part of (7.2) has to vanish due to Ward identity<sup>8</sup>. Hence, the Feynman diagrams match with the expression (6.16) obtained from one-loop CHY.

## 7.2 The extensions to multi-trace YMS and YM

Although all the previous discussions are carried around single-trace YMS amplitudes, it is straightforward to generalize them to multi-trace YMS amplitudes with a pure scalar loop. This is because the multi-trace YMS amplitudes that are derived from tree-level CHY formula can be obtained via introducing another type of components: components with a gluon trace as stated in appendix B. Such a component has an equal status with the components containing a type-1 line. Therefore, one just includes these new components in the previous discussions, and finally also arrives at the conclusion (6.16). But in this case, the graphs  $\mathcal{F}_{jL}$ ,  $\mathcal{F}_{jR}$  referred in (6.15) can be those with both gluons and scalar traces<sup>9</sup>. Note that the

<sup>8</sup>The detail of this statement will be presented in a coming work.

<sup>9</sup>On the Feynman diagram side, this feature naturally implies the four-scalar vertex for multi-trace YMS amplitudes.

multi-trace case discussed above is only the case that all loop propagators are scalar ones and the two particles  $\pm$  with the forward limit are adjacent to each other in the  $(n+2)$ -point tree-level half integrand. As classified in [33], according to distinct orders of coupling constants, there still exist (i). half integrands which contribute only scalar loop propagators but the particles  $\pm$  are not adjacent to each other, and (ii). the half integrands which contribute gluon propagators on the loop. The former case is related to the results in the current paper via a KK relation at one-loop level (see appendix K), while we leave a detailed study of the latter case in future work.

For YM amplitudes, we have to expand the reduced Pfaffian (see table 2) with  $n+2$  external particles in terms of tree-level PT factors and then take the forward limit. This can be achieved via eq. (2.17) where each term is accompanied by a Pfaffian for YMS. More specifically, apart from the prefactor  $\text{Tr}[F_{i_1} \cdot F_{i_2} \cdot \dots \cdot F_{i_l}]$ , each term in eq. (2.17) is a YMS half integrand with the scalar trace  $+, i_1, i_2, \dots, i_l, -$ . Hence, together with the other half integrand, which is expressed as an  $(n+2)$ -point PT factor where the  $\pm$  are considered as the two ends and the cyclic permutations over other  $n$  elements are summed over, such a term will produce

$$(-1)^l \text{Tr}[F_{i_1} \cdot F_{i_2} \cdot \dots \cdot F_{i_l}] \sum_{\{A_1, A_2, \dots, A_I\}} \text{gon}(A_1, A_2, \dots, A_I) \prod_{j=1}^I J[A_j], \quad (7.6)$$

where the cyclic symmetry of  $\text{Tr}[F_{i_1} \cdot F_{i_2} \cdot \dots \cdot F_{i_l}]$  has been applied. We summed over all possible cyclic partitions  $\{A_1, A_2, \dots, A_I\}$  of external particles such that the relative cyclic ordering of  $i_1, i_2, \dots, i_l$  is preserved. The  $J[A_j]$  has been defined in (6.14) and (6.15), where elements of  $\{i_1, \dots, i_l\}$  are considered as scalars. If the set  $\{i_1, \dots, i_l\}$  is empty, we do not have the  $\text{Tr}[F_{i_1} \cdot F_{i_2} \cdot \dots \cdot F_{i_l}]$  and the extra factor  $(D-2)$  in eq. (2.17) should be dressed. For this special case, the  $J[A_j]$ 's are those defined in (6.15) which contains only external gluons. When all terms in eq. (2.17) are collected, one expresses the one-loop YM amplitudes in terms of expressions with quadratic propagators

$$I_{\text{YM}}^{1\text{-loop}} = (D-2) \sum_{\{A_1, A_2, \dots, A_I\}} \text{gon}(A_1, A_2, \dots, A_I) \prod_{j=1}^I J[A_j] \quad (7.7)$$

$$+ \sum_{l=2}^n (-1)^l \sum_{\{i_1, i_2, \dots, i_l\} \in S_l \setminus Z_l} \text{Tr}[F_{i_1} \cdot F_{i_2} \cdot \dots \cdot F_{i_l}] \sum_{\{A_1, A_2, \dots, A_I\}} \text{gon}(A_1, A_2, \dots, A_I) \prod_{j=1}^I J[A_j],$$

where each  $A_j$  can at least contain one element. Hence the  $I$  in each term runs from 1 to  $n$  (the total number of external particles). Terms with all  $i_1, \dots, i_l$  belonging to a same subset have to vanish due to the  $U(1)$ -decoupling identity of YMS current.

## 8 Conclusions and further discussions

In this paper, we provided a general approach to converting the linear propagators which exist in the one-loop Cachazo-He-Yuan (CHY) formula [1–5] into quadratic propagators which exist in traditional Feynman

diagrams. We expanded  $n$ -point one-loop CHY half integrands for Yang-Mills-scalar (YMS) in terms of  $(n + 2)$ -point Parke-Taylor (PT) factors with forward limits, according to the tree-level refined graphic rule. Then decomposed a graph into subgraphs and established correspondence between subgraphs and subcurrents in the linear-propagator Feynman diagrams (LPFD). Nonlocalities occur when two subgraphs are contracted with each other but are separated by linear propagators in the LPFD. We treated the nonlocalities by combining two approaches. Once the nonlocalities are canceled, the expressions can always be arranged into a cyclic sum which implies a quadratic-propagator expression.

The formula with quadratic propagators has further been shown to match the traditional Feynman diagrams in YMS. The quadratic form reduced from CHY formula of multi-trace YMS amplitudes and pure Yang-Mills (YM) amplitudes were obtained via the single-trace YMS. Although, the starting point of this work is the one-loop CHY formula, the full discussion essentially relies only on the forward limit. Therefore, the discussion in this paper may be directly extended to other approaches which are based on forward limit. Moreover, since the quadratic form of the pure YM amplitudes has been obtained, it is straightforward to generalize the results to super-Yang-Mills theories and the gluon amplitudes with fermions circulating in the loop.

There are still some related problems that deserve further study. The first one is to implement the conversion from linear to quadratic propagators for YMS with gluon propagators on the loop, Einstein-Yang-Mills (EYM) and gravity (GR) integrands, which have more complicated CHY half integrands. Being different from the situation studied in this paper, they do not have a half integrand that can be directly expressed as a scalar PT factor with a cyclic symmetry [24], which means that the contribution of the tadpole diagrams needs to be revisited and cannot be straightforwardly canceled out by U(1)-decoupling. The second is how to expand the CHY half integrands into combinations of tensorial PT factors in a generic way. The third is, we can analyze the algebraic structures of results in this paper and further study the construction of BCJ numerators [35, 36] at one-loop (see e.g. [48–52]). The relations between BCJ numerators in various theories at tree-level [53, 54] may further help one to extend the discussions to one-loop amplitudes in different theories. Last but not least, although we have already analyzed the relationship between the result in the current paper and Feynman diagrams for YMS, it is still worth working out the full connection between the YM results and the YM Feynman diagrams.

## Acknowledgements

We would like to thank Bo Feng, Song He, Yong Zhang and Kang Zhou for helpful suggestions and comments on the draft. We also thank Chih-Hao Fu and Yihong Wang for helpful discussions on kinematic algebra. We thank Yixiao Tao, Xinhao Tong and Konglong Wu for helpful discussions on the decomposition of Berends-Giele currents in YMS. We acknowledge the referees of this paper for helpful suggestions. The authors acknowledge the organizers of “3rd seminar on quantum field theory and its applications” (2023, Beijing, China). YD would like to thank the organizers of “4th seminar on field theory and string theory in China” (2023, Nanjing, China) as well as Fudan University, Tianjin University for kind invitation. CX

would like to thank the organizers of “2023 Frontier Summer School on String Theory, Field Theory, and Holography” (2023, Nanjing, China). This work is supported by NSFC under Grant No. 11875206.

## A Expansion formula of $\text{PT}(+, x_1, \dots, x_r, -) \text{Pf}[\Psi_G]$

The expansion formula (2.12) can be equivalently expressed by the strength tensors  $F_i^{\mu\nu}$  as follows:

- Define reference order for gluons by an ordered set  $R = \{\gamma_1, \dots, \gamma_s\}$  and define the root set by  $\mathcal{R} = \{+, x_1, x_2, \dots, x_r\}$ .
- Pick out the highest-weight element  $a = \gamma_s$  and possible other elements  $i_1, \dots, i_l$  from the ordered set  $R$ . Construct a chain towards an element  $b$  in the root set  $\mathcal{R}$

$$\epsilon_a \cdot F_{i_1} \cdot F_{i_2} \cdot \dots \cdot F_{i_l} \cdot k_b. \quad (\text{A.1})$$

Redefine the ordered set and the root set by moving  $a, i_1, \dots, i_l$  from  $R$  to  $\mathcal{R}$ .

- Repeating the previous step by the new defined  $R$  and  $\mathcal{R}$  until the ordered set  $R$  has been cleared up, we finally get a fully connected tree graph  $\mathcal{F}$ . This graph is accompanied by a coefficient  $\mathcal{C}^{\mathcal{F}}$  which is a product of Lorentz contractions between  $\epsilon^\mu$ ,  $F^{\rho\sigma}$  and  $k^\nu$ . Permutations established by  $\mathcal{F}$  are determined in the same way with those in section 2.3.
- When all graphs are summed over, we get an expansion formula of  $\text{PT}(+, x_1, \dots, x_r, -) \text{Pf}[\Psi_G]$ .

When all strength tensors  $F_i^{\mu\nu}$  are expanded into  $k_i^\mu \epsilon_i^\nu - \epsilon_i^\mu k_i^\nu$ , the result turns into that was generated in section 2.3. This has been proven in [7].

## B Expansion of $\text{PT}(+, \sigma_1, -) \text{PT}(\sigma_2) \cdots \text{PT}(\sigma_m) \mathcal{P}$

We provide the graphic rule for the half integrand  $\text{PT}(+, \sigma_1, -) \text{PT}(\sigma_2) \cdots \text{PT}(\sigma_m) \mathcal{P}$  which exists in a multi-trace amplitude with  $m$  traces  $\mathbf{tr}_1 = \{+, \sigma_1, -\}$ ,  $\mathbf{tr}_2 = \{\sigma_2\}$ , ...,  $\mathbf{tr}_m = \{\sigma_m\}$ . We define a KK basis for a trace  $\mathbf{tr}_i$  by

$$\text{KK}[i, a_i, b_i] \equiv (-1)^{|\beta|} \{a_i, \boldsymbol{\alpha} \sqcup \boldsymbol{\beta}^T, b_i\}, \quad (\text{B.1})$$

where the trace  $\mathbf{tr}_i$  can be expressed as  $\mathbf{tr}_i = \{a_i, \boldsymbol{\alpha}, b_i, \boldsymbol{\beta}\}$ . As proven in [8], the refined graphic rule for  $\text{PT}(+, \sigma_1, -) \text{PT}(\sigma_2) \cdots \text{PT}(\sigma_m) \mathcal{P}$  can be obtained by adjusting the rules in section 2.3.1 as follows:

- Enlarge the reference order set  $R = \{\gamma_1, \dots, \gamma_s\}$  in step-1 by including the traces  $\{\mathbf{tr}_2, \dots, \mathbf{tr}_m\}$ , the reference order then becomes  $R = \{\gamma_1, \dots, \gamma_{s+m-1}\}$ .

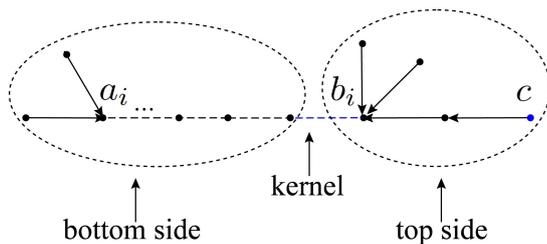


**Figure 43.** In the multitrace case, there exists a new type of component. In such a component, a trace is characterized by a simple chain where nodes are connected via type-4 lines, possible type-2 lines are connected to the trace. If the highest-weight node in this component is a gluon  $c$ , the contribution of the graph can always be expanded in terms of those graphs where  $c$  is connected to an end node  $b_i$  of the trace  $\text{KK}[i, a_i, b_i]$  via type-2 lines. The path from this gluon to root must pass through the full trace  $\text{KK}[i, a_i, b_i]$  where  $a_i$  is the nearest-to-root scalar. If the weight of the trace  $\mathbf{tr}_i$  is higher than all gluons in that component, the node  $b_i$  carries the weight of the trace. In both cases, the kernel is defined by the type-4 line attached to  $b_i$ . The top side is the side containing  $b_i$ .

- Consider the  $C_0$  (defined in section 2.3) as the component involving  $\mathbf{tr}_1$ . Enlarge the kernel set by including traces  $\{\mathbf{tr}_2, \dots, \mathbf{tr}_m\}$ . For each trace  $\mathbf{tr}_i$  ( $i = 2, \dots, m$ ), we choose a pair  $a_i, b_i \in \mathbf{tr}_i$  and then arrange the elements of  $\mathbf{tr}_i$  as  $\text{KK}[i, a_i, b_i]$ . For a given permutation in  $\text{KK}[i, a_i, b_i]$ , two adjacent nodes are connected by a type-4 line. As demonstrated by Fig. 43, components containing the trace  $\mathbf{tr}_i$  are constructed as follows: (i). If the trace has the highest weight in the component, we plant gluons to scalars of the trace via type-2 lines. (ii). If the highest-weight element is a gluon say  $c$ , we further require that  $c$  is connected to  $b_i$  via type-2 lines. *The kernel of such a component is defined as the type-4 line attached to  $b_i$ . The top side of this component is defined by the side containing  $b_i$ .*

With the above adjustment, one finally gets all possible graphs  $\mathcal{F}$  which include graphs with  $k$  pairs of type-2 lines and  $m$  traces. The summation over  $\mathcal{F}$  in eq. (2.12) means summing over all possible values of  $k$  ( $k = 1, \dots, \lfloor \frac{s}{2} \rfloor$ ), all possible graphs corresponding to a given  $k$ . Given trace  $\mathbf{tr}_i$ , we sum over all possible  $a_i \in \mathbf{tr}_i$  ( $a_i \neq b_i$ ) for a fixed  $b_i \in \mathbf{tr}_i$  when the following two conditions are satisfied simultaneously: (i). the trace  $\mathbf{tr}_i$  is involved in a starting component of a chain and (ii). the trace  $\mathbf{tr}_i$  has the highest weight in this component. For other cases, all ordered pairs of  $\{a_i, b_i\}$  in  $\mathbf{tr}_i$  are summed over. The kinematic coefficient  $\mathcal{C}^{\mathcal{F}}$  is also given by the product of the kinematic factors corresponding to the lines, reminding that a type-4 line does not bring any kinematic factor. In addition to the signs counted in the single-trace case, each trace is also accompanied by a sign  $(-1)^{|\beta_i|}$ .

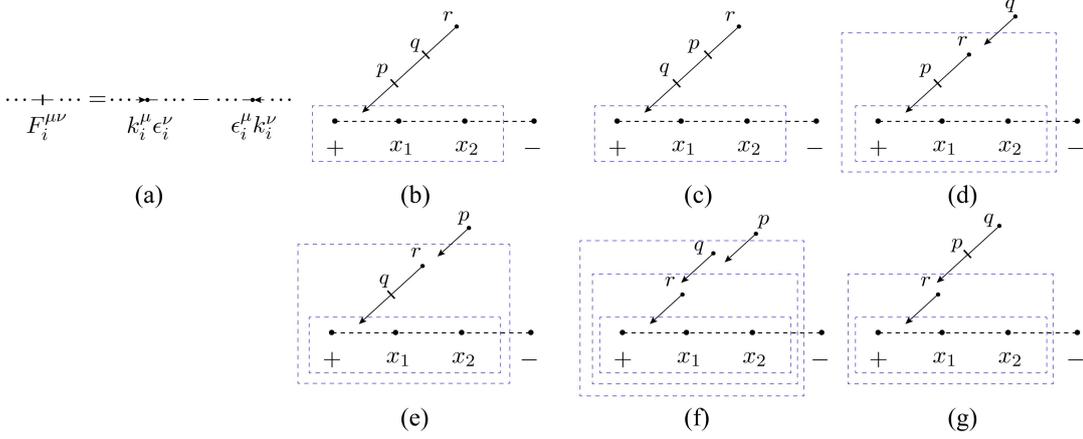


**Figure 44.** When we introduce the compact expression (a) for the strength tensor, all graphs for three-gluon two-scalar integrands are presented by graphs (b)-(g). The reference order is fixed as  $p \prec q \prec r$ .

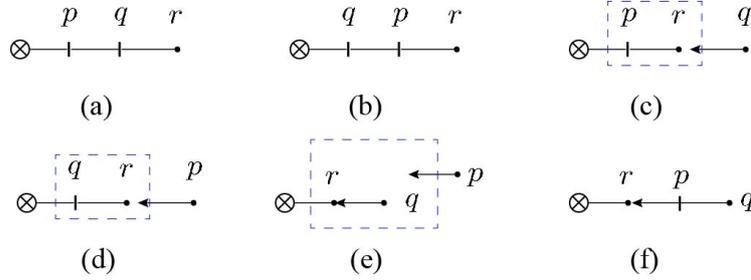


**Figure 45.** All graphs for the effective current  $\tilde{J}^\mu(p, q, r)$  with the reference order  $p \prec q \prec r$ .

### C All graphs with three gluons and all graphs for the effective current $\tilde{J}^\mu(p, q, r)$

We present all graphs with three gluons and two scalars in Fig. 44 and all graphs for the effective current  $\tilde{J}^\mu(p, q, r)$  in Fig. 45. The reference order is supposed to be  $p \prec q \prec r$ . The compact form, which is expressed by strength tensors  $F_i^{\mu\nu} = k_i^\mu \epsilon_i^\nu - \epsilon_i^\mu k_i^\nu$  in Fig. 44 (a), is directly generated by the rule in appendix A. The graphs in Fig. 45 can be obtained from Fig. 44 (b)-(g), via replacing the root set by a cross node which stands for other structure contracted with  $\tilde{J}^\mu(p, q, r)$ , and deleting the disconnected graphs which have to vanish due to generalized  $U(1)$ -decoupling identity. The explicit expression of  $\tilde{J}^\mu(p, q, r)$  is

$$\begin{aligned}
\tilde{J}^\mu(p, q, r) &= (\epsilon_r \cdot F_q \cdot F_p)^\mu \phi_{pqr|a_1 a_2 a_3} + (\epsilon_r \cdot F_p \cdot F_q)^\mu \phi_{qpr|a_1 a_2 a_3} \\
&+ \left[ (\epsilon_q \cdot k_r) \phi_{prq|a_1 a_2 a_3} + (\epsilon_q \cdot k_p) \phi_{p\{r\sqcup q\}|a_1 a_2 a_3} \right] (\epsilon_r \cdot F_p)^\mu \\
&+ \left[ (\epsilon_p \cdot k_r) \phi_{qrp|a_1 a_2 a_3} + (\epsilon_p \cdot k_q) \phi_{q\{r\sqcup p\}|a_1 a_2 a_3} \right] (\epsilon_r \cdot F_q)^\mu \\
&+ \left[ (\epsilon_q \cdot k_r) (\epsilon_p \cdot k_q) \phi_{rqp|a_1 a_2 a_3} + (\epsilon_q \cdot k_r) (\epsilon_p \cdot k_r) \phi_{r\{q\sqcup p\}|a_1 a_2 a_3} \right] \epsilon_r^\mu + (\epsilon_q \cdot F_p \cdot k_r) \epsilon_r^\mu \phi_{r pq|a_1 a_2 a_3}.
\end{aligned} \tag{C.1}$$

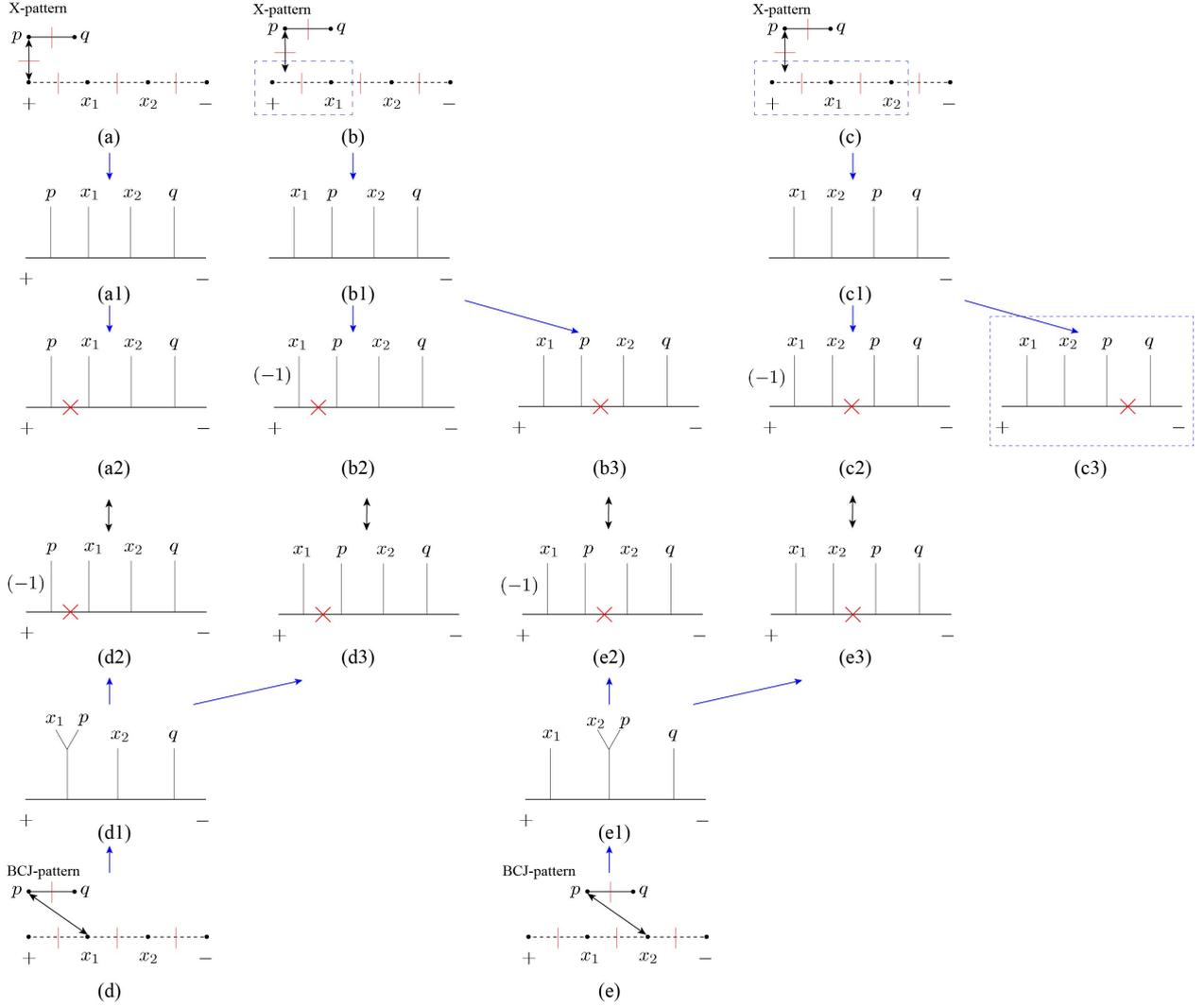


Figure 46. The cancellation map for the example in section 3.4

## D The cancellation map for the example in section 3.4

Fig. 46 presents the cancellation map between X- and BCJ-patterns for the example in section 3.4. The diagram (c3) in Fig. 46 is the surviving term, corresponding to the second term of the second line in (3.28).

## E Two versions of graphic rules for a subgraph

When a partition  $\{A_1, A_2, \dots, A_j, \dots\}$  and a topology for this partition are fixed, we can construct subgraphs for a subset  $A_j$  via graphic rule, which mostly inherits the rule for a full graph, see section 2.3. Some adjustments have to be introduced to adapt the fact that the subgraph contains off-shell nodes:

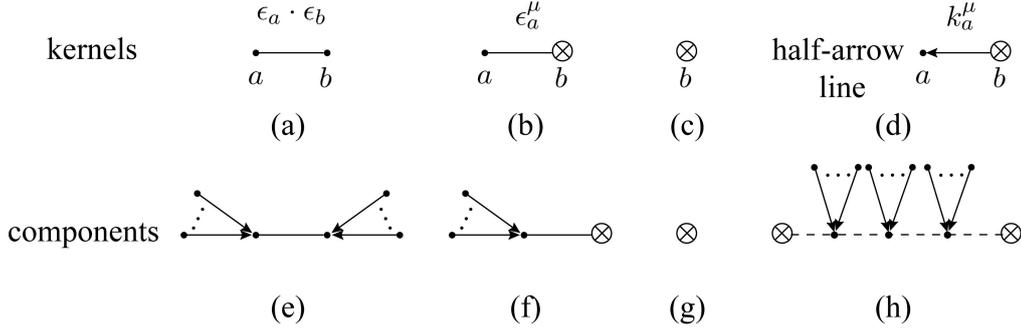


**Figure 47.** Graphs (a), (b) and (c) are possible kernels in a subgraph. Graphs (e), (f), (g) and (h) are possible components in a subgraph. A line between an on-shell node and a cross node can either be a half line (with no arrow) or a half-arrow line, as shown by (b) and (d), respectively.

### Version-1 rule for a subgraph

- For a given subset  $A_j$ , we not only have the on-shell nodes in  $\mathcal{F}_j$ , but also have off-shell nodes, i.e., the subtree structures attached to  $\mathcal{F}_j$ , as shown by Fig. 38 (c). Specifically, the off-shell nodes locating above  $\mathcal{F}_j$  (e.g.,  $b_1$  and  $b_2$  in Fig. 38 (c)) stand for the corresponding *full subtree structures attached to  $\mathcal{F}_j$*  whose distance from root are larger than that of  $\mathcal{F}_j$ . The off-shell node below  $\mathcal{F}_j$  only represents *the subgraph below  $\mathcal{F}_j$* . The weights of off-shell nodes above  $\mathcal{F}_j$  are defined by the highest-weight nodes in the corresponding subtree structure. The reference order between these nodes inherits the reference order for the full integrand.
- *If the subset  $A_j$  contains only gluons*, we construct  $k$  kernels which can be obtained by (i). connecting a type-1 line between two on-shell gluons, as shown by Fig. 47 (a), (ii). connecting a half line (with no arrow) between an on-shell gluon and an off-shell node, as shown by Fig. 47 (b), or (iii). a single cross node, see Fig. 47 (c). All off-shell nodes are contained by kernels. Connect other on-shell gluons towards the on-shell nodes in kernels (i) and (ii) via type-2 ( $\epsilon \cdot k$ ) lines, together with possible single cross nodes, we get  $k$  components, as shown by Fig. 47 (e), (f) and (g). In the component with both off-shell node above the subset and on-shell nodes, we require that the weight of the off-shell node is higher than those of on-shell nodes in this component. *If the subset  $A_j$  contains scalars*, apart from the possible components which have been introduced previously, we also have a component involving scalars, as shown by Fig. 47 (h). These scalars must live on the path from a cross node to another (both cross nodes also involve scalars) and are interconnected via type-4 lines, in accordance with the relative order of the scalar set. The gluons are connected to the scalars via type-2 lines.
- Consider the component containing the off-shell node below  $\mathcal{F}_j$  (e.g., the off-shell node representing  $\mathcal{F}_1$  in Fig. 38 (c)) as root. Construct COC's following step-3 in section 2.3 and require:

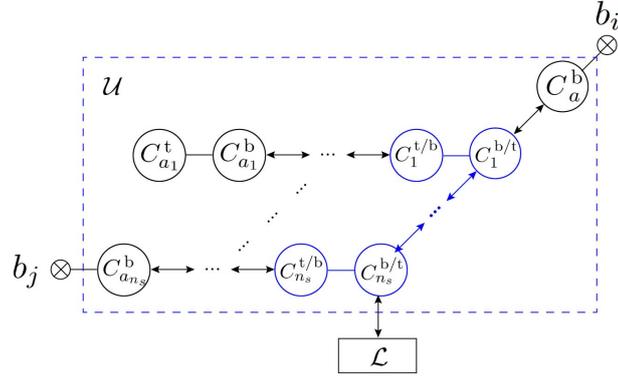


**Figure 48.** In this spurious graph, the cross node  $b_i$  is supposed to be the highest-weight node. In the upper block  $\mathcal{U}$  attached to  $b_i$ , there are  $n_s$  components (mentioned as *spurious components*) whose single sides are passed through by the path from  $b_i$  to the lower component  $\mathcal{L}$ .

- (a). The lines between on-shell nodes of two components are type-3 ( $k \cdot k$ ) lines. The line between an off-shell node and an on-shell node of two components should be a half-arrow line (shown by Fig. 47 (d)) pointing towards the on-shell node.
- (b). An off-shell node above the subgraph can only live in the starting component (the  $C_a$  in (2.13)) of a COC.

An example for subgraphs constructed by version-1 rule is given by Fig. 52 in appendix G.

In order to cancel the nonlocalities following approach-1 and -2, we have to further introduce spurious graphs so that X- and BCJ-patterns are explicitly constructed. To achieve this, we provide the following equivalent construction rule.

#### Version-2 rule for a subgraph

- **Step-1** Pick out a component led by an off-shell node  $b_i$ . Construct COC's, which are led by components with higher weights than that of  $b_i$ , towards root following version-1 rule.
- **Step-2** Define the *lower block*  $\mathcal{L}$  by the subgraph constructed in the above step, the *upper block*  $\mathcal{U}$  by the component containing  $b_i$  (the highest-weight cross node among the remaining on-shell and off-shell nodes). Construct a COC towards either  $\mathcal{L}$  or  $\mathcal{U}$ .
- **Step-3** Redefine the upper and lower blocks  $\mathcal{U}$  and  $\mathcal{L}$  by absorbing the COC which has been constructed in step-2. Repeat step-2 using the new defined  $\mathcal{U}$  and  $\mathcal{L}$  until all components have been used, we get the final configurations of  $\mathcal{U}$  and  $\mathcal{L}$ , which are two subgraphs separated from each other.
- **Step-4** If both  $\mathcal{U}$  and  $\mathcal{L}$  involve on-shell nodes, connect a type-3 line between them. If one of  $\mathcal{U}$  and  $\mathcal{L}$  is a single cross node, connect a half-arrow line pointing to the other block.

Following these steps, we finally get fully connected tree graphs. *A part of them are those constructed according to version-1 rule, while the other part are pairs of spurious graphs with opposite signs [7].* The

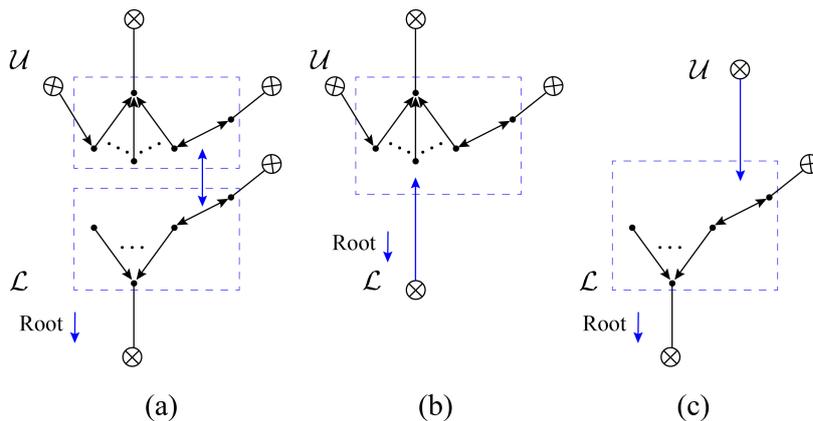


**Figure 49.** Possible structures of subgraphs

sign of a spurious graph is given by  $(-1)^{n_s+n_a}$  where (i).  $n_s$  denotes the number of spurious components in the upper block, as shown by Fig. 48, (ii).  $n_a$  denotes the number of arrows pointing away from root.

A graph constructed by version-2 rule consists of the upper and lower blocks  $\mathcal{U}$  and  $\mathcal{L}$ , which are interconnected to each other. The structures of subgraphs can further be classified according to whether the  $\mathcal{U}$  or  $\mathcal{L}$  contains on-shell nodes:

- **Both  $\mathcal{U}$  and  $\mathcal{L}$  contain on-shell nodes, as shown by Fig. 49 (a).** The line between them is a type-3 line. When the kinematic coefficients of  $\mathcal{U}$  and  $\mathcal{L}$  are extracted out, we get a BCJ-pattern with correct signs in each term [7].
- **The lower block  $\mathcal{L}$  contains no on-shell node, as shown by Fig. 49 (b).** Denote such subgraph and the subgraph below by  $\mathcal{F}_j$  and  $\mathcal{F}_l$ , respectively. If the upper block of  $\mathcal{F}_l$  has no on-shell node (as shown by Fig. 49 (c)),  $\mathcal{F}_j$  makes a contribution  $(-k_{A_j} \cdot k_{A_l})$  to an X-pattern  $(-k_{A_j} \cdot X_{A_j})$ . Else, if the upper block of  $\mathcal{F}_l$  has on-shell nodes (as shown by Fig. 49 (a) and (b)), the  $\mathcal{F}_j$  is neither a BCJ-pattern nor a part of the X-pattern with  $-k_{A_j} \cdot X_{A_j}$ . Subgraph in this case should be treated differently according to different configurations of  $\mathcal{F}_l$ .
- **The upper block  $\mathcal{U}$  contains no on-shell node, as shown by Fig. 49 (c).** In this case, the upper block has only one cross node which can further be extracted out as a  $C \cdot k_{A_j}$  factor. When the cross node is extracted out, the subgraph becomes a physical graph constructed by version-1 rule.

## F Constructing a subgraph in a given partition and topology

In this section, we construct subgraphs  $\mathcal{F}_j$  for a given partition and a fixed topology. To achieve this, we can *combine the two versions of graphic rules in appendix E for subgraphs in various ways*. Different approaches are equivalent to each other since they must be reduced into the same set of physical graphs when pairs of spurious graphs are canceled out. Here, we provide two possible approaches to the construction of subgraphs for a given partition  $\{A_1, A_2, \dots, A_j, \dots, A_i\}$  and a given topology.

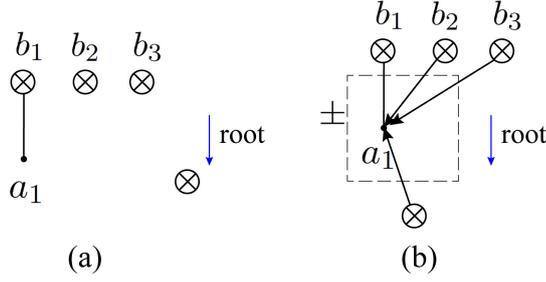


**Figure 50.** Suppose the reference order is  $a_1 \prec b_1 \prec b_2 \prec b_3$ . If the components of a subgraph are shown by (a), there does not exist physical graph constructed by step-1 in approach-1. However, we may introduce a pair of spurious graphs (b) with opposite signs so that the cancellations totally follow from section 6.2.

### F.1 Approach-1

We assume the cross nodes for the subgraph  $A_j$  are  $b_1, \dots, b_s$  (the reference order is  $b_1 \prec \dots \prec b_s$ ) whose highest-weight nodes are  $c_1, \dots, c_s$ , respectively. The nodes  $c_1, \dots, c_s$  must belong to different subsets to the right side of  $A_j$  in the partition. Supposing that the nodes  $c_1, \dots, c_s$  in the partition from left to right are  $c_{\sigma_1}, \dots, c_{\sigma_s}$ , we further generate all subgraphs properly in the following way:

- **Step-1** Generate all possible subgraphs according to version-1 rule.
- **Step-2** Turn back to the step that generates the COC led by  $b_{\sigma_s}$ . Considering  $b_{\sigma_s}$  as the upper block, the tree structure which has already been constructed as the lower block, we apply version-2 rule to generate possible graphs. As demonstrated before, such graphs may (a). contain X- or BCJ-pattern, (b). provide a  $C \cdot k_{A_j}$  factor when  $b_{\sigma_s}$  is extracted out, or (c). be neither the case (a) nor (b) and can be treated when the subgraph below is taken into account. Further treatment of cases (a) and (c) are given in section 6.2. For (b), we get a physical subgraph (a subgraph generated by version-1 rule) with  $b_{\sigma_s}$  extracted out.
- **Step-3** For the physical graph in (b) with  $b_{\sigma_s}$  extracted out, we repeat step-2 for cross nodes  $b_{\sigma_{s-1}}, \dots, b_{\sigma_2}$  in turn.
- **Step-4** When all cross nodes  $b_{\sigma_s}, \dots, b_{\sigma_2}$  have been extracted out, we have a physical graph which has only one cross node above  $\mathcal{F}_j$ , i.e.,  $b_{\sigma_1}$ . We finally consider  $b_{\sigma_1}$  as the upper block, the component containing the cross node below  $\mathcal{F}_j$  as the lower one, and apply version-2 rule. We again obtain subgraphs, each of which (a). contains X- or BCJ-pattern, (b). provides a  $C \cdot k_{A_j}$  factor with  $b_{\sigma_1}$  extracted out, or (c). is neither the case (a) nor (b).

*Comment on the boundary:* If there does not exist physical subgraph constructed in the first step, as shown by Fig. 50 (a), the total contribution of this subset must be zero. Nevertheless, we may construct pairs of spurious graphs from step-2 (as shown by Fig. 50 (b)) so that all cancellations follow from the way pointed in section 6.2.

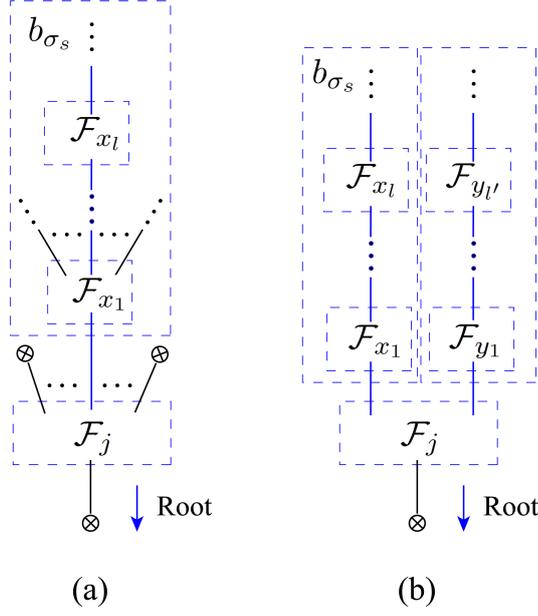


**Figure 51.** Assuming that the  $c_{\sigma_s} \in \mathcal{F}_{x_l}$ , the subgraphs in (a) on the path from  $c_{\sigma_s}$  to  $\mathcal{F}_j$  are not separated by other subsets in the partition  $\{A_1, \dots, A_j, \dots, A_{x_1}, \dots, A_{x_l}, \dots, A_i\}$  where  $A_{x_1}, \dots, A_{x_l}$  are the subsets corresponding to  $\mathcal{F}_{x_1}, \dots, \mathcal{F}_{x_l}$ . In graph (b), the subgraphs on the path from  $c_{\sigma_s}$  to  $\mathcal{F}_j$  are separated in the partition  $\{\dots, A_j, \dots, A_{x_1}, \dots, A_{x_{l-k}}, A_{y_1}, \dots, A_{y_{l'}}, A_{x_{l-k+1}}, \dots, A_{x_l}, \dots\}$ .

- (i). If  $b_{\sigma_s}$  is not the highest-weight node  $b_s$  and the component with  $b_{\sigma_s}$  contains on-shell nodes, we do not further construct subgraphs and this case has no contribution to the final result.
- (ii). If  $b_{\sigma_s}$  is not the highest-weight node and the component with  $b_{\sigma_s}$  is a single cross node, the construction can further be performed as:
  - (a). If the subgraphs on the path from  $c_{\sigma_s}$  to  $\mathcal{F}_j$  (including the subgraph containing  $c_{\sigma_s}$  but excluding  $\mathcal{F}_j$ ) are not separated by other subsets in the partition (as demonstrated by Fig. 51 (a)), the cross node  $b_{\sigma_s}$  can be extracted out and provides a  $C \cdot k_{A_j}$  factor. We may have pairs of spurious graphs generated at the next step when  $b_{\sigma_{s-1}}$  is considered as the upper block.
  - (b). If the subgraphs on the path from  $c_{\sigma_s}$  to  $\mathcal{F}_j$  are separated by other subsets in the partition (as shown by Fig. 51 (b)), we do not have any reasonable subgraph  $\mathcal{F}_j$ .
- (iii). If  $b_{\sigma_s}$  is the highest-weight node  $b_s$ , we consider it as the upper block and construct subgraphs (pairs of spurious graphs) from step-2. In the special case that no such subgraph can be produced, we follow the (a) and (b) in (ii).

In the cases with  $b_{\sigma_s}$  extracted out, we return to step-3 and perform a further construction.

As an example of the boundary case, we assume that  $A_{m_i}$  ( $i = 1, 2, 3$ ) is the subset containing the highest-weight node in Fig. 50 for each cross node  $b_i$ . For partition  $\{\dots, A_j, \dots, A_{m_2}, \dots, A_{m_3}, \dots, A_{m_1}, \dots\}$ ,

we do not construct any subgraph according to (i). For partition  $\{\dots, A_j, \dots, A_{m_1}, \dots, A_{m_3}, \dots, A_{m_2}, \dots\}$ , if the subgraphs on the path from  $\mathcal{F}_{m_2}$  to  $\mathcal{F}_j$  are not separated by other subsets, the cross node  $b_2$  can be extracted out and produces a  $C \cdot k_{A_j}$  factor, according to (a) in (ii). After this step, we must turn to  $b_3$  and construct a pair of subgraphs, as shown by Fig. 50 (b).

## F.2 Approach-2

Now we provide another possible approach to constructing subgraphs. Assuming the relative order of cross nodes above  $\mathcal{F}_j$  is  $b_1 \prec \dots \prec b_k \prec \dots \prec b_s$ , there are two possible situations depending on different relative positions of the subgraphs contained by cross nodes of  $\mathcal{F}_j$  in the partition:

- **Situation (i).** Assuming that the highest-weight node  $c_k$  in the cross node  $b_k$  is contained by subgraph  $\mathcal{F}_{x_l}$ , graphs on the path between  $\mathcal{F}_j$  and  $\mathcal{F}_{x_l}$  (including  $\mathcal{F}_j$  and  $\mathcal{F}_{x_l}$ ) are not separated by other subset in the partition

$$\{A_1, \dots, A_j, A_{x_1}, \dots, A_{x_l}, \dots, A_i\}, \quad (\text{F.1})$$

where  $A_{x_1}, \dots, A_{x_l}$  are the subsets corresponding to  $\mathcal{F}_{x_1}, \dots, \mathcal{F}_{x_l}$ , as shown by Fig. 51 (a) (when  $b_{\sigma_s}$  is replaced by  $b_k$ ).

- **Situation (ii).** For any cross node  $b_k$  above  $\mathcal{F}_j$ , the path from  $\mathcal{F}_j$  to  $c_k$  in  $b_k$  (including  $\mathcal{F}_j$  and the subgraph containing  $c_k$ ) is always separated by other subsets in the partition. For example in Fig. 51 (b) (when  $b_{\sigma_s}$  is replaced by  $b_k$ ), there are two cross nodes whose highest-weight nodes are involved in  $\mathcal{F}_{x_l}$  and  $\mathcal{F}_{y_{l'}}$ , respectively. The subgraph  $\mathcal{F}_j$  in Fig. 51 (b) with the partition

$$\{\dots, A_j, A_{x_1}, \dots, A_{x_{l-k}}, A_{y_1}, \dots, A_{y_{l'-k'}}, A_{x_{l-k+1}}, \dots, A_{x_l}, A_{y_{l'-k'+1}}, \dots, A_{y_{l'}}, \dots\} \quad (\text{F.2})$$

is a graph in this situation.

For **situation (i)**, we generate all possible subgraphs according to version-1 rule and then extract cross nodes according to the order  $b_2, \dots, b_{k-1}, b_s, b_{s-1}, \dots, b_{k+1}, b_k$  in turn by version-2 rule. For **situation (ii)**, we extract cross nodes  $b_1, b_2, \dots, b_s$  in turn. Similar with the treatment in approach-1, this approach also produces X- and BCJ-patterns. Thus the cancellations in section 6.2 can also be applied while proper boundaries (pairs of spurious graphs) are further introduced.

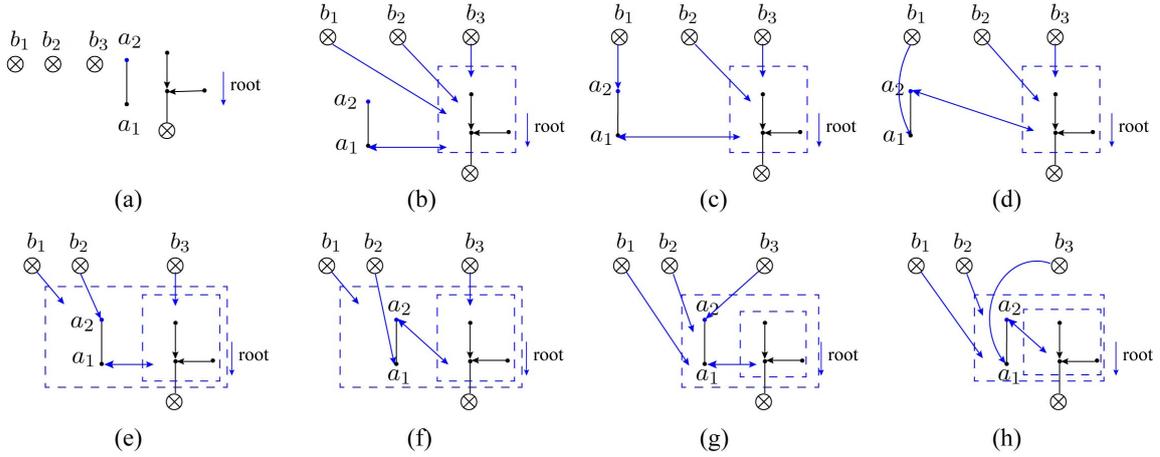


**Figure 52.** Graph (a) present five components including three off-shell nodes  $b_1, b_2, b_3$ , the component consisting of two on-shell nodes  $a_1, a_2$ , and the component below the subgraph. The reference order of nodes is supposed to be  $a_1 \prec a_2 \prec b_1 \prec b_2 \prec b_3$ . Graphs (b)-(h) are all possible graphs constructed by these components, via version-1 rule.

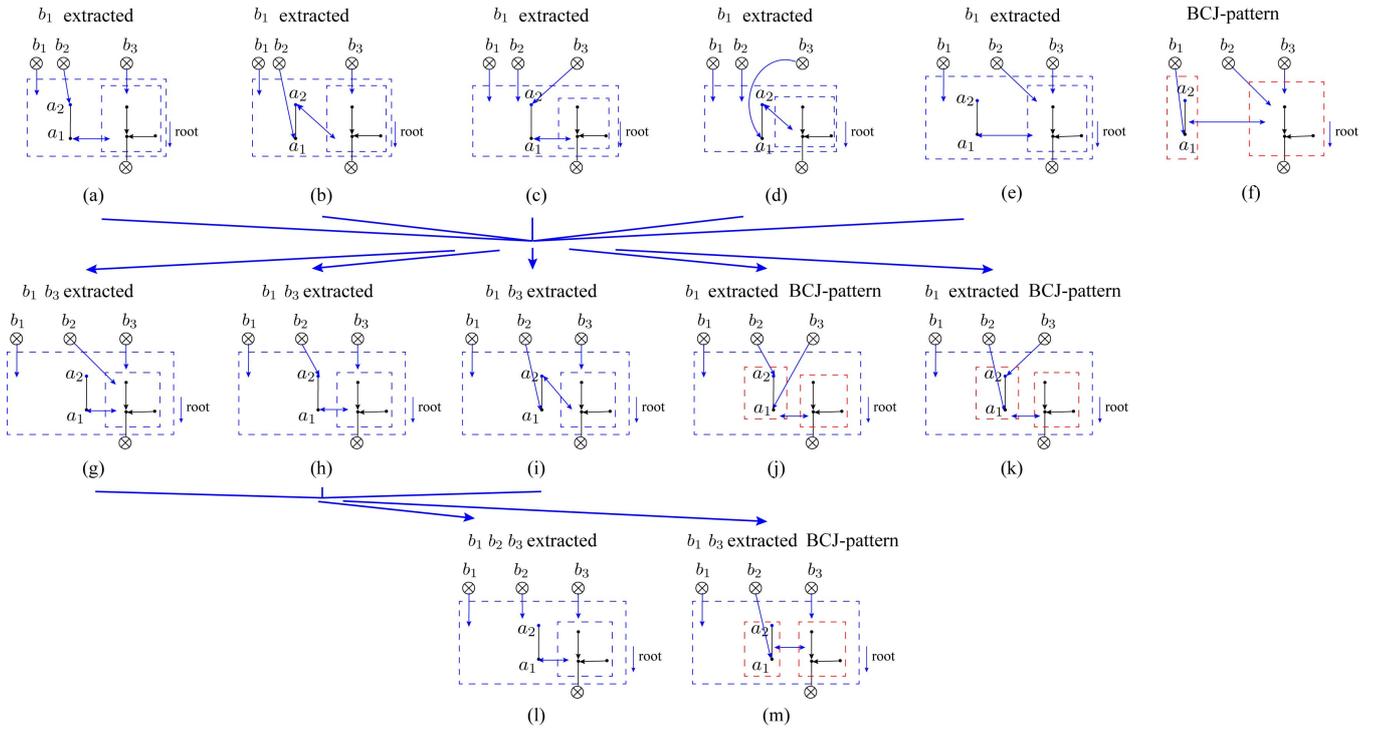


**Figure 53.** Subgraphs constructed by combining version-1 and version-2 rules, using the components in Fig. 52 (a) with the same reference order  $a_1 \prec a_2 \prec b_1 \prec b_2 \prec b_3$ . These graphs not only reproduce the physical graphs Fig. 52, but also introduce pairs of spurious graphs. Each of the final constructed subgraphs either contains BCJ-pattern or has all cross nodes extracted out.

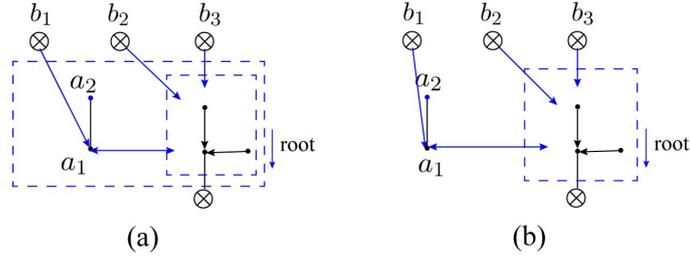


**Figure 54.** Graphs (a) and (b) are the same spurious graph coming from Fig. 53 (e) and (f), respectively. The sign for (b) is minus, while that for (a) is plus. Thus they cancel each other.

## G Explicit examples for the construction of subgraphs

Fig. 52 (b)-(h) present an example for graphs constructed by five components as shown by Fig. 52 (a), via version-1 rule in appendix E. Graphs in Fig. 53 are generated by combining version-1 and -2 rules, with the same components in Fig. 52 (a). These graphs can be considered as those constructed according to approach-1 in appendix F for the partition  $\{\dots, A_j, \dots, A_{m_2}, \dots, A_{m_3}, \dots, A_{m_1}, \dots\}$ , where the highest-weight nodes in  $b_1, b_2, b_3$  are respectively contained by  $A_{m_1}, A_{m_2}, A_{m_3}$ . On another hand, graphs in Fig. 53 can be obtained by approach-2 when partition is given as  $\{\dots, A_j, A_{j+1}, \dots, A_{m_2}, \dots, A_{m_1}, \dots, A_{m_3}, \dots\}$  or  $\{\dots, A_j, A_{j+1}, \dots, A_{m_2}, \dots, A_{m_3}, \dots, A_{m_1}, \dots\}$ . Here, all the subsets  $A_{j+1}, \dots, A_{m_2}$  correspond to the subgraphs which belong to  $b_2$  and live on the path from  $\mathcal{F}_{m_2}$  to  $\mathcal{F}_j$ . In Fig. 53, there are pairs of spurious graphs with opposite signs, e.g., Fig. 54 (a) and (b). When all pairs of spurious graphs are canceled out, graphs in Fig. 53 become Fig. 52 (b)-(h).

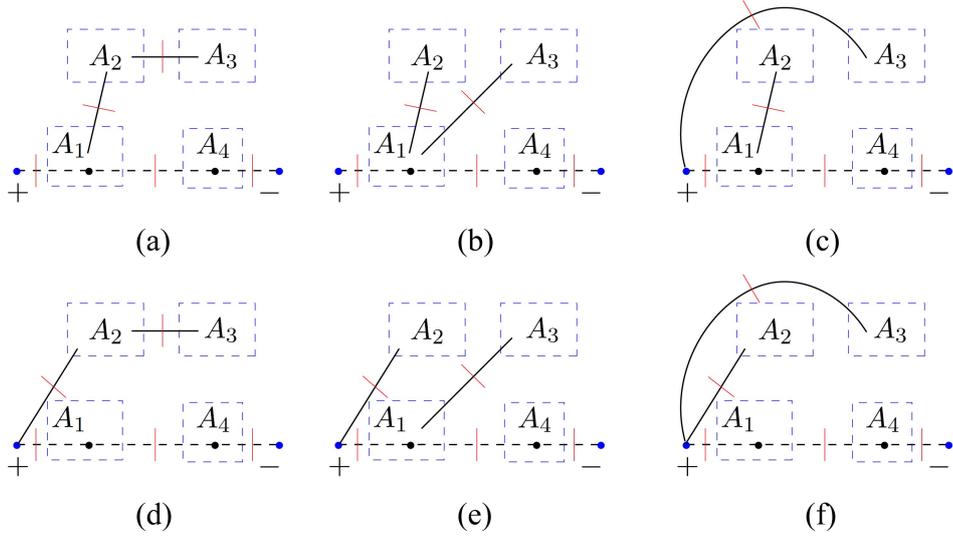


**Figure 55.** All topologies for the partition  $\{A_1, A_2, A_3, A_4\} = \{x_1, \{p, q\}, \{r, s\}, x_2\}$ .

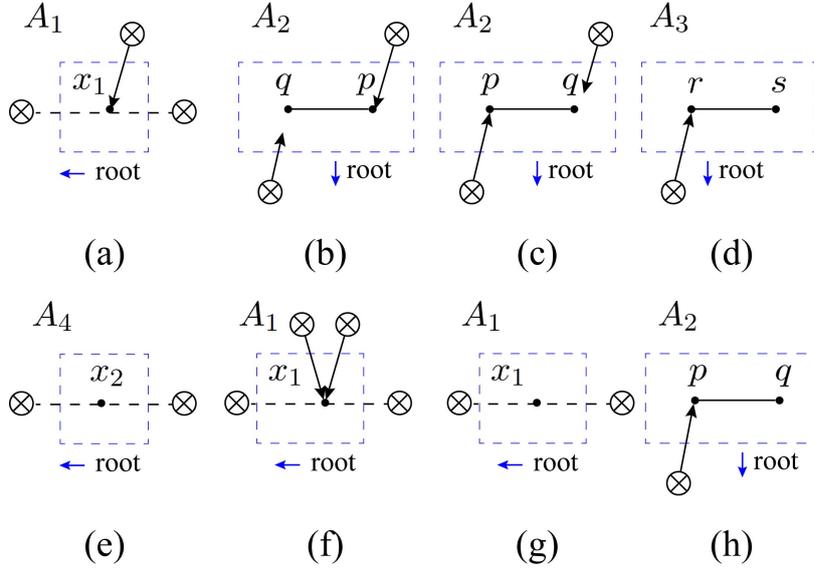


**Figure 56.** All possible structures of subgraphs for topologies in Fig. 55, which contribute a factor  $(\epsilon_p \cdot \epsilon_q)(\epsilon_r \cdot \epsilon_s)$ . The reference order is assumed to be  $p < q < r < s$ .

## H Quadratic propagators from refined graphic rule: an example with four gluons

By an example with four gluons and two scalars, we show the cancellation between diagrams and the final quadratic propagator form, using the general method in section 6. We focus on the partition  $\{x_1, \{p, q\}, \{r, s\}, x_2\}$  and only consider terms with a factor  $(\epsilon_p \cdot \epsilon_q)(\epsilon_r \cdot \epsilon_s)$ . All possible topologies for the partition  $\{x_1, \{p, q\}, \{r, s\}, x_2\}$  are given by Fig. 55, where  $A_1 = \{x_1\}$ ,  $A_2 = \{p, q\}$ ,  $A_3 = \{r, s\}$  and  $A_4 = \{x_2\}$ . All structure of subgraphs are displayed in Fig. 56. The choice of a subgraph for a subset

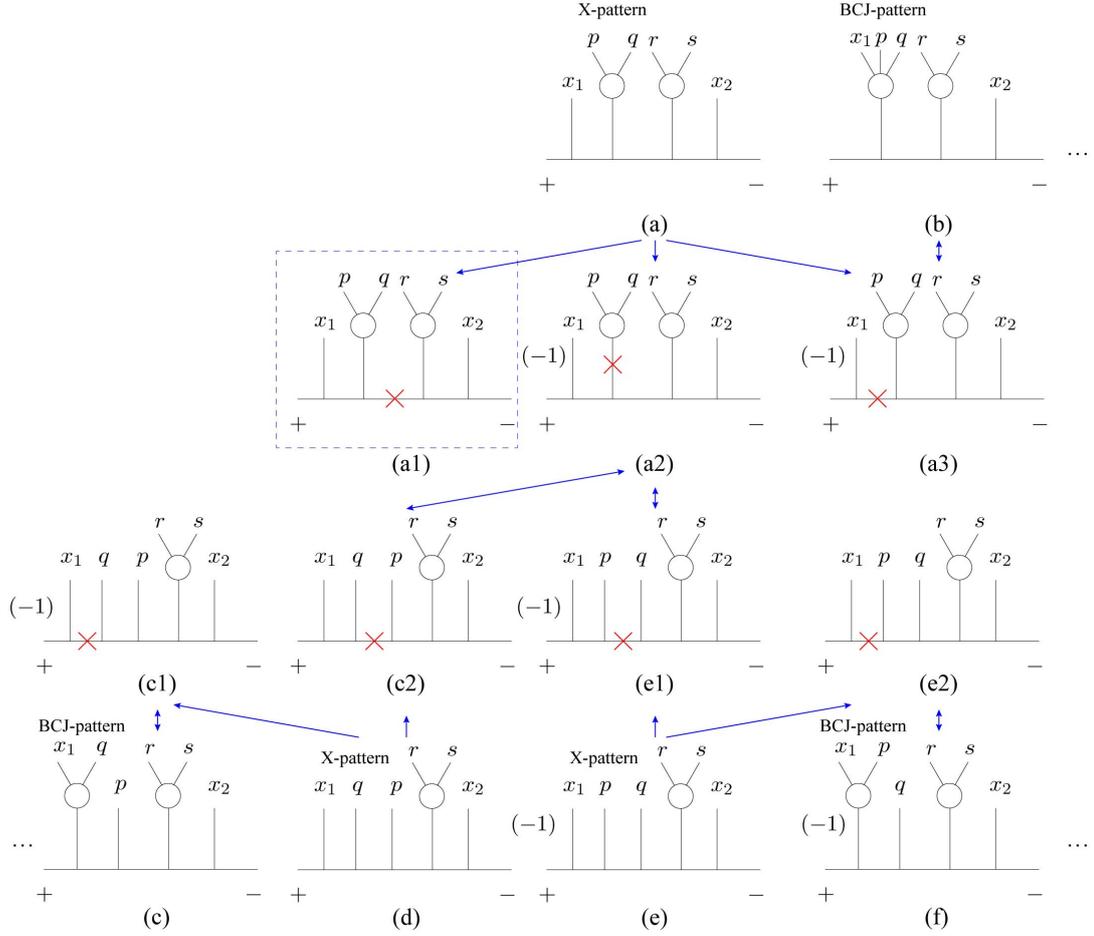


**Figure 57.** Cancellation map related to the topology Fig. 55 (a) when the subgraph of  $A_2$  is chosen as Fig. 56 (b). The ‘X-pattern’ or ‘BCJ-pattern’ for a diagram means the graph accompanying to this diagram contains the corresponding pattern. The minus signs in (a2), (a3) and (c1) come from the decomposition of an X-pattern, see Fig. 18. The minus in (e) and (f) are induced by spurious graph. The signs of (e1) and (e2) are resulted by both X-pattern and the spurious graph associating with (e).

relies on topology. For example, corresponding to the topology Fig. 55 (a), subgraphs of  $A_1$ ,  $A_3$  and  $A_4$  are shown by Fig. 56 (a), (d) and (e), while the subgraph of  $A_2$  has two distinct structures Fig. 56 (b) and (c). Another example is given by the topology Fig. 55 (b), possible subgraphs are Fig. 56 (d), (e), (f), (h).

For the topology Fig. 55 (a), if the subgraph for  $A_2$  is chosen as Fig. 56 (b), the cancellation map is shown by Fig. 57. After cancellation, the remaining diagram resulted by Fig. 57 (a) is Fig. 57 (a1), which is expressed as

$$\phi_{x_1} \left[ -\frac{1}{2} (\epsilon_q \cdot \epsilon_p) (-k_p \cdot k_r) (\epsilon_r \cdot \epsilon_s) \phi_{qp} \phi_{rs} \right] \phi_{x_2} \frac{1}{l^2} \frac{1}{s_{x_1, l}} \frac{1}{s_{x_1 p q r s, l}}. \quad (\text{H.1})$$

When all cyclic permutations of  $(x_1 x_2)$  and cyclic permutations of all elements in the right half integrand

are considered, graphic rule allows all cyclic permutations of  $A_1, A_2, A_3, A_4$ . Altogether provides a term with quadratic propagators

$$\phi_{x_1} \left[ -\frac{1}{2} (\epsilon_q \cdot \epsilon_p) (-k_p \cdot k_r) (\epsilon_r \cdot \epsilon_s) \phi_{qp} \phi_{rs} \right] \phi_{x_2} \frac{1}{l^2} \frac{1}{l_{x_1}^2} \frac{1}{l_{x_1 p q r s}^2}, \quad (\text{H.2})$$

where the expression inside the squarebrackets contributes one term to  $(-\frac{1}{2}) \tilde{J}(p, q) \cdot \tilde{J}(r, s)$ , agrees with (6.15). The  $\phi_{x_1}$  and  $\phi_{x_2}$  are  $\tilde{J}(x_1)$  and  $\tilde{J}(x_2)$  which are the currents containing scalars (defined by (6.14)).

When the subgraph of  $A_2$  is chosen as Fig. 56 (c), the topology Fig. 55 (a) and other topologies Fig. 55 (b) and (c) together provide

$$\phi_{x_1} \left[ (\epsilon_p \cdot \epsilon_q) (-k_p \cdot x_1) \phi_{pq} \right] \left[ (\epsilon_r \cdot \epsilon_s) (-k_r \cdot X_r) \phi_{rs} \right] \phi_{x_2} \frac{1}{l^2} \frac{1}{s_{x_1, l}} \frac{1}{s_{x_1 p q, l}} \frac{1}{s_{x_1 p q r s, l}}, \quad (\text{H.3})$$

where,  $X_r^\mu = l^\mu + k_{x_1}^\mu + k_p^\mu + k_q^\mu$ . We have used the fact that the subgraphs for the topology Fig. 55 (b) are Fig. 56 (d), (e), (f), (h) and the subgraphs for Fig. 55 (c) are Fig. 56 (a), (d), (e), (h). Similarly, the topologies Fig. 55 (d), (e) and (f) produce

$$\phi_{x_1} \left[ (\epsilon_p \cdot \epsilon_q) (-k_p \cdot l) \phi_{pq} \right] \left[ (\epsilon_r \cdot \epsilon_s) (-k_r \cdot X_r) \phi_{rs} \right] \phi_{x_2} \frac{1}{l^2} \frac{1}{s_{x_1, l}} \frac{1}{s_{x_1 p q, l}} \frac{1}{s_{x_1 p q r s, l}}. \quad (\text{H.4})$$

The sum of (H.3) and (H.4) gives rise

$$\phi_{x_1} \left[ (\epsilon_p \cdot \epsilon_q) (-k_p \cdot X_p) \phi_{pq} \right] \left[ (\epsilon_r \cdot \epsilon_s) (-k_r \cdot X_r) \phi_{rs} \right] \phi_{x_2} \frac{1}{l^2} \frac{1}{s_{x_1, l}} \frac{1}{s_{x_1 p q, l}} \frac{1}{s_{x_1 p q r s, l}}, \quad (\text{H.5})$$

where  $X_p^\mu = l^\mu + k_{x_1}^\mu$ . After summing over cyclic permutations  $A_1, A_2, A_3, A_4$ , we get the quadratic propagator form

$$\tilde{J}(x_1) \left[ (\epsilon_p \cdot \epsilon_q) (-k_p \cdot X_p) \phi_{pq} \right] \left[ (\epsilon_r \cdot \epsilon_s) (-k_r \cdot X_r) \phi_{rs} \right] \tilde{J}(x_2) \frac{1}{l^2} \frac{1}{l_{x_1}^2} \frac{1}{l_{x_1 p q}^2} \frac{1}{l_{x_1 p q r s}^2}. \quad (\text{H.6})$$

The expressions in the squarebrackets contribute to  $\tilde{J}(p, q) \cdot X_{\{p, q\}}$ ,  $\tilde{J}(r, s) \cdot X_{\{r, s\}}$ , agree with (6.15). The definition of subcurrent with scalars (6.14) was applied again.

In the above, we only presented the remaining terms with  $(\epsilon_p \cdot \epsilon_q)(\epsilon_r \cdot \epsilon_s)$  after cancellation, for the partition  $\{x_1, \{p, q\}, \{r, s\}, x_2\}$  with topology Fig. 55 (a). In fact, all surviving terms in the cancellations for all partitions and all topologies can be obtained in a similar way. Terms expressed by effective currents are further demonstrated in the next section.

## I Expressions of terms in (6.16): demonstrated by explicit examples

We display terms in (6.16) for the integrand  $I^{1\text{-loop}}(x_1, x_2 | \{p, q, r, s\} | x_1, x_2, p, q, r, s)$  with four gluons  $p, q, r, s$  and two scalars  $x_1, x_2$ , by partitions with four to six subsets. All partitions with four to six subsets

are given by

$$\begin{aligned}
& \{x_1, x_2, p, q, r, s\}, & \{x_1, \{x_2, p\}, q, r, s\}, & \{x_1, x_2, \{p, q\}, r, s\}, & \{x_1, x_2, p, \{q, r\}, s\}, \\
& \{x_1, x_2, p, q, \{r, s\}\}, & \{\{s, x_1\}, x_2, p, q, r\}, & \{x_1, \{x_2, p, q\}, r, s\}, & \{x_1, x_2, \{p, q, r\}, s\}, \\
& \{x_1, x_2, p, \{q, r, s\}\}, & \{\{r, s, x_1\}, x_2, p, q\}, & \{x_1, \{x_2, p\}, \{q, r\}, s\}, & \{x_1, \{x_2, p\}, q, \{r, s\}\}, \\
& \{\{s, x_1\}, \{x_2, p\}, q, r\}, & \{x_1, x_2, \{p, q\}, \{r, s\}\}, & \{\{s, x_1\}, x_2, \{p, q\}, r\}, & \{\{s, x_1\}, x_2, p, \{q, r\}\}, \quad (\text{I.1})
\end{aligned}$$

where those partitions with  $x_1, x_2$  in the same subset vanishes due to  $U(1)$ -decoupling identity, partitions related by cyclic permutations of subsets are equivalent to each other.

The expression accompanying to the partition  $\{x_1, x_2, \{p, q, r\}, s\}$  is explicitly given by

$$\begin{aligned}
& \frac{1}{l^2} \tilde{J}(x_1) \frac{1}{l_{x_1}^2} \tilde{J}(x_2) \frac{1}{l_{x_1 x_2}^2} \left\{ \tilde{J}(p, q, r) \cdot l_{x_1 x_2} \right. \\
& \quad \left. + \left( -\frac{1}{2} \right) \left[ \tilde{J}(p) \cdot \tilde{J}(q, r) + \tilde{J}(q) \cdot \tilde{J}(p, r) + \tilde{J}(p, q) \cdot \tilde{J}(r) \right] \right\} \frac{1}{l_{x_1 x_2 p q r}^2} \tilde{J}(s) \cdot l_{x_1 x_2 p q r}, \quad (\text{I.2})
\end{aligned}$$

in which,  $\tilde{J}(x_1) = \phi_{x_1|x_1}$ ,  $\tilde{J}(x_2) = \phi_{x_2|x_2}$ ,  $\tilde{J}^\mu(p)$ ,  $\tilde{J}^\mu(q)$  and  $\tilde{J}^\mu(r)$  are respectively given by  $\epsilon_p^\mu \phi_{p|p}$ ,  $\epsilon_q^\mu \phi_{q|q}$  and  $\epsilon_r^\mu \phi_{r|r}$ . The effective current  $\tilde{J}^\mu(p, q, r)$  is given by (C.1), while the currents  $\tilde{J}^\mu(q, r)$ ,  $\tilde{J}^\mu(p, r)$ ,  $\tilde{J}^\mu(p, q)$  are expressed as

$$\begin{aligned}
\tilde{J}^\mu(q, r) &= (\epsilon_r \cdot F_q)^\mu \phi_{qr|qr} + (\epsilon_q \cdot k_r) \epsilon_r^\mu \phi_{rq|qr}, \\
\tilde{J}^\mu(p, r) &= (\epsilon_r \cdot F_p)^\mu \phi_{pr|qr} + (\epsilon_p \cdot k_r) \epsilon_r^\mu \phi_{rp|qr}, \\
\tilde{J}^\mu(p, q) &= (\epsilon_q \cdot F_p)^\mu \phi_{pq|pq} + (\epsilon_p \cdot k_q) \epsilon_q^\mu \phi_{qp|pq},
\end{aligned}$$

where the current  $\tilde{J}^\mu(p, r)$  finally vanishes since  $\phi_{pr|qr} = \phi_{rp|qr} = 0$ . The expression for the partition  $\{x_1, \{x_2, p\}, \{q, r\}, s\}$  is written as

$$\frac{1}{l^2} \tilde{J}(x_1) \frac{1}{l_{x_1}^2} \tilde{J}(x_2, p) \frac{1}{l_{x_1 x_2 p}^2} \left[ \tilde{J}(q, r) \cdot l_{x_1 x_2 p} + \left( -\frac{1}{2} \right) \tilde{J}(q) \cdot \tilde{J}(r) \right] \frac{1}{l_{x_1 x_2 p q r}^2} \tilde{J}(s) \cdot l_{x_1 x_2 p q r}, \quad (\text{I.3})$$

where the current  $\tilde{J}(x_2, p)$  is explicitly written as

$$\tilde{J}(x_2, p) = (\epsilon_p \cdot k_{x_2}) \phi_{x_2 p|x_2 p}. \quad (\text{I.4})$$

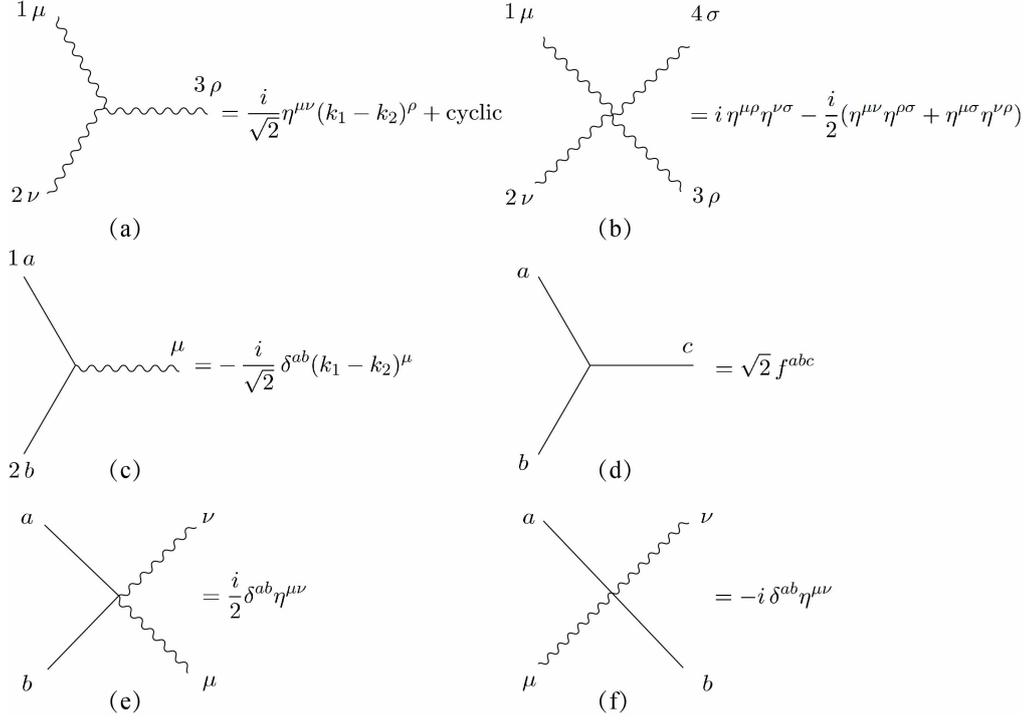


**Figure 58.** Vertices in the Feynman rule for single-trace YMS amplitudes (see [55])

## J Feynman rule in YMS

The vertices for single-trace YMS amplitudes are given by Fig. 58. This Feynman rule evaluates the color-ordered YMS amplitude of gluons and color-scalars. When the color factors for color-scalars are further extracted out, the kinematic part becomes the YMS amplitudes discussed in this paper.

## K KK relation for one-loop half integrands

As pointed in [33], there are three types of one-loop CHY half integrands  $I_L^{1\text{-loop}}(\sigma_1; \dots; \sigma_m || \mathbf{G})$ , which depend on different orders in the couplings  $g$  and  $\lambda$ , in the YMS theory. Specifically

$$I_L^{1\text{-loop}}(\sigma_1; \dots; \sigma_m || \mathbf{G})|_{g^n \lambda^{r-2m+4}} = \sum_{1 \leq i < j \leq m} \sum_{\substack{Q \in \text{cyc } \sigma_i \\ R \in \text{cyc } \sigma_j}} I_L^{\text{tree}}(+, Q, -, R; \sigma_1; \dots; \sigma_i; \dots; \sigma_j; \dots; \sigma_m || \mathbf{G}) + (+ \leftrightarrow -),$$

$$I_L^{1\text{-loop}}(\sigma_1; \dots; \sigma_m || \mathbf{G})|_{g^n \lambda^{r-2m+2}} = N \sum_{j=1}^m \sum_{Q \in \text{cyc } \sigma_i} I_L^{\text{tree}}(+, Q, -, \sigma_1; \dots; \sigma_i; \dots; \sigma_m || \mathbf{G}) + (+ \leftrightarrow -),$$

$$I_L^{1\text{-loop}}(\sigma_1; \dots; \sigma_m || \mathbf{G})|_{g^n \lambda^{r-2m}} = N c_2 I_L^{\text{tree}}(\sigma_1; \dots; \sigma_m; +, - || \mathbf{G}) + I_L^{\text{tree}}(\sigma_1; \dots; \sigma_m || \mathbf{G}, +, -),$$

$$+ \sum_{j=1}^m \left\{ \sum_{\substack{\sigma_j=QR \\ |Q|, |R| \neq 0}} I_L^{\text{tree}}(Q, +; R, -; \sigma_1; \dots; \cancel{\sigma_j}; \dots; \sigma_m || \mathbf{G}) + \text{cyc } \sigma_j \right\}, \quad (\text{K.1})$$

where  $N$  referred to the  $U(N)$  or  $SU(N)$  group for the color scalar, while the coefficient  $c_2$  is  $N$  for  $U(N)$  group and  $\frac{N^2-1}{N}$  for  $SU(N)$  group. The sets  $Q$  and  $R$  are two ordered sets of scalars, the set  $\mathbf{G}$  denotes the gluon set, and  $\cancel{\sigma_i}$  represents that the  $i$ -th trace  $\sigma_i$  is removed. The number of total particles and scalars are supposed to be  $n$  and  $r$ , respectively. In the above expression, the RHS of the first and the second equations as well as the first term on the RHS of the third equation correspond to the case that there are only scalar propagators on the loop. On the contrary, the second and the third terms on the RHS of the third equation contribute to loops with at least one gluon propagator.

The one-loop YMS integrands (in both single- and multi-trace cases) with quadratic propagators, which come from the forward limit of the tree-level amplitudes whose particles  $+$  and  $-$  are in the same trace and adjacent to each other, are directly obtained from (6.16) and the discussions in section 7. Now we show that the tree-level CHY half integrands  $I_L^{\text{tree}}(+, Q, -, R; \dots || \mathbf{G})$  with particles  $+$  and  $-$  separated by the scalars belonging to the same trace, can be rewritten as

$$\begin{aligned} & \sum_{\substack{Q \in \text{cyc } \sigma_i \\ R \in \text{cyc } \sigma_j}} I_L^{\text{tree}}(+, Q, -, R; \sigma_1; \dots; \cancel{\sigma_i}; \dots; \cancel{\sigma_j}; \dots; \sigma_m || \mathbf{G}) \\ &= \sum_{\text{cyc } \rho} \sum_{R^T \in \text{cyc } \sigma_j^T} (-1)^{|\sigma_j|} I_L^{\text{tree}}(+, Q_1, \{Q_2, \dots\} \sqcup R^T, -; \sigma_1; \dots; \cancel{\sigma_i}; \dots; \cancel{\sigma_j}; \dots; \sigma_m || \mathbf{G}), \end{aligned} \quad (\text{K.2})$$

where the ordered sets  $\sigma_i$  and  $\rho$  in the above summations are defined by  $\sigma_i = Q_1, Q_2, \dots$ , and  $\rho = Q_1, \{Q_2, \dots\} \sqcup R^T$ . The  $|\sigma_j|$ ,  $\sigma_j^T$  denote the number of elements and the inverse of the permutation  $\sigma_j$ , respectively. To prove eq. (K.2), we arrange the tree-level PT factors as

$$\begin{aligned} \sum_{\substack{\text{cyc } \alpha \\ \text{cyc } \beta}} \text{PT}(+, \alpha, -, \beta) &= \sum_{\substack{\text{cyc } \alpha \\ \text{cyc } \beta^T}} (-1)^{|\beta|} \text{PT}(+, \alpha \sqcup \beta^T, -) \\ &= \sum_{\text{cyc } \rho} \sum_{\text{cyc } \beta^T} (-1)^{|\beta|} \text{PT}(+, \alpha_1, \{\alpha_2, \dots, \alpha_s\} \sqcup \beta^T, -), \end{aligned} \quad (\text{K.3})$$

where  $\alpha = \alpha_1, \alpha_2, \dots, \alpha_s$ ,  $\rho = \alpha_1, \{\alpha_2, \dots, \alpha_s\} \sqcup \beta^T$ . The first equality is the KK relation, while the second can be checked by comparing the permutations on both sides of this equation. For any permutation on the LHS, one can always find it on the RHS of the second equality. Both sides of this equation have the number of permutations  $\frac{(s+t)!}{(s-1)!(t-1)!}$ , where  $s$  and  $t$  are the number of elements of  $\alpha$  and  $\beta$ . For example, we choose  $\alpha = 1, 2$  and  $\beta = 3, 4$ , then both the LHS of the first line and the RHS of the second line have the following 24 permutations: 1234, 2341, 3412, 4123, 1324, 3241, 2413, 4132, 1342, 3421, 4213, 2134, 1243, 2431, 4312, 3124, 1423, 4231, 2314, 3142, 1432, 4321, 3214, 2143. This observation can be straightforwardly extended

to general permutations, therefore eq. (K.2) is proven.

This relation of PT factors can be considered as the CHY version of the one-loop KK relation (the one for YM amplitudes was proposed in [56])

$$A^{1\text{-loop}}(\boldsymbol{\alpha}; \boldsymbol{\beta}) = \sum_{\boldsymbol{\rho} \in \text{COP}(\boldsymbol{\alpha} \cup \boldsymbol{\beta}^T)} (-1)^{|\boldsymbol{\beta}|} A^{1\text{-loop}}(\boldsymbol{\rho}), \quad (\text{K.4})$$

where  $A^{1\text{-loop}}(\boldsymbol{\alpha}; \boldsymbol{\beta})$  refers to a one-loop multi-trace amplitude and  $A^{1\text{-loop}}(\boldsymbol{\rho})$  denote a one-loop amplitude with one less trace. The  $\text{COP}(\boldsymbol{\alpha} \cup \boldsymbol{\beta}^T)$  denotes the summation of all possible permutations that keep  $\boldsymbol{\alpha}$ ,  $\boldsymbol{\beta}^T$  in their own cyclic order.

## References

- [1] F. Cachazo, S. He, and E. Y. Yuan, *Scattering equations and Kawai-Lewellen-Tye orthogonality*, *Phys. Rev. D* **90** (2014), no. 6 065001, [[arXiv:1306.6575](#)].
- [2] F. Cachazo, S. He, and E. Y. Yuan, *Scattering of Massless Particles in Arbitrary Dimensions*, *Phys. Rev. Lett.* **113** (2014), no. 17 171601, [[arXiv:1307.2199](#)].
- [3] F. Cachazo, S. He, and E. Y. Yuan, *Scattering of Massless Particles: Scalars, Gluons and Gravitons*, *JHEP* **07** (2014) 033, [[arXiv:1309.0885](#)].
- [4] F. Cachazo, S. He, and E. Y. Yuan, *Einstein-Yang-Mills Scattering Amplitudes From Scattering Equations*, *JHEP* **01** (2015) 121, [[arXiv:1409.8256](#)].
- [5] F. Cachazo, S. He, and E. Y. Yuan, *Scattering Equations and Matrices: From Einstein To Yang-Mills, DBI and NLSM*, *JHEP* **07** (2015) 149, [[arXiv:1412.3479](#)].
- [6] S. J. Parke and T. R. Taylor, *An Amplitude for n Gluon Scattering*, *Phys. Rev. Lett.* **56** (1986) 2459.
- [7] L. Hou and Y.-J. Du, *A graphic approach to gauge invariance induced identity*, *JHEP* **05** (2019) 012, [[arXiv:1811.12653](#)].
- [8] Y.-J. Du and L. Hou, *A graphic approach to identities induced from multi-trace Einstein-Yang-Mills amplitudes*, *JHEP* **05** (2020) 008, [[arXiv:1910.04014](#)].
- [9] S. Stieberger and T. R. Taylor, *New relations for Einstein–Yang–Mills amplitudes*, *Nucl. Phys. B* **913** (2016) 151–162, [[arXiv:1606.09616](#)].
- [10] D. Nandan, J. Plefka, O. Schlotterer, and C. Wen, *Einstein-Yang-Mills from pure Yang-Mills amplitudes*, *JHEP* **10** (2016) 070, [[arXiv:1607.05701](#)].
- [11] O. Schlotterer, *Amplitude relations in heterotic string theory and Einstein-Yang-Mills*, *JHEP* **11** (2016) 074, [[arXiv:1608.00130](#)].
- [12] C.-H. Fu, Y.-J. Du, R. Huang, and B. Feng, *Expansion of Einstein-Yang-Mills Amplitude*, *JHEP* **09** (2017) 021, [[arXiv:1702.08158](#)].
- [13] M. Chiodaroli, M. Gunaydin, H. Johansson, and R. Roiban, *Explicit Formulae for Yang-Mills-Einstein Amplitudes from the Double Copy*, *JHEP* **07** (2017) 002, [[arXiv:1703.00421](#)].

- [14] F. Teng and B. Feng, *Expanding Einstein-Yang-Mills by Yang-Mills in CHY frame*, *JHEP* **05** (2017) 075, [[arXiv:1703.01269](#)].
- [15] Y.-J. Du, B. Feng, and F. Teng, *Expansion of All Multitrace Tree Level EYM Amplitudes*, *JHEP* **12** (2017) 038, [[arXiv:1708.04514](#)].
- [16] Y.-J. Du and F. Teng, *BCJ numerators from reduced Pfaffian*, *JHEP* **04** (2017) 033, [[arXiv:1703.05717](#)].
- [17] L. Mason and D. Skinner, *Ambitwistor strings and the scattering equations*, *JHEP* **07** (2014) 048, [[arXiv:1311.2564](#)].
- [18] S. He and E. Y. Yuan, *One-loop Scattering Equations and Amplitudes from Forward Limit*, *Phys. Rev. D* **92** (2015), no. 10 105004, [[arXiv:1508.06027](#)].
- [19] F. Cachazo, S. He, and E. Y. Yuan, *One-Loop Corrections from Higher Dimensional Tree Amplitudes*, *JHEP* **08** (2016) 008, [[arXiv:1512.05001](#)].
- [20] S. He and O. Schlotterer, *New Relations for Gauge-Theory and Gravity Amplitudes at Loop Level*, *Phys. Rev. Lett.* **118** (2017), no. 16 161601, [[arXiv:1612.00417](#)].
- [21] Y. Geyer, L. Mason, R. Monteiro, and P. Tourkine, *One-loop amplitudes on the Riemann sphere*, *JHEP* **03** (2016) 114, [[arXiv:1511.06315](#)].
- [22] Y. Geyer and R. Monteiro, *Gluons and gravitons at one loop from ambitwistor strings*, *JHEP* **03** (2018) 068, [[arXiv:1711.09923](#)].
- [23] A. Edison, S. He, O. Schlotterer, and F. Teng, *One-loop Correlators and BCJ Numerators from Forward Limits*, *JHEP* **09** (2020) 079, [[arXiv:2005.03639](#)].
- [24] B. Feng, S. He, Y. Zhang, and Y.-Q. Zhang, *One-loop diagrams with quadratic propagators from the worldsheet*, *JHEP* **08** (2022) 240, [[arXiv:2204.13659](#)].
- [25] C. Baadsgaard, N. E. J. Bjerrum-Bohr, J. L. Bourjaily, P. H. Damgaard, and B. Feng, *Integration Rules for Loop Scattering Equations*, *JHEP* **11** (2015) 080, [[arXiv:1508.03627](#)].
- [26] C. Cardona and H. Gomez, *Elliptic scattering equations*, *JHEP* **06** (2016) 094, [[arXiv:1605.01446](#)].
- [27] C. Cardona and H. Gomez, *CHY-Graphs on a Torus*, *JHEP* **10** (2016) 116, [[arXiv:1607.01871](#)].
- [28] H. Gomez, S. Mizera, and G. Zhang, *CHY Loop Integrands from Holomorphic Forms*, *JHEP* **03** (2017) 092, [[arXiv:1612.06854](#)].
- [29] H. Gomez, *Quadratic Feynman Loop Integrands From Massless Scattering Equations*, *Phys. Rev. D* **95** (2017), no. 10 106006, [[arXiv:1703.04714](#)].
- [30] N. Ahmadinia, H. Gomez, and C. Lopez-Arcos, *Non-planar one-loop Parke-Taylor factors in the CHY approach for quadratic propagators*, *JHEP* **05** (2018) 055, [[arXiv:1802.00015](#)].
- [31] J. Agerskov, N. E. J. Bjerrum-Bohr, H. Gomez, and C. Lopez-Arcos, *One-Loop Yang-Mills Integrands from Scattering Equations*, *Phys. Rev. D* **102** (2020), no. 4 045023, [[arXiv:1910.03602](#)].
- [32] J. A. Farrow, Y. Geyer, A. E. Lipstein, R. Monteiro, and R. Stark-Muchão, *Propagators, BCFW recursion and new scattering equations at one loop*, *JHEP* **10** (2020) 074, [[arXiv:2007.00623](#)].

- [33] F. Porkert and O. Schlotterer, *One-loop amplitudes in Einstein-Yang-Mills from forward limits*, *JHEP* **02** (2023) 122, [[arXiv:2201.12072](#)].
- [34] J. Dong, Y.-Q. Zhang, and Y. Zhang, *One-loop BCJ Numerators on Quadratic Propagators from the Worldsheet*, [arXiv:2312.01580](#).
- [35] Z. Bern, J. J. M. Carrasco, and H. Johansson, *New Relations for Gauge-Theory Amplitudes*, *Phys. Rev. D* **78** (2008) 085011, [[arXiv:0805.3993](#)].
- [36] Z. Bern, J. J. M. Carrasco, and H. Johansson, *Perturbative Quantum Gravity as a Double Copy of Gauge Theory*, *Phys. Rev. Lett.* **105** (2010) 061602, [[arXiv:1004.0476](#)].
- [37] K. Wu and Y.-J. Du, *Off-shell extended graphic rule and the expansion of Berends-Giele currents in Yang-Mills theory*, *JHEP* **01** (2022) 162, [[arXiv:2109.14462](#)].
- [38] Y.-J. Du and K. Wu, *Note on graph-based BCJ relation for Berends-Giele currents*, *JHEP* **12** (2022) 080, [[arXiv:2207.02374](#)].
- [39] R. Kleiss and H. Kuijf, *Multi - Gluon Cross-sections and Five Jet Production at Hadron Colliders*, *Nucl. Phys. B* **312** (1989) 616–644.
- [40] F. A. Berends and W. T. Giele, *Recursive Calculations for Processes with  $n$  Gluons*, *Nucl. Phys. B* **306** (1988) 759–808.
- [41] C. R. Mafra, *Berends-Giele recursion for double-color-ordered amplitudes*, *JHEP* **07** (2016) 080, [[arXiv:1603.09731](#)].
- [42] Y.-J. Du, B. Feng, and C.-H. Fu, *BCJ Relation of Color Scalar Theory and KLT Relation of Gauge Theory*, *JHEP* **08** (2011) 129, [[arXiv:1105.3503](#)].
- [43] H. Frost, C. R. Mafra, and L. Mason, *A Lie Bracket for the Momentum Kernel*, *Commun. Math. Phys.* **402** (2023), no. 2 1307–1343, [[arXiv:2012.00519](#)].
- [44] S. Lee, C. R. Mafra, and O. Schlotterer, *Non-linear gauge transformations in  $D = 10$  SYM theory and the BCJ duality*, *JHEP* **03** (2016) 090, [[arXiv:1510.08843](#)].
- [45] E. Bridges and C. R. Mafra, *Algorithmic construction of SYM multiparticle superfields in the BCJ gauge*, *JHEP* **10** (2019) 022, [[arXiv:1906.12252](#)].
- [46] R. H. Boels and R. S. Isermann, *New relations for scattering amplitudes in Yang-Mills theory at loop level*, *Phys. Rev. D* **85** (2012) 021701, [[arXiv:1109.5888](#)].
- [47] Y.-J. Du and H. Luo, *On General BCJ Relation at One-loop Level in Yang-Mills Theory*, *JHEP* **01** (2013) 129, [[arXiv:1207.4549](#)].
- [48] Z. Bern, S. Davies, T. Dennen, Y.-t. Huang, and J. Nohle, *Color-Kinematics Duality for Pure Yang-Mills and Gravity at One and Two Loops*, *Phys. Rev. D* **92** (2015), no. 4 045041, [[arXiv:1303.6605](#)].
- [49] M. Chiodaroli, Q. Jin, and R. Roiban, *Color/kinematics duality for general abelian orbifolds of  $N=4$  super Yang-Mills theory*, *JHEP* **01** (2014) 152, [[arXiv:1311.3600](#)].
- [50] H. Johansson and A. Ochirov, *Pure Gravities via Color-Kinematics Duality for Fundamental Matter*, *JHEP* **11** (2015) 046, [[arXiv:1407.4772](#)].

- [51] M. Berg, I. Buchberger, and O. Schlotterer, *String-motivated one-loop amplitudes in gauge theories with half-maximal supersymmetry*, *JHEP* **07** (2017) 138, [[arXiv:1611.03459](#)].
- [52] A. Edison, S. He, H. Johansson, O. Schlotterer, F. Teng, and Y. Zhang, *Perfecting one-loop BCJ numerators in SYM and supergravity*, *JHEP* **02** (2023) 164, [[arXiv:2211.00638](#)].
- [53] J. Dong, S. He, and L. Hou, *Universal expansions of scattering amplitudes for gravitons, gluons, and Goldstone particles*, *Phys. Rev. D* **105** (2022), no. 10 105007, [[arXiv:2111.10525](#)].
- [54] Q. Cao, J. Dong, S. He, and Y.-Q. Zhang, *Covariant color-kinematics duality, Hopf algebras, and permutohedra*, *Phys. Rev. D* **107** (2023), no. 2 026022, [[arXiv:2211.05404](#)].
- [55] Z. Bern, A. De Freitas, and H. L. Wong, *On the coupling of gravitons to matter*, *Phys. Rev. Lett.* **84** (2000) 3531, [[hep-th/9912033](#)].
- [56] V. Del Duca, L. J. Dixon, and F. Maltoni, *New color decompositions for gauge amplitudes at tree and loop level*, *Nucl. Phys. B* **571** (2000) 51–70, [[hep-ph/9910563](#)].